

STATUS OF THESIS

Title of thesis

Development of Mixed Matrix Membranes for Separation of CO ₂ from CH ₄
--

I, AMELIA SUYONO WIRYOATMOJO

hereby allow my thesis to be placed at the Information Resource Center (IRC) of Universiti Teknologi PETRONAS (UTP) with the following conditions:

1. The thesis becomes the property of UTP
2. The IRC of UTP may make copies of the thesis for academic purposes only
3. This thesis classified as

Confidential

Non-confidential

If the thesis is confidential, please state the reason:

The contents of the thesis will remain confidential for _____ years.

Remarks on disclosure:

Endorsed by

Signature of Author
Amelia Suyono Wiryoatmojo

Kopo Permai II A12/18
Bandung 40239
Indonesia

Date: _____

Signature of Supervisor
Assoc. Prof. Dr. Hilmi Mukhtar

Department of Chemical Engineering
Universiti Teknologi PETRONAS
Bandar Seri Iskandar, Perak
Malaysia

Date: _____

UNIVERSITI TEKNOLOGI PETRONAS
DEVELOPMENT OF MIXED MATRIX MEMBRANES
FOR SEPARATION OF CO₂ FROM CH₄

by

AMELIA SUYONO WIRYOATMOJO

The undersigned certify that they have read, and recommend to the Postgraduate Studies Programme for acceptance this thesis for the fulfilment of the requirements for the degree stated.

Signature: _____

Main Supervisor: Assoc. Prof. Dr. Hilmi Mukhtar

Signature: _____

Co-Supervisor: Assoc. Prof. Dr. Zakaria Man

Signature: _____

Head of Department: Dr. Suhaimi Mahadzir

Date: _____

DEVELOPMENT OF MIXED MATRIX MEMBRANES
FOR SEPARATION OF CO₂ FROM CH₄

by

AMELIA SUYONO WIRYOATMOJO

A Thesis

Submitted to the Postgraduate Studies Programme

as a Requirement for the Degree of

MASTER OF SCIENCE

CHEMICAL ENGINEERING DEPARTMENT

UNIVERSITI TEKNOLOGI PETRONAS

BANDAR SERI ISKANDAR,

PERAK

JULY 2010

DECLARATION OF THESIS

Title of thesis

Development of Mixed Matrix Membranes for Separation of CO ₂ from CH ₄
--

I, AMELIA SUYONO WIRYOATMOJO

hereby declare that the thesis is based on my original work except for quotations and citations which have been duly acknowledged. I also declare that it has not been previously or concurrently submitted for any other degree at UTP or other institutions.

Witnessed by

Signature of Author

Kopo Permai II A12/18
Bandung 40239
Indonesia

Date : _____

Signature of Supervisor

Assoc. Prof. Dr. Hilmi Mukhtar

Date : _____

ACKNOWLEDGEMENTS

I thank all people who have taught me and contribute in so many ways during my years in graduate studies. I am especially grateful to my beloved mother, father, sisters, and husband, who never stop encouraging me to keep striving forward towards completion of my degree. Secondly I would like to thank Assoc. Prof. Dr. Hilmi Mukhtar and Assoc. Prof. Dr. Zakaria Man for their supports and guidances through my research activities. I also want to thank Professor Thanabalan Murugesan for his thoughtful inputs and his supports through some rough times.

Lastly, I would like to thank numerous fellow graduate and undergraduate students, which without them graduate life would not be as wonderful and fun as it has been. I am very fortunate to have met and developed friendship with them.

ABSTRACT

The rapid development in membrane technology for gas separation application to seek membrane with higher permeability and selectivity has motivated the present study to develop mixed matrix membranes. This is done by incorporating carbon molecular sieves (CMS) particles within polysulfone (PSU) matrix. The effect of CMS loading, annealing treatment and functionalization of CMS surface to the membrane morphology, mechanical, and viscoelastic properties were evaluated. The performance of fabricated membranes was evaluated in term of permeability and selectivity of CO₂ and CH₄.

Morphology analysis found that CMS and PSU have a good adhesion. It was also found that the introduction of CMS led to the formation of restricted mobility polymer regions surrounded CMS particles, indicated by the appearance of dual glass transition temperature (T_g). Adhesion of PSU-CMS within the membranes was explained using the profile of $\tan \delta$ and storage modulus, and the stress-strain curve. Membranes with annealing treatment have shown better adhesion between the two phases indicated by the reduction of $\tan \delta$ peaks area with the shifting of the second T_g to a lower temperature, higher storage modulus, and the occurrence of necking process. It was also found that functionalization of CMS surface by nitric acid oxidation further enhanced PSU-CMS adhesion. The formation of functional groups on CMS surface was confirmed by FTIR spectra and the reduction of its intermolecular distance.

Permeability of CO₂ and CH₄ indicated that the mixed matrix membrane has high ideal selectivity of CO₂/CH₄ compare to PSU membrane. Within the pressure range of CO₂ from 2 to 10 bar, the addition of 30 wt.% of CMS has increased the permeability of CO₂ and the ideal selectivity of CO₂/CH₄ up to 7-37% and 132-344%, respectively. However annealing treatment decreased the permeability of CO₂ as much as 12-29%, but increased its ideal selectivity as much as 165-823%. Similarly by using surface

functionalized CMS, the permeability of CO₂ was decreased as much as 2-5% and increased its ideal selectivity as much as 183-516%. Mixed matrix membranes modified by annealing treatment and employing surface functionalized CMS had successfully surpassed the upper-bound trade-off limit of polymeric membranes.

Keywords: Mixed matrix membranes; Carbon molecular sieves; CO₂ separation.

ABSTRAK

Perkembangan pesat dalam teknologi membran untuk aplikasi pemisahan gas bagi mencari membran dengan ketelapan dan kepemilihan yang lebih tinggi telah mendorong kajian ini untuk menghasilkan membran matrik campuran. Ini dilakukan dengan memasukkan zarah karbon penapis molekul (CMS) dalam matrik polisulfon (PSU). Kesan campuran CMS, rawatan pemanasan dan permukaan CMS difungsikan terhadap sifat-sifat morfologi, mekanik, dan viskoelastisitas membrane telah dikaji. Prestasi membran ini telah dinilai dengan ketelapan dan kepemilihan ideal terhadap gas karbon dioksida (CO₂) dan metana (CH₄).

Analisis morfologi mendapati bahawa pelekatan antara CMS dan matrik PSU sangat baik. Kajian ini juga mendapati bahawa memasukkan CMS mengarah pada pembentukan rantai polimer dengan mobility terhad mengelilingi zarah CMS. Ini ditunjukkan oleh keberadaan suhu peralihan gelas (T_g) ganda. Pelekatan daripada PSU-CMS dalam membran dijelaskan menggunakan profil daripada $\tan \delta$, simpanan modulus, dan graf tegangan-regangan. Membran dengan rawatan pemanasan telah menunjukkan pelekatan yang lebih baik antara kedua fasa. Ini ditunjukkan dengan pengurangan daerah puncak-puncak $\tan \delta$ dan pergeseran T_g kedua kepada suhu yang lebih rendah, modulus simpanan yang lebih tinggi, serta berlakunya penciutan muat. Kajian ini mendapati bahawa pengoksidasian CMS dengan asid nitrik lebih meningkatkan lagi pelekatan PSU-CMS. Pembentukan kelompok fungsional pada permukaan CMS disahkan oleh spektrum FTIR, dan pengurangan daripada jarak antarmolekul.

Ketelapan CO₂ dan CH₄ menunjukkan bahawa membran matrik campuran mempunyai kepemilihan ideal yang tinggi untuk CO₂/CH₄ dibandingkan dengan membran PSU. Dalam rentang tekanan CO₂ dari 2 sampai 10 bar, penambahan 30 wt.% CMS telah meningkatkan ketelapan CO₂ dan kepemilihan ideal CO₂/CH₄ sebanyak 7-37% dan 132-344%, secara urutan. Walaubagaimanapun, rawatan

pemanasan telah menurunkan ketelapan CO₂ sebanyak 12-29%, namun meningkatkan kepemilihan ideal sebanyak 165-823%. Keputusan yang serupa telah didapati pada membran menggunakan CMS permukaan difungsikan, ketelapan CO₂ berkurang sebesar 2-5% dan meningkatkan kepemilihan ideal sebanyak 183-516%. Membran matrik campuran yang diubahsuai dengan rawatan pemanasan dan menggunakan CMS permukaan yang difungsikan telah berjaya mengatasi batas atas garisan membran polimer.

Kata kunci: Campuran matriks membrane; Tapisan molekul karbon; Pemisahan CO₂.

In compliance with the terms of the Copyright Act 1987 and the IP Policy of the university, the copyright of this thesis has been reassigned by the author to the legal entity of the university,

Institute of Technology PETRONAS Sdn Bhd.

Due acknowledgement shall always be made of the use of any material contained in, or derived from, this thesis.

© Amelia Suyono Wiryoatmojo, 2010

Institute of Technology PETRONAS Sdn Bhd

All rights reserved.

TABLE OF CONTENTS

STATUS OF THESIS	i
APPROVAL PAGE	ii
TITLE PAGE	iii
DECLARATION OF THESIS	iv
ACKNOWLEDGEMENTS	v
ABSTRACT	vi
ABSTRAK	viii
DECLARATION OF THESIS	x
TABLE OF CONTENTS	xi
LIST OF FIGURE	xv
LIST OF TABLE	xix
ABBREVIATIONS	xxi
NOMENCLATURES	xxiii
CHAPTER 1 INTRODUCTION	1
1.1 Natural Gas	1
1.2 Gas Separation Technologies	6
1.2.1 Absorption Process	6
1.2.2 Adsorption Process	7
1.2.3 Cryogenic Process	8
1.2.4 Membrane Process	8
1.2.4.1 Polymeric Membranes	9
1.2.4.2 Inorganic Membranes	11
1.2.4.3 Mixed Matrix Membranes	12

1.2.4.4	Membrane Applications for Gas Separation	13
1.3	Problem Statement	15
1.4	Research Objectives	16
1.5	Scope of Study	17
1.6	Thesis Overview	18
CHAPTER 2	BACKGROUND AND THEORY	19
2.1	Review of Mixed Matrix Membranes Development	19
2.1.1	Selection of Polymer and Molecular Sieves Pair	20
2.1.2	Elimination of Interfacial Defects	23
2.2	Transport of Gas in Glassy Polymeric Membranes and Molecular Sieves Materials	31
2.2.1	Permeation	32
2.2.1.1	Permeation of Gas in Mixed Matrix Membrane	34
2.2.2	Sorption	35
2.2.3	Diffusion	37
2.2.3.1	Diffusion of Gas in Glassy Polymers	37
2.2.3.2	Diffusion of Gas in Molecular Sieves Particles	40
CHAPTER 3	MATERIAL AND METHODOLOGY	43
3.1	Material	43
3.1.1	Polysulfone	43
3.1.2	Solvents	44
3.1.3	Carbon Molecular Sieve	45
3.2	Fabrication of Membranes	47
3.2.1	Fabrication of Homogeneous Polysulfone Membrane	47
3.2.2	Mixed Matrix Membrane	49
3.3	Nitric Acid Oxidation of Carbon Molecular Sieve	50
3.4	Characterization of Homogeneous Polysulfone and Mixed Matrix Membranes	53
3.4.1	Field Emission Scanning Electron Microscope	53
3.4.2	Tensile Test	55
3.4.3	Dynamic Mechanical Analysis	57

3.4.4	Particle Size Analysis	58
3.4.5	X-Ray Diffraction	58
3.4.6	Density Measurement	59
3.4.7	Fourier Transform Infrared Spectroscopy	60
3.4.8	Determination of Acidic Functionality on Carbon Molecular Sieves Surface	62
3.5	Gas Permeation Study	62
CHAPTER 4 RESULTS AND DISCUSSIONS		66
4.1	Formation of Homogeneous Polysulfone Membranes	66
4.1.1	Effect of Polysulfone Concentration	66
4.2	Formation of Mixed Matrix Membranes with Carbon Molecular Sieves	71
4.2.1	Characterization of Carbon Molecular Sieves	71
4.2.2	Characterization of Mixed Matrix Membranes	73
4.2.2.1	Effect of Carbon Molecular Sieves Loading	73
4.2.2.2	Effect of Annealing Treatment	82
4.3	Formation of Mixed Matrix Membranes using Oxidized-Carbon Molecular Sieves	87
4.3.1	Nitric Acid Oxidation of Carbon Molecular Sieves	88
4.3.2	Characterization of Mixed Matrix Membranes with Oxidized- Carbon Molecular Sieves	94
4.4	Permeability Studies	99
4.4.1	Effect of Carbon Molecular Sieves Loading	99
4.4.2	Effect of Annealing Treatment	103
4.4.3	Effect of Using Oxidized-Carbon Molecular Sieves	106
CHAPTER 5 CONCLUSIONS AND RECCOMENDATIONS		110
5.1	Conclusions	110
5.2	Recommendations	112
REFERENCES		114
PUBLICATION		122

APPENDIX A ACIDIC CAPACITY OF CARBON MOLECULAR SIEVES 123

APPENDIX B PERMEABILITY OF MEMBRANE CALCULATION 127

LIST OF FIGURE

Figure 1.1: Natural gas use by sector. Adapted from [7].	3
Figure 1.2: Schematic mechanism for permeation of gases through porous and dense membranes.	9
Figure 1.3: Trade-off plot between membrane CO ₂ /CH ₄ selectivity and CO ₂ permeability for polymeric membranes. Adapted from [26].	11
Figure 1.4: Schematic diagram of a mixed matrix membrane.	13
Figure 2.1: Strategies to improve the adhesion between molecular sieves particles and polymer matrix in mixed matrix membranes fabrication.	24
Figure 2.2: CO ₂ /CH ₄ selectivity and CO ₂ permeability for various mixed matrix membranes.	31
Figure 2.4: Solution-diffusion mechanism.	32
Figure 2.5: Gas permeation through mixed matrix membrane containing different amounts of dispersed filler particles. Adapted from [10].	34
Figure 2.6: Sorption mechanisms contribute to the gas sorption in dual-sorption model: (a) Langmuir sorption and (b) Henry's law sorption.	36
Figure 2.7: Dual-sorption model in glassy polymer.	37
Figure 2.8: Diffusion of gas penetrant through glassy polymer. Adapted from [62].	39
Figure 2.9: The structure models of carbon materials: (a) for a nongraphitizable carbons by Franklin and (b) ribbon model for glass-like carbon by Jenkins-Kawamura. Adapted from [67].	41
Figure 3.1: Chemical structure of PSU. Adapted from [68].	44
Figure 3.2: CMS particle size distribution for various grinding period.	46
Figure 3.3: Experimental methodology of the study.	47
Figure 3.4: Casting steps of homogeneous dense membrane.	48
Figure 3.5: Preparation of casting solution to form mixed matrix membrane.	50

Figure 3.6: Experiment set-ups for: (a) reflux of CMS by HNO ₃ and (b) Soxhlet extraction of CMS by distilled water.	51
Figure 3.7: Schematic diagram of stirred filtration cell.	52
Figure 3.8: The schematic diagram of SEM instrument.	54
Figure 3.9: The stress-strain curve.	55
Figure 3.10: The illustration of tensile test.	56
Figure 3.11: The sinusoidal wave of stress and strain in DMA.	57
Figure 3.12: Bragg's diffraction.	59
Figure 3.13: Schematic of a gas pycnometer.	60
Figure 3.14: Schematic of FTIR instrument.	61
Figure 3.15: Schematic of gas membrane permeation test unit.	63
Figure 3.16: Schematic of the membrane module.	64
Figure 4.1: Field emission scanning electron micrographs of 15 wt.% polysulfone membrane: (a) cross-section (700 ×); (b) top section (10K ×); (c) bottom section (10K ×).	67
Figure 4.2: Stress-strain curve of homogeneous PSU membranes in different polymer concentrations.	68
Figure 4.3: Tan δ and storage modulus profile of homogeneous PSU membrane.	70
Figure 4.4: Field emission scanning electron micrograph of CMS powder (30K ×).	71
Figure 4.5: XRD spectra of CMS particle.	72
Figure 4.6: Field emission scanning electron micrograph of mixed matrix membrane using CMS in different loadings: (a) 10 (700 ×); (b) 20 (700 ×); and (c) 30 wt.%	74
Figure 4.7: Field scanning electron micrograph of CMS and PSU interaction (25K ×).	75
Figure 4.8: Tan δ profile for mixed matrix membranes with different CMS loadings.	76
Figure 4.9: Storage modulus profile for mixed matrix membranes with different CMS loadings.	77
Figure 4.10: Schematic model of the morphological transformation in filled polymer by Tsagaropoulos and Eisenberg [85].	78

Figure 4.11: Stress-strain curve of mixed matrix membranes in different CMS loadings.	80
Figure 4.12: Schematic illustration of debonding mechanism of one particle in a pair by Lauke [87].	81
Figure 4.13: Comparison of mixed matrix membranes: (a) with annealing (5K ×) and (b) without annealing treatment (5K ×).	83
Figure 4.14: Comparisons of: (a) $\tan \delta$ and (b) storage modulus profile of mixed matrix membranes with and without annealing treatment in different CMS loadings.	84
Figure 4.15: Comparisons of stress-strain curve of mixed matrix membranes with and without annealing treatment: (a) 10 wt.%; (b) 20 wt.%; and (c) 30 wt.% CMS.	86
Figure 4.16: FTIR spectra of surface CMS treated with various HNO ₃ concentrations.	88
Figure 4.17: Possible acidic groups attached to the CMS surface [96].	89
Figure 4.18: Nitric acid oxidation of 9,10-dihydrophenanthrene (a) and diphenylmethane (b). Adapted from Vinke et al. [71].	90
Figure 4.19: Acidic capacity of oxidized CMS treated with several HNO ₃ concentrations.	90
Figure 4.20: Filtered NaOH solution after reflux treatment.	91
Figure 4.21: Possible structure of oxidized graphitic fragment. Adapted from Wu et al. [73].	92
Figure 4.22: The comparison of CMS surface: a) without oxidation (200K ×) and b) with oxidation treatment using 11 M of HNO ₃ (200K ×).	92
Figure 4.23: XRD spectra of CMS particle before and after oxidation process.	93
Figure 4.24: Field emission scanning electron micrographs of mixed matrix membranes using ox-CMS in different loadings: (a) 10 (700 ×); (b) 20 (700 ×); and (c) 30 wt.% (700 ×).	95
Figure 4.25: Comparison of mixed matrix membranes using: (a) ox-CMS (25K ×) and (b) CMS (25K ×).	96
Figure 4.26: Comparisons of $\tan \delta$ (a) and storage modulus (b) profile of mixed matrix membranes using CMS and ox-CMS in different loadings.	98

Figure 4.27: CO ₂ and CH ₄ permeabilities of mixed matrix membranes with different CMS loading in various feed pressures.	100
Figure 4.28: CO ₂ /CH ₄ ideal selectivities of mixed matrix membranes with different CMS loading in various feed pressures.	101
Figure 4.29: CO ₂ /CH ₄ ideal selectivity vs CO ₂ permeability for mixed matrix membranes using CMS in various feed pressures.	103
Figure 4.30: CO ₂ and CH ₄ permeabilities of mixed matrix membranes using CMS with annealing treatment in various feed pressures.	104
Figure 4.31: CO ₂ /CH ₄ ideal selectivities of mixed matrix membranes using CMS with annealing treatment in various feed pressures.	105
Figure 4.32: CO ₂ /CH ₄ ideal selectivity vs CO ₂ permeability for mixed matrix membranes using CMS with annealing treatment in various feed pressures.	106
Figure 4.33: CO ₂ and CH ₄ permeabilities of mixed matrix membranes using oxidized-CMS in various feed pressures.	107
Figure 4.34: CO ₂ /CH ₄ ideal selectivities of mixed matrix membranes using oxidized-CMS in various feed pressures.	108
Figure 4.35: CO ₂ /CH ₄ selectivity vs CO ₂ permeability for mixed matrix membranes using oxidized-CMS in various feed pressures.	109

LIST OF TABLE

Table 1.1:	Fossil fuel emission levels in pounds per billion BTU of energy input. Adapted from [4].	2
Table 1.2:	Malaysia's natural gas energy data. Adapted from [9].	4
Table 1.3:	Composition of natural gas reservoirs in volume %. Adapted from [1].	5
Table 1.4:	Pipeline natural gas specifications. Adapted from [12].	5
Table 1.5:	Status of membrane gas separation process. Adapted from [10].	14
Table 2.1:	Comparison of rubbery and glassy polymer for zeolite-based mixed matrix membranes.	22
Table 2.2:	Selected studies in the mixed matrix membranes fabrication.	27
Table 2.3:	Units of permeability and permeance coefficient.	33
Table 2.4:	Molecular dimensions of gas penetrants.	42
Table 3.1:	Chemical and physical properties of PSU.	44
Table 3.2:	Chemical and physical properties of typical organic solvents for PSU.	45
Table 3.3:	Carbon molecular sieve characteristics.	46
Table 3.5:	Mixed matrix membranes composition.	49
Table 4.1:	Effect of polymer concentration to the mechanical properties of the membrane films.	69
Table 4.2:	Tan δ curve properties of mixed matrix membranes with different CMS loadings.	76
Table 4.3:	Effect of CMS loading to the mechanical properties of mixed matrix membranes.	80
Table 4.4:	Tan δ curve properties of mixed matrix membranes with annealing treatment.	85
Table 4.5:	Effect of annealing treatment to the mechanical properties of mixed matrix membranes.	87

Table 4.6:	Tan δ curve properties of mixed matrix membranes with different loadings of oxidized-CMS.	99
Table A.1:	Acid-base titration data of oxidized-carbon molecular sieves.	125
Table A.2:	Total acidic capacity of oxidized-carbon molecular sieves.	126
Table B.1:	Gas permeation results of polysulfone membranes.	130
Table B.2:	Gas permeation results of mixed matrix membranes contain 10 wt.% CMS.	131
Table B.3:	Gas permeation results of mixed matrix membranes contain 20 wt.% CMS.	132
Table B.4:	Gas permeation results of mixed matrix membranes contain 30 wt.% CMS.	133
Table B.5:	Gas permeation results of mixed matrix membranes contain 10 wt.% CMS with annealing treatment.	134
Table B.6:	Gas permeation results of mixed matrix membranes contain 20 wt.% CMS with annealing treatment.	135
Table B.7:	Gas permeation results of mixed matrix membranes contain 30 wt.% CMS with annealing treatment.	136
Table B.8:	Gas permeation results of mixed matrix membranes contain 10 wt.% oxidized-CMS.	137
Table B.9:	Gas permeation results of mixed matrix membranes contain 20 wt.% oxidized-CMS.	138
Table B.10:	Gas permeation results of mixed matrix membranes contain 30 wt.% oxidized-CMS.	139

ABBREVIATIONS

ABS	Acrylonitrile-butadiene-styrene
AC	Activated Carbons
APTS	(γ -aminopropyl)triethoxysilane
APDEMS	(3-aminopropyl)-diethoxymethyl silane
CA	Cellulose acetate
CMS	Carbon Molecular Sieves
CNT	Carbon nanotubes
DCM	Dichloromethane
DEA	Diethanolamine
DMA	Dynamic Mechanical Analysis
DMAc	N,N-dimethylacetamide
DMF	N,N-dimethylformamide
EPDM	Ethylene-propylene rubber
FESEM	Field Emission Scanning Electron Microscope
FTIR	Fourier Transform Infrared Spectroscopy
LNG	Liquid Natural Gas
MEA	Monoethanolamine
MWCNT	Multi-walled Carbon Nanotubes
NBR	Nitrile butadiene rubber
NMP	1-methyl-2-pyrrolidone
ODA	Octadecylamine
Ox-CMS	Oxidized Carbon Molecular Sieves
PA	Polyamide
PCP	Polychloroprene
PDMS	Polydimethylsiloxane
PES	Polyethersulfone
PI	Polyimide

PP	Polypropylene
PSA	Pressure Swing Adsorption
PSU	Polysulfone
PTFE	Polytetrafluoroethylene
PVP	Poly(vinyl pyrrolidone)
SEM	Scanning Electron Microscope
SWCNT	Single-walled Carbon Nanotubes
TAC	Total Acidic Content
TAP	2,4,6-triaminopyrimidine
THF	Tetrahydrofuran
TSA	Temperature Swing Adsorption
XRD	X-Ray Diffraction

NOMENCLATURES

A	Area of membrane	m^2
A_0	Initial cross-sectional film area	m^2
b	Langmuir affinity constant	-
b.p.	Boiling point	$^{\circ}\text{C}$
C_D	Concentration of dissolved gas in Henry's law environments	kg/m^3
C_H	Concentration of dissolved gas in Langmuir environments	kg/m^3
C'_H	Hole saturation constant	$\text{m}^3(\text{STP})/\text{m}^3$
D	Diffusion coefficient	m^2/s
d	Interparticle distance	-
d_{cr}	Critical interparticle distance	-
D_D	Diffusion coefficients of gas in Henry's law environments	m^2/s
D_H	Diffusion coefficients of gas in Langmuir environments	m^2/s
D_0	Pre-exponential term	-
dC_A/dx	Concentration gradient across the membrane	-
E	Young's modulus	MPa
E_D	Activation energy of diffusion jump	J/mole
E^*	Complex modulus	MPa
E'	Storage modulus	MPa
E''	Loss modulus	MPa
J	Flux	m/s
K_D	Henry's law constant	$\text{m}^3(\text{STP})/\text{m}^3 \cdot \text{atm}$
L_0	Initial film length	m
ℓ	Thickness of membrane film	μm

MW	Molecular weight	g/mole
N	Avogadro's number	l/mole
n	Integer number	-
P	Load	N
P	Permeability coefficient	Barrer
p	Partial pressure	bar
Δp	Pressure difference across the membrane	bar
P_c	Permeability of polymer phase	Barrer
P_d	Permeability of dispersed particles	Barrer
P/ℓ	Permeance	GPU
Q	Volumetric flowrate	cm ³ /s
R	Universal gas constant	J/mole.K
r	Pore radius of membrane	m
r_A	Spherical radius of the diffusing particle A	m
S	Solubility coefficient	m ³ /m ³ .Pa
T	Absolute temperature	K
T_g	Glass transition temperature	°C
u	Displacement	-
v.p	Vapour pressure	kPa
$\alpha_{A/B}$	Ideal selectivity of component A over component B	-
γ	Strain (from dynamic mechanical analysis)	%
δ	Solubility parameter	J ^{1/2} /cm ^{3/2}
δ'	Deflection	-
ε	Strain (from tensile test)	mm/mm
η	Viscosity	Pa.s
θ	Incident angle	-
λ	Wavelength	cm ⁻¹
ρ	Density	kg/m ³
σ	Stress	MPa
ϕ	Volume fraction of dispersed particles in mixed matrix membrane	-

CHAPTER 1

INTRODUCTION

With the increasing attention from the world to seek more environmental friendly fuel sources, natural gas has emerged as important energy resources for the future. Sour natural gas needed to be purified by removing impurities present such as carbon dioxide (CO₂) and hydrogen sulphide (H₂S). This is critical to increase its energy values and also reducing the operation issues due to corrosion and pipeline blockage. Various technologies have been employed for natural gas purification including absorption, adsorption, cryogenic, and membrane process. The detailed descriptions on those technologies are discussed in Section 1.2. More elaborative discussion is given to membrane process since the present study concentrated on the development of mixed matrix membranes for gas separations.

1.1 Natural Gas

Natural gas is being considered as a valuable alternative energy resources to replace oil. Even though oil dominates the world's energy supply, the usage of natural gas is rapidly increasing [1]. In the world's energy consumption, natural gas is ranked as the third most consumed energy (23.8%), while oil (35.6%) and coal (28.6%) occupy the first and second, respectively [2]. Rapid growth in natural gas demand is attributed to the advantages of natural gas over other fossil fuels in promoting clean air, abundant reserves and rapidly expanding infrastructure. While burning, natural gas produces less CO₂, carbon monoxide (CO), nitrogen oxides (NO_x), and sulphur dioxide (SO₂) as compared to oil and coal [3]. Typical amount of compounds emitted during the combustion of natural gas, oil, and coal are compared in Table 1.1.

Table 1.1: Fossil fuel emission levels in pounds per billion BTU of energy input. Adapted from [4].

Compound	Natural Gas	Oil	Coal
CO ₂	117,000	164,000	208,000
CO	40	33	208
NO _x	92	448	457
SO ₂	1	1,122	2,591
Particulates	7	84	2,744
Formaldehyde (CH ₂ O)	0.750	0.220	0.221
Mercury (Hg)	0	0.007	0.016

As a non-renewable fossil fuel, natural gas is formed due to a decaying process of living matter over millions of years. It is believed that when enormous number of microscopic marine organisms died, they piled up on the seabed as a thick sludge and gradually buried deeper by layers of sediment that turns into rocks. By the action of bacteria the remains were decomposed into organic mixture. Over the years, layers of the sedimentary rocks became thousands of meters thick, creates pressure and the heat that transformed organic mixture into oil and natural gas. Specific conditions, such as low oxygen level, are necessary for this process to occur. Natural gas was then either trapped in porous rock layers or in underground reservoirs where the oil is formed [5].

It was only during 1950s the story of natural gas began to raise worldwide interest. For decades natural gas was seen as a form of energy that was difficult to exploit, particularly due to the amount of investment and transport cost to the end user [1]. The invention of the modern seamless pipe allowed gas to transport in high pressure and large quantities. Since then, natural gas transportation become profitable and its demand continue to grow until today.

As one of the world's primary energy source, natural gas worldwide consumption has been projected to increase by an average of 1.6% annually from 2006 to 2030 [6]. It is projected by the year of 2030 natural gas consumption will reach 4,284 billion cubic meters, which is 40% higher than the amount of natural gas consumed in 2008

worldwide. Natural gas is used across all sectors in varying amounts. The proportion of natural gas uses per sector is given in Figure 1.1. Natural gas is mostly used as a heat source, feedstock in petrochemical plants, and as a fuel for power generation plants. Recently, natural gas is used as transportation fuel. Due to the wide application of natural gas, there is a need to increase the production of natural gas to meet its market demand.

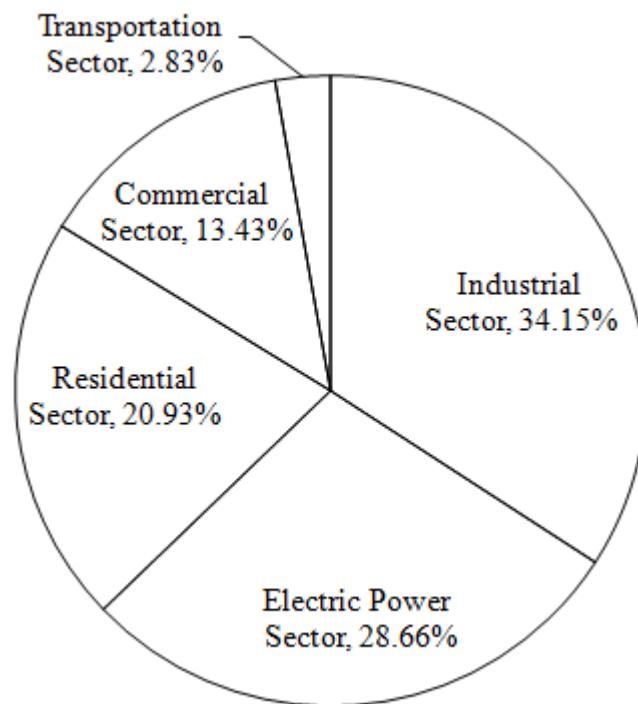


Figure 1.1: Natural gas use by sector. Adapted from [7].

Malaysia, as one of the natural gas producers rendering 62.5 billion cubic meters to the total 3065.6 billion cubic meters of world's natural gas production in 2008 [8]. At the end of 2008, Malaysia's natural gas reserves stood at the 16th place in the world with 2,390 billion cubic meters with a reserves-to-production ratio as high as 38.2. During March 2008, Malaysia had 27 gas fields, and about 50% of them are solely operated by PETRONAS. The profile of Malaysia's natural gas data series for the past ten years is shown in Table 1.2.

Table 1.2: Malaysia’s natural gas energy data. Adapted from [9].

Activity	Year									
	1999	2000	2001	2002	2003	2004	2005	2006	2007	2008
Production (bcf)	1422	1600	1687	1706	1836	1900	1967	1973	1962	2024
Consumption (bcf)	653	820	896	983	968	879	914	940	856	928
Exports (bcf)	769	780	719	723	868	1021	1053	1033	1105	1096
Proved reserves (tcf)	81.7	81.7	81.7	75	75	75	75	75	75	83

bcf: billion cubic feet; tcf: trillion cubic feet

During the production process, natural gas found in the reservoirs is not necessarily free from impurities. Although methane is always the major component, natural gas contains significant amounts of ethane (C₂H₆), propane (C₃H₈), butanes (C₄H₁₀), and other higher hydrocarbons. In addition, natural gas also contains undesirable impurities such as moisture, CO₂, N₂, and hydrogen sulphide (H₂S) [10]. The composition of natural gas may vary depends on the reservoir location. Examples of the composition of natural gas reservoirs are shown in Table 1.3. These undesirable materials must be reduced to a very low concentration to meet pipeline and commercial specifications. A typical pipeline natural gas specification is given in Table 1.4.

CO₂ is the most undesirable compound found in sour natural gas. The composition of CO₂ is typically in the range of 0.5 – 10% with a maximum of 70% in some operated reservoirs [1]. It is generally known that the presence of CO₂ in natural gas stream made it highly corrosive, particularly in combination with water, and could rapidly destroy pipelines and equipments. In LNG plant, solidification of CO₂ may cause pipeline blockage and impede the transportation system. CO₂ also reduces the heating value of the natural gas stream and eventually lower the selling price of the gas [11]. Therefore, the purification process has become an important step in natural gas processing.

Table 1.3: Composition of natural gas reservoirs in volume %. Adapted from [1].

Component	Reservoir				
	Groningen (Netherlands)	Lacq (France)	Uch (Pakistan)	Uthmaniyah (Saudi Arabia)	Ardjuna (Indonesia)
CH ₄	81.3	69.0	27.3	55.5	65.7
C ₂ H ₆	2.9	3.0	0.7	18.0	8.5
C ₃ H ₈	0.4	0.9	0.3	9.8	14.5
C ₄ H ₁₀	0.1	0.5	0.3	4.5	5.1
C ₅₊	0.1	0.5	-	1.6	0.8
N ₂	14.3	1.5	25.2	0.2	1.3
H ₂ S	-	15.3	-	1.5	-
CO ₂	0.9	9.3	46.2	8.9	4.1

Table 1.4: Pipeline natural gas specifications. Adapted from [12].

Component	Typical Analysis (mole %)	Range (mole %)
CH ₄	94.9	87.0 - 96.0
C ₂ H ₆	2.5	1.8 – 5.1
C ₃ H ₈	0.2	0.1 – 5.1
iso-Butane (C ₄ H ₁₀)	0.3	0.01 – 0.3
n-Butane (C ₄ H ₁₀)	0.03	0.01 – 0.3
iso-Pentane (C ₅ H ₁₂)	0.01	trace – 0.14
n-Pentane (C ₅ H ₁₂)	0.01	trace – 0.04
C ₆₊	0.01	trace – 0.06
N ₂	1.6	1.3 – 5.6
CO ₂	0.7	0.1 – 1.0
O ₂	0.02	0.01 – 0.1
H ₂	trace	trace – 0.02
Sulphur	-	< 5.5 mg/m ³
Water	16 - 32 mg/m ³	< 80 mg/m ³

1.2 Gas Separation Technologies

A wide variety of technologies are currently being used for the removal of CO₂ from natural gas. They include absorption process, adsorption process, cryogenic condensation, and permeation through membrane. Apart from membrane application, other separation processes are based on the principle of a phase change, where the component desired is selectively transferred from gas phase to liquid or solid phase [1]. The membrane separation process involves the difference in transport rates of the components to be separated across the membrane.

1.2.1 Absorption Process

Absorption process is the most common technique used in natural gas processing. The gas to be processed is contacted counter currently with the selective solvent in a plate or packed column. Based on the interaction of the solvent and the absorbed gas component, absorption process could be classified into physical and chemical absorption. Physical absorption occurs when the desired gas component is more soluble in the solvent among other components in the gas phase. Wherein chemical absorption, the gas component chemically react with the solvent or a component within the solvent. Once the solvent reach its saturation level, it requires regeneration, which for physical solvent is achieved by a reduction of pressure and for chemical solvent, by the action of thermal driving force or by chemical means [13]. Currently, amine based solvents are widely used for natural gas purification. The amine absorption process has the capability to purify the natural gas having acid gases from 5-15% down to pipeline quality in a single process. Common amine based solvents used for the absorption process are monoethanolamine (MEA) and diethanolamine (DEA). Absorption process is usually applied for CO₂, H₂S, and SO₂ removal.

Although absorption offer a simple process, on the other hand it is also has some disadvantages. The stoichiometric reaction between the absorbed component and the solvent used become the limitation when chemical absorption is employed [14]. Corrosive characteristic of amine based solvents made it necessary to add anti-corrosion agent frequently to the system. Anti foaming agent is injected to reduce the

surface tension of the solvent and to ensure better contact between the solvent and CO₂. Since the used of solvent may harm the environment, therefore before being discharged a post-treatment should be subjected to solvent [15].

1.2.2 Adsorption Process

Adsorption process uses a solid surface to remove one component in an analogous way to the solvent in absorption. Adsorption process is applied when a high purity is required in the process [1]. The adsorbent is characterized by its microporous structure, which afford a very large specific surface area. Typical adsorbents used include zeolites, activated carbons, molecular sieves, silica gel, alumina, etc.

Adsorbents are usually not suitable for continuous process, owing to mechanical problems and also due to the risk of attrition. Therefore, it is normally used in fixed beds with periodic sequencing. In the simplest case, one bed operates in adsorption, while the second operates in desorption, and both are switching periodically [1]. Based on the regeneration method, adsorption process could be differentiated as temperature swing adsorption (TSA) and pressure swing adsorption (PSA). Desorption process could be carried out by raising the temperature in TSA system or lowering the pressure in PSA system. TSA is generally chosen for purification process, while PSA is suitable for bulk separation [16].

The selection of TSA and PSA for a particular separation is based on the technical and economical consideration. Compared to PSA application, TSA system requires more time to heat, desorbs, and cool the bed [16]. Due to the time limitation, TSA is more suitable for the removal of impurities from feed in a small concentration. TSA is used in natural gas sweetening and gas drying process. On the contrary, PSA system offers a faster time cycle. Short cycle of PSA makes it more attractive for bulk separation where impurities are present in higher concentration. However, PSA has some disadvantages, its high pressure leads to high operational cost. PSA is used in the recovery of CO, CO₂, H₂, CH₄, N₂, O₂, and other gases. Both PSA and TSA are able to produce low CO₂ concentration stream down to pipeline quality.

1.2.3 Cryogenic Process

Cryogenic separation uses a very low temperature to separate gas mixtures. Liquid and vapour phases are produced and separation is achieved by distillation or analogous process [13]. The main principle of cryogenic separation lies on the boiling temperature difference of each gas. Cryogenic distillation involves a sequence of vaporizations and condensations, where the high boiling species concentrated in liquid phase flowing down in the column and the low boiling constituents concentrated in vapour phase flowing up in the column. The low-temperature in cryogenic separation is achieved through compression followed by cooling, followed by refrigeration and Joule-Thompson expansion. Product from cryogenic separation may be a cryogenic liquid or a gas. Cryogenic is used in the separation of atmospheric gases, CH₄ from N₂, and in H₂ separation, etc. This method is worth considering when there is a high CO₂ present in the stream [17]. The advantage of this method is that it produces a liquid CO₂ ready for transportation by pipeline, and since there is no additional chemical required in cryogenic separation, no further separation is required. The main disadvantages of cryogenic separation is the high energy consumption for the refrigerant compressor, therefore this process is not cost effective for commercial applications [18].

1.2.4 Membrane Process

A membrane is defined as a selective barrier between two fluid phases, considered as feed phase (upstream) and permeate phase (downstream), which allow a preferential flow of the desired components under the influence of driving forces. Membranes can be made from a large number different material, ranging from organic to inorganic materials, depending on the nature of their application. The application of membrane technology in gas separation can be considered as a recent development, but the study of gas transport in membranes has been actively pursued for over 100 years [13]. Polymeric membranes are typically employed in gas separation process. Compared to earlier separation methods, membrane offers many attractive opportunities such as low capital and operational costs, reduced energy consumption, enhanced weight and space efficiency, operational simplicity, separation under low pressure and

temperature, easy to combine with other separation process, and other chemicals are not required [19-22]. Brief explanation of transport mechanisms of gas through membranes, commercial applications of gas membrane separations, and the challenges faced by membranes in gas separation are described in the following Sections.

1.2.4.1 Polymeric Membranes

Polymeric membranes perform their separation through a variety of mechanism based on the membrane properties (physical and chemical structure), the nature of the gas (size, shape, and polarity), and the interaction between membrane and components [23]. Both dense and porous membranes can be utilized in gas separation process. Gas molecules are transported across the membranes through several types of mechanism depending on the properties of both the gas and the membrane. Figure 1.2 illustrates the mechanisms of gas permeation in porous (with different pore size) as well as dense nonporous membranes.

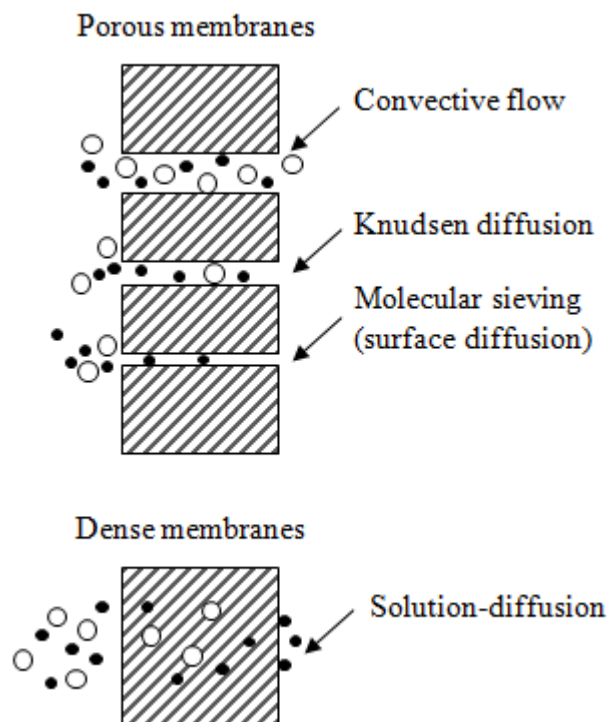


Figure 1.2: Schematic mechanism for permeation of gases through porous and dense membranes.

When a membrane having relatively large pore size, in the range between 0.1-10 μm , gas molecules will collide exclusively with each other and pass through the membrane by convective flow. There will be no separation and the flow is proportional to r^4 (where r is pore radius). This type of membrane is suitable for microfiltration applications. If the pores are smaller than 0.1 μm , the pore size is the same as or smaller than the mean free path of the gas molecules. Transport through such pores will take place via Knudsen flow, where the ideal separation factor for binary gas mixtures can be estimated from the square root of the ratio of the molecular weights. If the membrane has extremely small pores, in the range of 5-20 \AA , then gases are separated via molecular sieving. In molecular sieving mechanism, the membrane pore size should be between those of the gas molecules to be separated. Transport through this kind of membrane includes both diffusion in the gas phase and diffusion of adsorbed component on the pore surface (surface diffusion). This kind of membranes are not preferred for large scale applications [10]. While in dense membranes the gas is being transported via solution-diffusion mechanism. In solution-diffusion mechanism, the gas molecules are adsorbed onto the surface of membrane in the feed side, diffuses across the membrane, and finally desorbed in the permeate phase of the membrane. The mechanism is described more detail in Section 2.2.

Dense polymeric membranes are generally employed in gas separation process. Since gas separation through membranes is a pressure driven process, it is considered ideal as separating media in natural gas purification process due to the high pressure of the gas feed stream [24]. When natural gas stream passes through the membrane film, the fast-permeating gases (CO_2 , O_2 , H_2 , H_2S) will be transported to the permeate phase, while the slow-permeating gases (N_2 , CH_4 , and heavier hydrocarbons) are held up in the feed phase.

Polymeric membranes have typically been used for gas separation because of their robustness and capability to withstand mechanical abuse. Based on the chemical composition and structural flexibility of the polymer chains, dense polymers membranes can distinguish between different gas species in a mixture. The utility of polymeric membranes lies in their relative ease in processing, formation, and

manufacturing cost when compared to inorganic membranes [25]. In spite of their advantages, tailoring the structure of polymeric membrane had seemingly reached a limit in the trade-off between productivity and selectivity as shown by Robeson [20, 26] in the upper bound limit on Figure 1.3. Even though considerable efforts in developing new polymer structure to enhance its separation properties have been done in the past two decades, further progress in exceeding the upper-bound limit seem to have not much significance [27, 28].

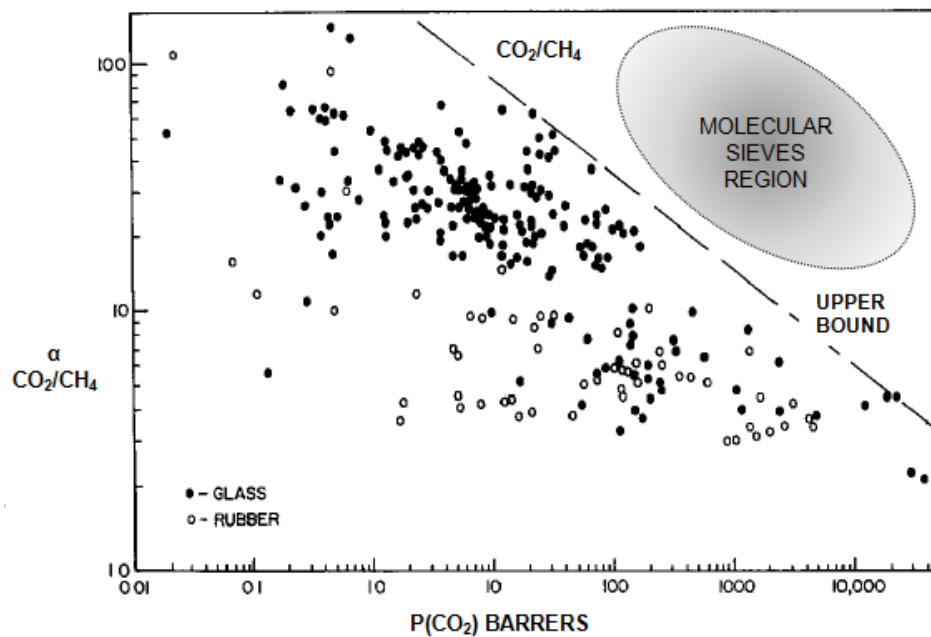


Figure 1.3: Trade-off plot between membrane CO_2/CH_4 selectivity and CO_2 permeability for polymeric membranes. Adapted from [26].

1.2.4.2 Inorganic Membranes

Similar to polymeric membranes, inorganic membranes can be formed in dense and porous structures. Porous inorganic membranes include oxides (alumina, titania, zirconia), carbon, glass (silica), metal, and zeolite based membranes. These membranes vary greatly in pore size, support material, and configuration. These membranes usually have higher permeability compared to polymeric membranes. On the other hand, dense inorganic membranes include metal (palladium, silver, and their alloys), solid electrolytes (zirconia), and nickel based membranes are very specific in

their separation behaviours. Low permeability of dense inorganic membranes have limited their industrial application [29].

During the last few years, ceramic and zeolite based membranes have begun to be used for a few commercial separations. Both Mitsui and Sulzer have commercialized these membranes for dehydration of alcohols by pervaporation. Extraordinarily high selectivities and high fluxes have been reported for these membranes. However, the membranes are not easy to made and consequently are prohibitively expensive for many applications [10]. It is estimated that a zeolite membrane module would cost around US\$ 3000/m² of active area, compared to US\$ 20/m² for the existing gas separation hollow-fiber membrane modules [30]. Therefore, industrial applications of inorganic membrane is still hindered due to their extremely high cost of production, lack of technology to develop continuous and defect-free membranes, and handling issues due to their inherent brittleness [20, 27, 31].

1.2.4.3 Mixed Matrix Membranes

In an effort to increase its permeability-selectivity limitation of polymeric membranes, selective molecular sieves are incorporated in the polymer matrix forming a mixed matrix membrane, as illustrated in Figure 1.4. Mixed matrix membranes have the potential to achieve higher permeability and selectivity due to the superior permeability and selectivity govern by molecular sieves particles, and at the same time hindered the costly process and fragility of inorganic membranes by using cost-effective and flexible polymer as the continuous matrix [20, 27]. The successful key for implementation lies on both, the selection of polymer matrix and molecular sieve, and the elimination of interfacial defects [27, 28, 32]. The transport of gases within mixed matrix membranes are described by Maxwell equation, later discussed more detail in Section 2.2.1.1. The incorporation of molecular sieves has been done not only to improve its separation performance, but its mechanical properties and thermal properties as well [33-35].

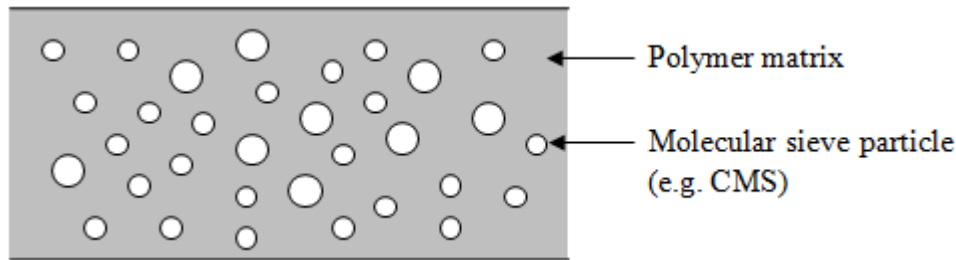


Figure 1.4: Schematic diagram of a mixed matrix membrane.

1.2.4.4 Membrane Applications for Gas Separation

The investigations on gas separation using membranes were started during 1829, when Thomas Graham performed the first experiment on the transport of gases and vapors in polymeric membranes, but it is only since 1970 gas separation membranes became economically competitive in industry [10, 36]. During mid-80s, Cyanara, Separex, and Grace Membrane System produced membranes to remove carbon dioxide from methane in natural gas [10]. This application, although hindered by low price of natural gas in 1990s, has grown significantly over the years. The interest in this area resulted in making gas separation membranes as major industrial application for the recent 20 years. More than 90% of this business involves the separation of noncondensable gases: nitrogen from air; carbon dioxide from methane; and hydrogen from nitrogen, argon, or methane. The market for gas separation membranes is estimated to reach US\$ 350 million in 2010 and rapidly grow to US\$ 760 million in 2020 [25, 37]. The current status of gas membrane processes are summarized in Table 1.5.

Table 1.5: Status of membrane gas separation process. Adapted from [10].

Process	Application	Comments
Established processes		
O ₂ /N ₂	N ₂ production from air	Processes are well developed. Only incremental improvements in performance expected.
H ₂ /N ₂ ; H ₂ /CH ₄ ;	ammonia purge gas streams; H ₂ recovery	
H ₂ O/Air	Dehydration of air	
Developing processes		
VOC/Air	Air pollution control applications	Several applications being developed. Significant growth expected as the process becomes accepted.
CH ₃₊ /N ₂ ; CH ₃₊ /H ₂	Reactor purge gas, petrochemical process streams, refinery waste gas	Application is expanding rapidly.
CO ₂ /CH ₄	CO ₂ removal from natural gas	Many plants installed but better membranes are required to change market economics significantly.
To-be-developed processes		
C ₃₊ /CH ₄	NGL recovery from natural gas	Field trials and demonstration system tests under way. Potential market is large.
H ₂ S/CH ₄ H ₂ O/CH ₄	Natural gas treatment	Niche applications, difficult for membranes to compete with existing technology.
O ₂ /N ₂	O ₂ enriched air	Requires better membranes to become commercial.
Organic vapour mixtures	Separation of organic mixtures in refineries and petrochemical plants	Requires better membranes and modules. Potential size of application is large

From Table 1.5, it can be seen that the application of membrane separation processes particularly for CO₂ removal from natural gas is still under development. Low stability for long-term usage and high sensitivity to the presence of impurities other than CO₂ and/or H₂S in natural gas become major problems when membrane is used for this application. One-stage membrane units are preferable due to their low capital and operating costs, however, the high methane loss from a one-stage system made it is prohibitive to use. Two-stage and even three-stage of membrane units are commonly used to reduce the methane loss, which will increase the operating cost. In general, current membrane technology to remove high concentration of CO₂ (> 10%) is still too expensive and compete head-to-head with amine plants [10]. Therefore, further improvements are required to increase the performance of membranes for the separation of CO₂ from natural gas.

1.3 Problem Statement

In gas separation, the trade-off limitations of organic membranes and the economical considerations of inorganic membranes have opened wide range of research areas for searching better performance of membrane. Mixed matrix membranes offer a better alternative to improve the properties of polymeric and inorganic membranes, performances and economic wise. However, their performance still suffers from defects caused by poor contact between polymer and molecular sieves surface [38-42]. Voids appear at the interfacial region may allow the gases to bypass through the voids, resulting in high permeability of gas with no selectivity enhancement. When glassy polymers are used as the continuous phase, the adhesion between inorganic filler and polymer appear to be the major problem.

Most of researches in mixed matrix membranes were devoted to use polyimides (PI) as the continuous phase. PI was chosen due to its superior performance for gas separation application, excellent mechanical properties, and high temperature and chemical resistance [43]. However, PI are seriously affected by highly soluble penetrants such as CO₂, with plastization pressure varying between 10-20 bar [44],

and the rigid structure of PI somewhat causing the difficulties to form a good adhesion with the sieves particles. In view of this situation, less rigid glassy polymers, such as polysulfone (PSU), has promising potential to be used as an alternative polymer matrix to form a good adhesion with molecular sieves particles. PSU is valued as a high performance engineering thermoplastic polymer with resistance to degradation, good gas permeability and selectivity values, low cost and high critical pressure of plasticization (exceed 55 bar), and most importantly the degree of its chain rigidity is less than PI [44]. Therefore, in this study PSU was preferred as the continuous matrix.

With respect to the types of fillers, zeolites are predominantly used as the molecular sieve particles, the homogeneous pore size become one of the most interesting factor. However, most researchers found that the poor polymer-filler adhesion becomes the real challenge in developing successful film formation. Several attempts to enhance the polymer-filler adhesion by introducing mutual interactive functional groups on the polymer and the molecular sieves have lead to partial blockage of the sieve pores, thus hindering the separation performance [35]. In view of this situation, carbon molecular sieves (CMS) is selected for this study as a potential alternative molecular sieve material. CMS particles appear to have good affinity to glassy polymers with minimal preparation and casting modifications [20].

In this work, the adhesion of polymer-filler was enhanced via several strategies. To achieve a good polymer-filler adhesion, annealing treatment and introduction of mutual interaction functional groups were employed as a strategic way to enhance the compatibility of the two phases.

1.4 Research Objectives

Facing the current challenges of forming a high performance mixed matrix membrane with simple fabrication process, this study was carried out with the following objectives:

1. To develop mixed matrix membranes using the combination of polysulfone and carbon molecular sieves.
2. To characterize the physical and chemical properties of the developed mixed matrix membranes.
3. To evaluate the performance of the newly developed membranes in term of permeability and ideal selectivity for CO₂ and CH₄ against the feed pressures.

1.5 Scope of Study

This study is focused on the fabrication, characterization, and evaluation of mixed matrix membranes comprised of PSU and CMS. Detail of the study is described in the following:

1. Fabrication of polysulfone-carbon molecular sieves mixed matrix membranes

The research aims to explore the fabrication process of dense mixed matrix membranes using PSU-CMS system with dichloromethane (DCM) maintain as the solvent. Mixed matrix membranes were fabricated by using several filler loadings (10, 20, and 30 wt.%). Several attempts to achieve good polymer-filler adhesion were done by annealing treatment and introducing mutual interaction functional groups onto the sieves surface by oxidation treatment.

2. Characterization of polysulfone-carbon molecular sieves mixed matrix membranes and carbon molecular sieves particles

The resulting membranes were characterized in term of its morphology and physical properties. Membrane morphologies were carried out by using field emission scanning electron microscope (FESEM). The thermal and the dynamic mechanical properties were characterized by using dynamic mechanical analysis (DMA). Meanwhile, the physical and chemical properties of the inorganic filler used were characterized by using X-Ray diffraction

(XRD), particle size analyzer, gas pycnometer, Fourier transform infrared spectroscopy (FTIR), and simple acid-base titration.

3. Evaluation of polysulfone-carbon molecular sieves mixed matrix membranes

The capability and the performance of the present developed mixed matrix membranes were evaluated in term of CO₂ and CH₄ permeability against operating pressures of 2, 4, 6, 8, and 10 bars. The ideal selectivity was then calculated by dividing the permeability of CO₂ over CH₄.

1.6 Thesis Overview

Following this introductory chapter, this thesis is organized into 5 chapters. Chapter 2 presents the background and theory of gas transport in membranes and molecular sieves materials, along with a detailed literature review of mixed matrix membranes. Chapter 3 describes the details of materials used and the experimental work carried out in this study on the fabrication of dense homogeneous membranes and mixed matrix membranes. The details of the procedures adopted for the surface modification of carbon molecular sieves is also described. The experimental apparatus and the techniques used to characterize the properties of the membranes and evaluation of the membrane performance are described as well. The experimental results obtained in this study along with the detailed discussions are presented in Chapter 4, whereas Chapter 5 gives the summary and concluding remarks along with the recommendations for future study.

CHAPTER 2

BACKGROUND AND THEORY

As discussed earlier in Chapter 1, due to the market demand for efficient membrane separation technology, it is desirable to have a more durable membrane having greater permeability and selectivity compared to the existing membranes. An ideal membrane material should have three principal characteristics [45]: (i) sufficient mechanical strength to resist the trans-membrane pressures in the process, (ii) high product flow rate and maintain the flow rate for a long time, and (iii) high selectivity for the desired components.

A potential alternative way to improve the separation properties of membranes is achieved by incorporating molecular sieves particles such as zeolites and carbon molecular sieves homogeneously into a polymeric matrix, to form a mixed matrix membrane [20, 27, 46]. This approach combines the advantages of each material, high separation properties of molecular sieves materials, and the desirable mechanical and economical capabilities of polymers. Many researchers devoted their work to evaluate the performance and the material characteristic of mixed matrix membranes. In this Chapter, the development and the problems faced during mixed matrix membranes fabrication specifically in gas separations are discussed. The transport mechanisms of gas through polymeric and molecular sieves material are also highlighted.

2.1 Review of Mixed Matrix Membranes Development

Mixed matrix membranes could be comprised of wide range of rubbery or glassy polymers as continuous phase, pairs with various inorganic molecular sieves i.e. silicate, zeolites, activated carbon (AC), carbon molecular sieves (CMS), single-

walled and multi-walled carbon nanotubes (SWCNT and MWCNT) as dispersed phase. Polymers can be varying in their glass transition temperature (T_g) and polarity. Where molecular sieves particles could be varying in their pore size, pore structure, and surface polarity. Major concerns to fabricate a successful mixed matrix membrane are the selection of polymeric matrix and dispersed molecular sieves pair, and the elimination of interfacial defects between these two phases [27, 28]. The effect of polymer and molecular sieves selection to the membrane performance and various strategies to enhance polymer-filler adhesion are discussed in the following Sections.

2.1.1 Selection of Polymer and Molecular Sieves Pair

Research in the area of mixed matrix membranes for gas separations were started in early 1970s when Paul and Kemp [47] discovered a delayed diffusional time lag for CO₂ and CH₄, when zeolite 5A was incorporated in polydimethylsiloxane (PDMS) matrix. They observed that the addition of zeolite 5A creates an immobilizing adsorption of CO₂ and CH₄ which significantly increased the diffusion time lag but only had minor effects on the steady-state permeation. The same polymer were then used by Jia et al. [48] which found that the incorporation of silicate (70 wt.%) in PDMS matrix was able to slightly increase the selectivity of O₂/N₂ from 2.14 to 2.92 and the selectivity of CO₂/CH₄ from 3.42 to 8.86. It was suggested that silicate particle play a role as a sieves which permitting the smaller molecules to pass through the membrane faster than the larger molecules.

The effect of types of filler particles were examined by Duval et al. [38], which evaluated the effect of both zeolites (silicate-1, 13X, KY, 5A) and carbon molecular sieves (W20, Cecalite, Carbosieve) in poorly selective rubbery polymers of PDMS, ethylene-propylene rubber (EPDM), polychloroprene (PCP), nitrile butadiene rubber (NBR 45 and NBR 50). It was observed that in high loading of zeolites, nonselective voids appear. The optimum result reported was from nitrile butadiene rubber (NBR 45) filled by 46 vol.% of zeolite KY with CO₂ permeability of 14 Barrers and CO₂/CH₄ selectivity of 35. With carbon based filler, Duval et al. [38] founded that by incorporating 50 wt.% of Carbosieve in EPDM the permeability of CO₂ increased from 81 to 120 Barrer, and the CO₂/CH₄ selectivity increased from 4.3 to 8. From

Table 2.2 it can be seen that the performance of mixed matrix membranes derived from rubbery polymer are comparable to the pure glassy polymer membranes such as cellulose acetate (CA), Matrimid[®], polyethersulfone (PES), and polysulfone (PSU).

Continuous work in mixed matrix membrane were mostly done by employing glassy polymers as the continuous phase, since the intrinsic separation properties of rubbery polymer lying far below the upper-bound limit for polymeric membranes, mixed matrix membranes with rubbery polymer matrix did not give any significant enhancement compared to the pure glassy polymer membranes. Therefore, researchers shifted their interest to use the starting material such as CA, PSU, polyimide (PI), polyamide (PA), PES, etc. which has high separation performance, lying much closer to the upper-bound limit.

In 1988, Kulprathipanja et al. [49] investigated the possibility of incorporation of silicate in CA matrix. They observed that the incorporation of silicate (up to 25 wt.%) slightly increased the selectivity of O₂/N₂ from 2.99 to 4.33 at 150 psig, and significantly increased the selectivity of CO₂/H₂ from 0.7 to 9.6 at 50 psig. Suer et al. [50] found a slight increment in gas separation properties of PES by incorporating zeolite 4A and 13X, the selectivity of CO₂/N₂ appear to increase slightly from 3.7 to 4.4.

On the other hand, Gür [41] was unsuccessful incorporate zeolite 13X in PSU matrix due to the unsatisfactory adhesion of glassy polymer and zeolite. Up to 20 vol.% zeolite loading, no significant effect was found on gas permeabilities. Same problem was observed by Mahajan et al. [51] during the preparation of mixed matrix membranes using zeolite 4A in Matrimid[®] matrix. Transport results for O₂/N₂ separation, was reported to give the same selectivity O₂/N₂ value (7.2) with the Matrimid[®] intrinsic selectivity with higher permeability of O₂, increasing from 1.32 to 4 Barrers. Poor adhesion between zeolite and glassy polymer also found by Vankelecom et al. [40] when incorporated zeolites (silicate, borosilicate, zeolite Y) in polyimides (PI 2540, PI 2560, PI 2611, PMDA-ODA, and Kapton[®]). They found poor polymer-filler adhesion to be the main difference between the previous membranes prepared using PDMS due to the high chain rigidity of PI [52].

These results suggest that poor contact exists between the two phases, forming a “sieve-in-a-cage” phenomenon [40, 51]. In this case, the polymer intrinsic selectivity result in the mixed matrix membrane because of the gap between the sieve and the polymer provides a less resistive route to gas diffusion, and results in bypassing of the molecular sieve with higher permeability. The summary of the selection of polymer phase for zeolite-based molecular sieves is presented in Table 2.1 and Table 2.2.

Table 2.1: Comparison of rubbery and glassy polymer for zeolite-based mixed matrix membranes.

Continuous phase	Advantages	Disadvantages
Rubbery polymer	Provide good polymer-filler adhesion	No significant improvement
Glassy polymer	Provide better size-dependent separation characteristic	Show weak polymer-filler adhesion

Since many of the research using zeolite-based molecular sieves facing difficulties to have good polymer-filler adhesion with simple preparation steps, recently carbon-based molecular sieves are used in the mixed matrix membranes fabrication. Vu et al. [20] formed mixed matrix membranes by incorporating carbon molecular sieves (CMS) in two different polymer matrices, Matrimid[®] and Ultem[®]. Ultem[®]-CMS (35 wt.%) showed an enhancements of 40% in CO₂/CH₄ selectivity. Likewise, for Matrimid[®]-CMS mixed matrix films, enhancements by as much as 45% in CO₂/CH₄ selectivity (51.7) were observed with 36 wt.% of CMS loading. Similar enhancements were observed when these mixed matrix membrane films were examined for the O₂/N₂ separation. Vu et al. [20] identified several advantages of CMS over zeolites which exhibit better affinity to glassy polymer matrix, and the tailorable pore structure of self-pyrolyzed CMS makes the final membranes more adaptable for the desired gas separation. Significant improvement of membrane performance by carbon based molecular sieves also reported by Anson et al. [53] on the fabrication of activated carbon/acrylonitrile-butadiene-styrene (ABS) mixed matrix membranes. The resultant mixed matrix membranes showed a simultaneous increase of CO₂

permeabilities (40-600%) and CO₂/CH₄ selectivities (40-100%) over the intrinsic property of ABS membranes.

The most recent carbon-based molecular sieves used is carbon nanotubes (CNTs). Some of the attractive features of CNTs are their outstanding mechanical properties, their high strength-to-weight ratio, and their excellent thermal stability [54]. However, the long step of CNTs purification and the tendencies of agglomeration of CNTs in high loading make it necessary to do further modification in the mixed matrix membrane fabrication. Kim et al. [54] reported an increase in gas permeabilities in poly(imide siloxane) copolymer as CNTs added to the matrix. However, the selectivities of CO₂/CH₄ and O₂/N₂ of the final membranes showed a decreasing trend as CNTs added to the matrix. To depict the position of mixed matrix membranes performance in exceeding the upper bound limit of polymeric membranes, CO₂/CH₄ selectivity and CO₂ permeability of mixed matrix membranes comprised of zeolites and carbon-based molecular sieves summarized Table 2.2.

2.1.2 Elimination of Interfacial Defects

As described above, many researchers face the difficulties to obtain a good adhesion between molecular sieves, especially zeolites, and glassy polymers. From the literature survey, the compatibility of molecular sieves and polymer matrix could be enhanced by undergo three methods: (i) by using surface functionalized adsorbent, where mutual functional groups are attached to the surface of molecular sieve to promote similar characteristics with the polymer matrix, (ii) by priming technique, where a thin layer of polymer is introduced onto the sieve surface to promote compatibilization, (iii) by applying a heat treatment let the polymer chains to well-conform onto the sieves surface. The illustration of these strategies is depicted below, in Figure 2.1.

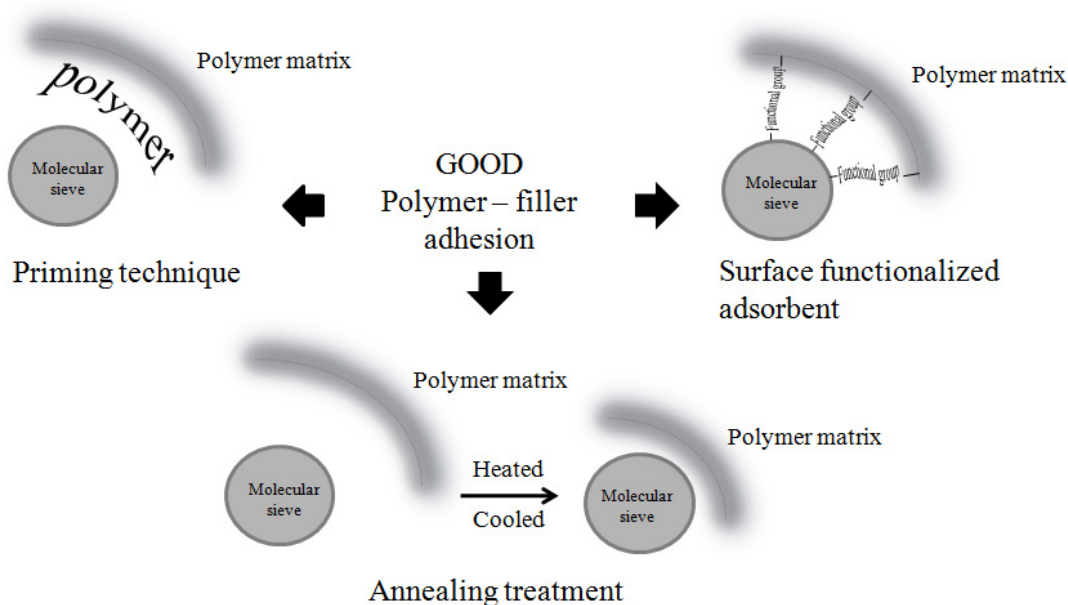


Figure 2.1: Strategies to improve the adhesion between molecular sieves particles and polymer matrix in mixed matrix membranes fabrication.

Common method to improve the performance of zeolite-glassy polymer membrane is by introducing mutual functional group on zeolite surface to enhance its compatibility with polymer matrix. Duval et al. [39] studied various silane coupling agents on silicate for a range of glassy polymers (PSU, Ultem[®], Udel[®], etc) in their subsequent work. Improved polymer-sieves adhesion was obtained as observed by SEM, but the influence on the gas separation properties was not in agreement with the observed structural improvements. Similar results were observed by Vankelecom et al. [55] when they used a silane coupling agent, (γ -aminopropyl)triethoxysilane (APTS), to improve the adhesion between zeolite (borosilicate molecular sieve, ZSM-5) in polyimide matrix in their subsequent work. Membranes with silylated borosilicate showed a higher tensile strength due to the covalent bond formed between the silylated borosilicate and the PI matrix, but no change was observed on their xylene sorption using the unsilylated and silylated borosilicate mixed matrix membranes.

Li et al. [56] used a novel silane coupling agent, (3-aminopropyl)-diethoxymethyl silane (APDEMS), to modify the zeolite surface prior to dispersed in PES matrix

which result in better adhesion with PES matrix. APDEMS also used by Husain and Koros [57] to incorporate zeolite (HSSZ-13) in Ultem[®] asymmetric hollow fiber membranes, but failed to enhancement the adhesion between the two phases. Meanwhile, on the same study HSSZ-13 also treated by Grignard reagent (methyl magnesium bromide) which showed significant selectivity enhancement of O₂/N₂, He/N₂, CO₂/CH₄ over pure polymer matrix. Yong et al. [58] introducing low molecular weight materials of 2,4,6-triaminopyrimidine (TAP) to enhance the adhesion of zeolites (4A, 13X, NaY, 5A, and NaSZ390HUA) in Matrimid[®], resulted in better mixed matrix membranes performance.

Not only in zeolite-based filler, several works has been done to improve carbon-based filler compatibility in glassy polymer by introducing mutual functional groups to its surface. Kim et al. [35] functionalized SWCNTs by long chain alkyl amine (octadecylamine, ODA) to facilitate its dispersion in PSU matrix. The permeabilities of all gases (He, CO₂, O₂, N₂, CH₄) showed an increase. However, in high loading of SWNTs, the tortuosity around the agglomerated SWCNTs domain limits futher increase in permeability. For the case of CO₂/CH₄ separation, the addition of SWCNTs showed a decreasing trend of CO₂/CH₄ selectivity due to the preferential sorption of CH₄ by the SWNTs. Singh et al. [34] also functionalized surface of MWCNT by acid and amide groups by chemical treatment with nitric acid and octadecylamine (ODA), respectively, to facilitate its dispersion in PI matrix. Functionalized MWCNTs showed better dispersion in polymer matrix, where amine-functionalized MWCNTs are relatively better dispersed compared to acid-functionalized MWCNTs. However, the thermal stability of composite material decreases by the addition of functionalized MWCNTs. Even so, compared to the amine-functionalized MWCNTs composites, acid-functionalized MWCNTs composites showed better thermal stability.

Mahajan et al. [42] made a new approach to imitate the use of low T_g polymer by actually forming the mixed matrix at condition close to the glass transition temperature of the polymer matrix used. Plasticizer was used to lower the T_g of rigid polymer, such as Matrimid[®], and the membrane film were casted at elevated temperature. Such modifications indeed eliminate the interfacial defect between

polymer and sieves surface, however, no improvement was observed in the gas separation performance.

Koros et al. [59] is the first researcher to introduce the priming technique, promoting the compatibilization of polymer onto the sieve surface, priming technique may aid in minimizing aggregation of sieves particles at high loadings. Similarly the effect of the selection of priming polymer on the fabrication of CMS-Matrimid[®] mixed matrix membranes was reported by Vu et al. [20]. When a rigid polymer having a poor affinity with the sieves surface is used as the continuous matrix, priming technique is foreseen to be advantageous. Another polymer which is miscible in the continuous matrix and has more flexible chain and better adhesion with the sieve surface may be used as the priming polymer. In their study, another strategy by annealing treatment above T_g also subjected to the membrane which produce mixed matrix membranes with selectivity enhancement of 70% and 22% for CO₂/CH₄ and O₂/N₂, respectively. Sizing treatment of CMS has also been done by Rafizah and Ismail [60] using poly(vinyl pyrrolidone) K-15 (PVP K-15) as the sizing agent. A dramatic improvement of PSU-CMS adhesion was observed upon incorporation of PVP K-15-sized-CMS due to the intermolecular interaction between PVP K-15 sizing layer with PSU matrix. Mixed matrix membrane with sizing treatment exhibited 1.7 times higher O₂/N₂ ideal selectivity compared to the unmodified mixed matrix membrane. The performance of mixed matrix membranes comprised of zeolite-based and carbon-based molecular sieves are presented in Table 2.2 and plotted in Figure 2.2. The upper-bound limit showed in Figure 2.2 was plotted from Robeson et al. [26].

Table 2.2: Selected studies in the mixed matrix membranes fabrication.

Author(s)	Components materials		Application	Membranes performance	
	Polymer	Molecular sieves		Pure polymer membranes	Mixed matrix membranes
Zeolite-based molecular sieves					
Jia et al. [48]	PDMS	Silicate (70 wt.%)	O ₂ /N ₂	$\alpha_{O_2/N_2} = 2.14$	$\alpha_{O_2/N_2} = 2.92$
			CO ₂ /CH ₄	$\alpha_{CO_2/CH_4} = 3.42$	$\alpha_{CO_2/CH_4} = 8.86$ $P_{CO_2} = 3835$ Barrer
Duval et al. [38]	NBR 45	Zeolite KY (46 wt.%)	CO ₂ /CH ₄	-	$\alpha_{CO_2/CH_4} = 35$ $P_{CO_2} = 14$ Barrer
Kulprathipanja et al. [49]	CA	Silicate (25 wt.%)	O ₂ /N ₂	$\alpha_{O_2/N_2} = 2.99$	$\alpha_{O_2/N_2} = 4.33$
			CO ₂ /H ₂	$\alpha_{CO_2/H_2} = 0.7$	$\alpha_{CO_2/H_2} = 9.6$
Suer et al. [50]	PES	Zeolite 4A (50 wt.%)	CO ₂ /N ₂	$\alpha_{CO_2/N_2} = 3.7$	$\alpha_{CO_2/N_2} = 4.4$
Mahajan et al. [42]	Matrimid [®]	Zeolite 4A (20 vol.%)	O ₂ /N ₂	$\alpha_{O_2/N_2} = 7.2$ $P_{O_2} = 1.32$ Barrer	$\alpha_{O_2/N_2} = 7.2$ $P_{O_2} = 4.0$ Barrer
	Matrimid [®] - RDP Fyroflex [®]	Zeolite 4A (15 vol.%)	O ₂ /N ₂	$\alpha_{O_2/N_2} = 7.8$ $P_{O_2} = 0.25$ Barrer	$\alpha_{O_2/N_2} = 8.6$ $P_{O_2} = 0.2$ Barrer

Table 2.2: Selected studies in the mixed matrix membranes fabrication (Continued).

Author(s)	Components materials		Application	Membranes performance	
	Polymer	Molecular sieves		Pure polymer membranes	Mixed matrix membranes
Yong et al. [58]	Matrimid [®]	Zeolite 4A-TAP	CO ₂ /CH ₄	$\alpha_{CO_2/CH_4} = 1$ $P_{CO_2} = 8.3$ Barrer	$\alpha_{CO_2/CH_4} = 617$ $P_{CO_2} = 0.2$ Barrer
Husain and Koros [57]	Ultem [®]	HSSZ-13 (Grignard treated)	O ₂ /N ₂	$\alpha_{CO_2/N_2} = 38$	$\alpha_{CO_2/N_2} = 74$
			O ₂ /N ₂	$\alpha_{O_2/N_2} = 7.6$ $P_{O_2} = 4.0$ GPU	$\alpha_{O_2/N_2} = 8.2 \pm 0.09$ $P_{O_2} = 1.7 \pm 0.02$ GPU
			CO ₂ /CH ₄	$\alpha_{CO_2/CH_4} = 37.4$ $P_{CO_2} = 13$ GPU	$\alpha_{CO_2/CH_4} = 43.9 \pm 0.3$ $P_{CO_2} = 6.23 \pm 0.02$ GPU
Li et al. [56]	PES	Zeolite 5A-APDEMS (50 WT.%)	CO ₂ /CH ₄	$\alpha_{CO_2/CH_4} = 31.6$ $P_{CO_2} = 2.6$ Barrer	$\alpha_{CO_2/CH_4} = 36.9$ $P_{CO_2} = 2.5$ Barrer
			O ₂ /N ₂	$\alpha_{O_2/N_2} = 5.8$ $P_{O_2} = 0.47$ Barrer	$\alpha_{O_2/N_2} = 7.4$ $P_{O_2} = 0.7$ Barrer

Table 2.2: Selected studies in the mixed matrix membranes fabrication (Continued).

Author(s)	Components materials		Application	Membranes performance	
	Polymer	Molecular sieves		Pure polymer membranes	Mixed matrix membranes
Carbon-based molecular sieves					
Duval et al. [38]	EPDM	Carbosieve (50 wt.%)	CO ₂ /CH ₄	$\alpha_{CO_2/CH_4} = 4.3$ $P_{CO_2} = 81$ Barrer	$\alpha_{CO_2/CH_4} = 8$ $P_{CO_2} = 120$ Barrer
Vu et al. [20]	Matrimid [®]	CMS (36 wt.%)	CO ₂ /CH ₄	$\alpha_{CO_2/CH_4} = 35.3$ $P_{CO_2} = 10$ Barrer	$\alpha_{CO_2/CH_4} = 51.7$ $P_{CO_2} = 12.6$ Barrer
			O ₂ /N ₂	$\alpha_{O_2/N_2} = 6.6$ $P_{O_2} = 2.12$ Barrer	$\alpha_{O_2/N_2} = 7.3$ $P_{O_2} = 3$ Barrer
Rafizah and Ismail [60]	PSU	PVP K-15-CMS (30 wt.%)	O ₂ /N ₂	$\alpha_{O_2/N_2} = 5.50$ $P_{O_2} = 1.58$ Barrer	$\alpha_{O_2/N_2} = 6.05$ $P_{O_2} = 1.08$ Barrer
Anson et al. [53]	ABS	Activated carbon (40 w/v%)	CO ₂ /CH ₄	$\alpha_{CO_2/CH_4} = 24.12$ $P_{CO_2} = 2.87$	$\alpha_{CO_2/CH_4} = 50.49$ $P_{CO_2} = 20.50$

Table 2.2: Selected studies in the mixed matrix membranes fabrication (Continued).

Author(s)	Components materials		Application	Membranes performance	
	Polymer	Molecular sieves		Pure polymer membranes	Mixed matrix membranes
Kim et al. [54]	Poly(imide siloxane)	CNT (10 wt.%)	CO ₂ /CH ₄	$\alpha_{CO_2/CH_4} = 5.89$ $P_{CO_2} = 166$ Barrer	$\alpha_{CO_2/CH_4} = 5.21$ $P_{CO_2} = 191.3$ Barrer
			O ₂ /N ₂	$\alpha_{O_2/N_2} = 2.69$ $P_{O_2} = 32.24$ Barrer	$\alpha_{O_2/N_2} = 2.23$ $P_{O_2} = 39.81$ Barrer
Kim et al. [35]	PSU	Amine functionalized-SWCNT (15 wt.%)	CO ₂ /CH ₄	$\alpha_{CO_2/CH_4} = 23.55$ $P_{CO_2} = 3.9$ Barrer	$\alpha_{CO_2/CH_4} = 16.09$ $P_{CO_2} = 4.52$ Barrer
			O ₂ /N ₂	$\alpha_{O_2/N_2} = 5.07$ $P_{O_2} = 0.84$ Barrer	$\alpha_{O_2/N_2} = 5.1$ $P_{O_2} = 1.11$ Barrer

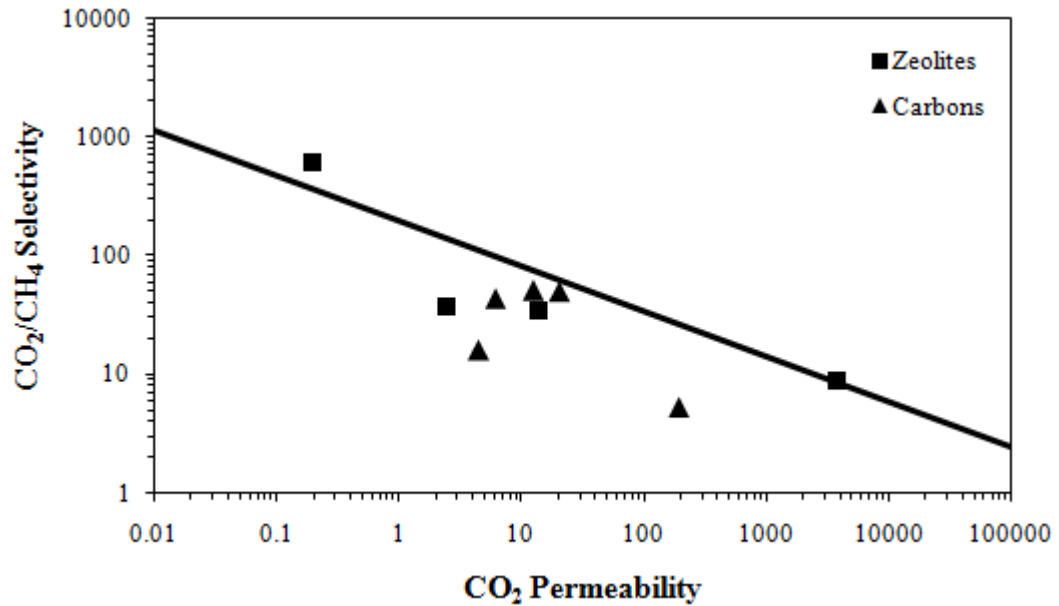


Figure 2.2: CO₂/CH₄ selectivity and CO₂ permeability for various mixed matrix membranes.

2.2 Transport of Gas in Glassy Polymeric Membranes and Molecular Sieves

Materials

Research of membrane technology in gas separations carried out mostly using dense membrane from glassy polymer, due to its ability to control the permeation of different species [36]. Solution-diffusion mechanism has been widely accepted to describe the transport of gas through dense polymeric membranes [29]. As in glassy polymer, gas transport in molecular sieving material also can be described using solution-diffusion mechanism [30, 46]. The mechanism could be divided into three steps: (i) a gas molecule in the feed phase is sorbed into the membrane interface, then (ii) diffuse across the membrane, and (iii) desorbed on the permeate phase side, as illustrated in Figure 2.3. The solution-diffusion mechanism is driven by the difference in thermodynamic activities (i.e. concentration gradient and pressure gradient) existing at the feed and permeate phase as well as the interaction forces acting between the penetrant and the membrane material [36]. The activity difference leads the penetrating molecule to travels towards the decreasing activity direction.

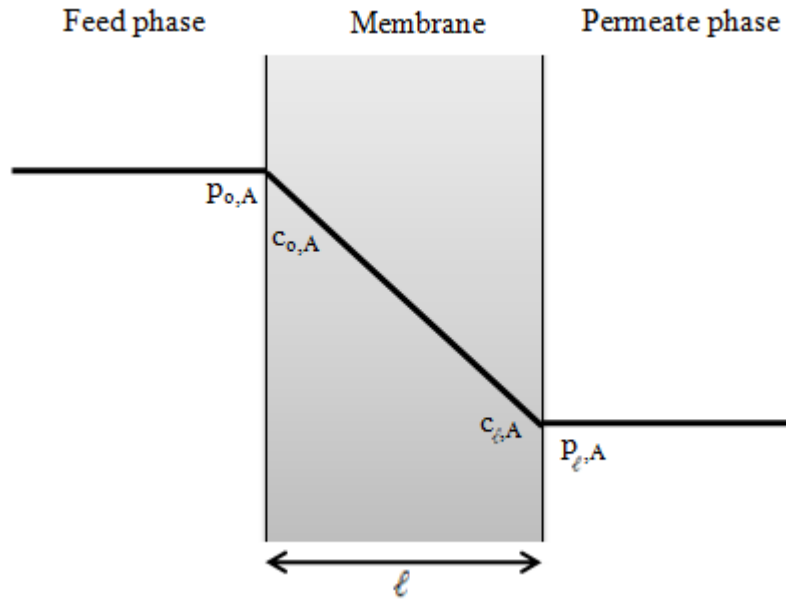


Figure 2.3: Solution-diffusion mechanism.

2.2.1 Permeation

In separation process, membrane performance is characterized by two main parameters: (i) the flux of a gas component across the membrane and (ii) the separation efficiency in separating gas components. A quantitative measure of the transport flux of a gas component A through a membrane is expressed as permeability coefficient (P_A), which is a pressure and thickness normalized flux:

$$P_A = \frac{J_A \cdot \ell}{\Delta p_A} \quad (2.1)$$

where J_A is the flux, ℓ is the thickness of the membrane film, and Δp_A is pressure difference across the membrane. However, when the thickness is difficult to define, such as in asymmetric membranes, pressure normalized flux or permeance (P_A/ℓ) is used. Permeance is defined as:

$$\frac{P_A}{\ell} = \frac{J_A}{\Delta p_A} \quad (2.2)$$

The units used to express permeability and permeance is given in Table 2.3. Based on solution-diffusion mechanism, the permeability of gas component A is a product of the diffusion coefficient (D_A) and the solubility coefficient (S_A), given by:

$$P_A = D_A \cdot S_A \quad (2.3)$$

Table 2.3: Units of permeability and permeance coefficient.

Coefficient	Units	Dimension
Permeability (P_A)	Barrer	$1 \times 10^{-10} \frac{\text{cm}^3(\text{STP}) \cdot \text{cm}}{\text{s} \cdot \text{cm}^2 \cdot \text{cmHg}}$
Permeance (P_A/ℓ)	GPU (Gas Permeation Unit)	$1 \times 10^{-6} \frac{\text{cm}^3(\text{STP})}{\text{s} \cdot \text{cm}^2 \cdot \text{cmHg}}$

The efficiency of the membrane in enriching a component over another component in the permeate phase can be expressed as ideal selectivity ($\alpha_{A/B}$), where its value is equal to the ratio of the permeability of the individual gases. For mixture of gas A and B the ideal selectivity is described by:

$$\alpha_{A/B} = \frac{P_A}{P_B} = \left(\frac{D_A}{D_B} \right) \left(\frac{S_A}{S_B} \right) \quad (2.4)$$

The selectivity could be separated into the product of the ration of diffusion coefficient and the ration of sorption coefficient. Thus, the membrane could be tailored to increase the permselectivity by adjusting sorption and diffusivity coefficient of the gas penetrant in membrane medium. The sorption selectivity is dependent on the relative condensability of gas penetrants and penetrant-membrane medium interactions, whereas diffusivity selectivity dependent on the relative differences of the diffusion coefficients of gas penetrants through the membrane material.

2.2.1.1 Permeation of Gas in Mixed Matrix Membrane

In mixed matrix membrane, permeation of gases occurs by a combination of diffusion through the polymer phase and the dispersed molecular sieves. Figure 2.4 shows the comparison of gas permeation in mixed matrix with low and high loading of filler. At relatively low loading of filler, the permeability can be expressed by Maxwell equation:

$$P = P_c \left(\frac{P_d + 2P_c - 2\phi(P_c - P_d)}{P_d + 2P_c + \phi(P_c - P_d)} \right) \quad (2.5)$$

where P is the overall permeability of the mixed-matrix membrane, ϕ is the volume fraction of the dispersed particles, P_c is the permeability of the continuous polymer phase, and P_d is the permeability of the dispersed particles. However, at loadings above a certain critical value, some of filler particles were interconnected with each other forming continuous channels within the membrane. This is called percolation threshold. At this particle loading, the Maxwell equation is no longer used to calculate the membrane permeability. The percolation threshold is believed to be achieved at particles loading of about 30 vol.% [10].

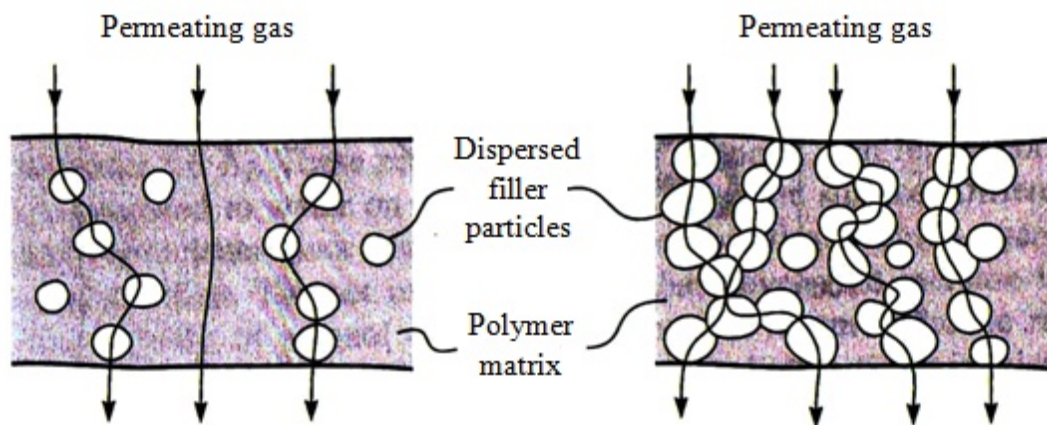


Figure 2.4: Gas permeation through mixed matrix membrane containing different amounts of dispersed filler particles. Adapted from [10].

2.2.2 Sorption

Sorption or solubility coefficient is a thermodynamic parameter which measures the amount of gas sorbed by the membrane material under equilibrium conditions at given pressure. The sorption behavior of gas molecules in polymeric membranes can be described by the dual-sorption model, which was originally proposed by Barrer et al. [10]. According to the dual-sorption model, gas sorption in a polymer occurs in two types of sites. The first type of site is filled by gas molecules dissolved in the equilibrium free volume portion of material (C_D) and the second type of site is the excess free volume due to the frozen conformation of polymer chain which forms microcavities in the matrix. The population of dissolved molecules (C_H) in the excess free volume is limited and ceases when all the sites are filled.

In rubbery polymers, the first site is the only sites that exist, therefore in rubbery polymers the amount of the sorbed gas can be related to the partial pressure of the gas by a linear expression according to the Henry's law, written as:

$$C_{DA} = S_A \cdot p_A \quad (2.6)$$

The Henry's law sorption is illustrated in Figure 2.5(a). While in glassy polymer, the second type of site exists. Sorption in the second type of sites is best approximated by Langmuir adsorption isotherm.

Not only for glassy polymers, porous molecular sieving materials, such as carbon molecular sieves (CMS) and zeolites, is commonly used the Langmuir adsorption isotherm to define its gas sorption. In Langmuir isotherm adsorption, the equilibrium is assumed to be dynamic, where the rate at which the gas molecules strike the adsorbent surface and condense on the bare sites is equal to the rate at which molecules evaporate from the occupied sites [61]. In other words, the rate of adsorption is equal to the rate of desorption. The Langmuir isotherm adsorption is expressed by:

$$C_{HA} = \frac{C'_{HA} b_A p_A}{1 + b_A p_A} \quad (2.7)$$

where C_{HA} is the amount of gas molecule A adsorbed with partial pressure p_A , C'_{HA} is the amount of gas molecule A required to form a monomolecular layer, and b_A is the

Langmuir affinity constant of gas molecule A . Depending upon pressure the Equation 2.7 can be reduced in two limiting parameters. At low pressure the value of bp is less than unity, such as at the beginning of adsorption, Equation 2.7 could be reduced as:

$$C_{HA} = C'_{HA} b_A p_A \quad (2.8)$$

showing a proportionality between the amount of gas adsorbed and the equilibrium pressure. Whereas at high pressure, Equation 2.7 could be reduced to:

$$C_{HA} = C'_{HA} \quad (2.9)$$

which indicates that at higher pressure the adsorption is independent to the pressure because it has attained the maximum capacity of A required to cover the surface by a monolayer. The Langmuir isotherm curve is shown in Figure 2.5(b).

From the description above, the total sorption of glassy polymer (C_A) is:

$$C_A = C_{DA} + C_{HA} \quad (2.10)$$

or in extended form:

$$C_A = K_{DA} p_A + \frac{C'_{HA} b_A p_A}{1 + b_A p_A} \quad (2.11)$$

where K_{DA} is the Henry's law constant for gas component A which is equal to the solubility coefficient. The illustration of dual-sorption model is given in Figure 2.6.

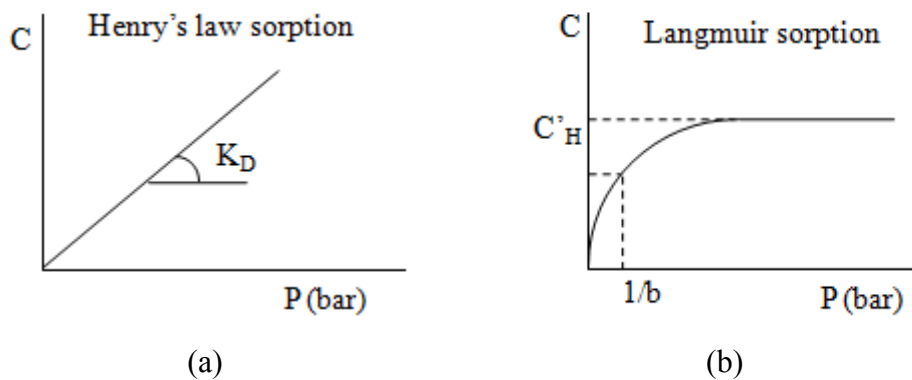


Figure 2.5: Sorption mechanisms contribute to the gas sorption in dual-sorption model: (a) Langmuir sorption and (b) Henry's law sorption.

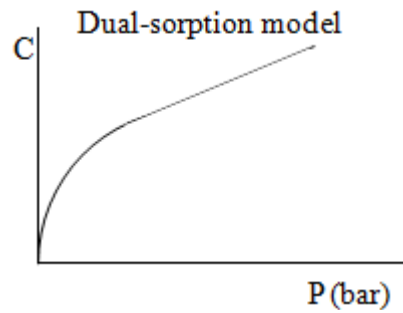


Figure 2.6: Dual-sorption model in glassy polymer.

2.2.3 Diffusion

The diffusion coefficient is a parameter which describes of the mobility of a gas penetrant through the membrane. Diffusivity is dependent on the geometry of the penetrant and on the nature of the material through which diffusion occurs. In general, diffusion coefficients decrease as the particle size increases, as described by Stokes-Einstein equation [62]:

$$D_A = \frac{RT}{N} \cdot \frac{1}{6\pi\eta r_A} \quad (2.12)$$

where R is the universal gas constant, T is the absolute temperature, N is the Avogadro's number, η is the viscosity of the medium, and r_A is the spherical radius of the diffusing particle A . This relationship shows that the diffusion coefficient is inversely proportional to the molecular size. The difference in diffusivity of gas components through the membrane and molecular sieves is a deciding factor to achieve separation. However, the mechanism of penetrant diffusion through molecular sieving materials and polymers matrix are different.

2.2.3.1 Diffusion of Gas in Glassy Polymers

Diffusion may be considered as statistical molecular transport as a result of the random motion of the molecules. The mechanism of gas diffusion through a polymeric membrane is via "zone of activation" where polymers are perturbed temporarily to allow penetrants making size-dependent diffusive jumps. Several models have been proposed to describe the transport of small penetrant molecules

through the polymer matrix, represented in Figure 2.7. A model from Brandt [63] (Figure 2.7(a)) shows that the activated state involving two polymer chains which have moved apart. In order to make the diffusive jump, the gas molecule pushes the polymer chains which lead to the partial rotation of each polymer backbone and jump into a new position. Another model by DiBenedetto and Paul [64], as depicted in Figure 2.7(b), assumed that a diffusive jump occur when four parallel polymer segments separate sufficiently to create a cylindrical void which the gas molecule can move and then returns to the normal configuration after the jump. Figure 2.7(c) shows the model proposed by Pace and Datyner [65] accounts for the structure of the polymer contributing to gas diffusions and incorporates features from DiBenedetto's model. It is proposed that noncrystalline polymer regions possess an approximate semicrystalline order with chain bundles that are locally parallel along distances of several nanometers and can be considered as tubules. Transport of gas molecules occur by leaps between tubules when thermal motions of local segments of the polymer chains open up a sufficiently large channel to a neighbouring gap. The gas penetrants can then move through this channel. Once the channel closes, the jump is successfully concluded. According to this model the diffusion selectivity of the membrane is controlled by the jump channel. A large opening causes large diffusion coefficient and activation energy for diffusion, whereas a smaller opening permits the smaller molecules to diffuse more readily than the larger particles. In contrary with the diffusion in polymers which can only occur when gaps with sufficient size are available, the diffusion of gas penetrants in molecular sieves occurs through rigid slit pores.

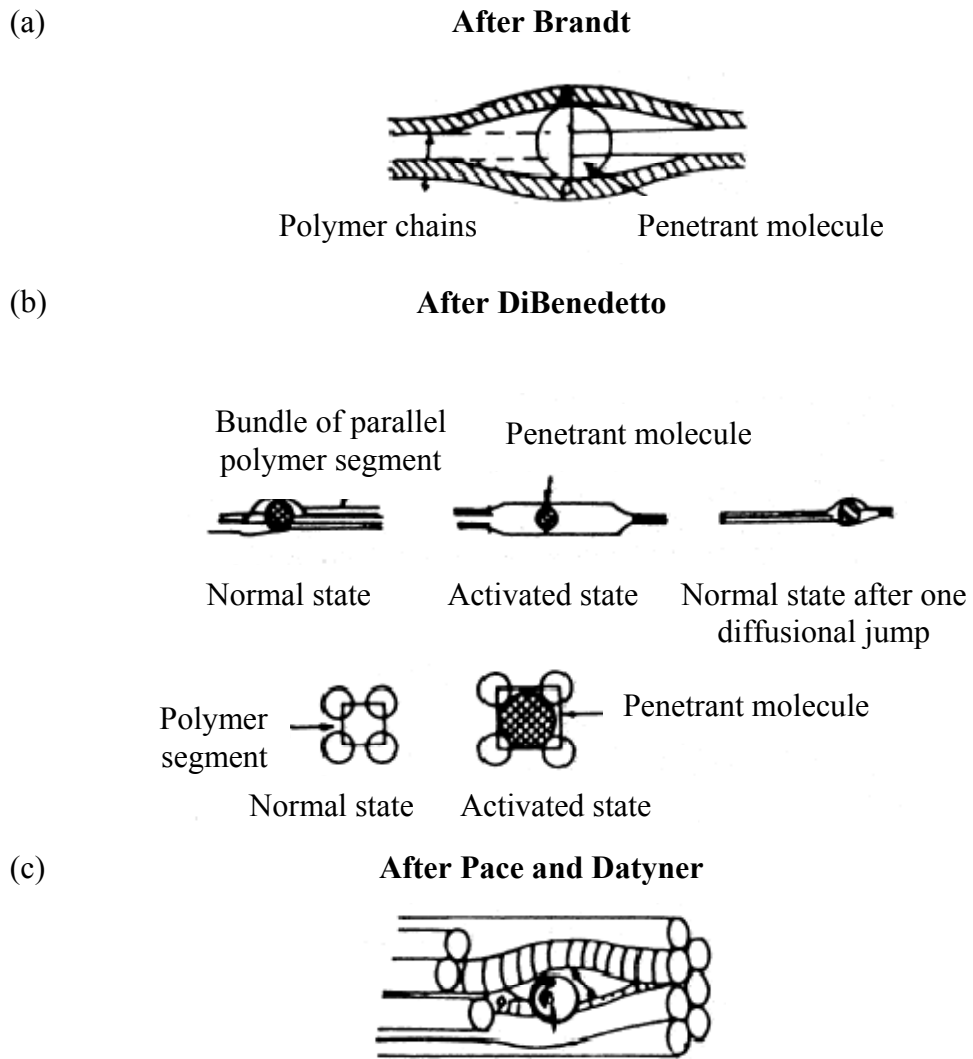


Figure 2.7: Diffusion of gas penetrant through glassy polymer. Adapted from [64].

The transport of gas diffusion through a non-porous membrane is described by Fick's first law, given by:

$$J_A = -D_A \frac{dC_A}{dx} \quad (2.13)$$

where J_A is the flux of gas molecule A through the membrane, D_A is the diffusion coefficient, and the driving force dC_A/dx is the concentration gradient across the membrane. The minus (-) sign refers to the direction of concentration gradient in which the gas molecules penetrating from high concentration to low concentration. Later, in the discussion of dual-sorption model, it was proposed that penetrants in the Langmuir mode may also have certain mobility. Hence, a dual-transport model, called

the partial immobilization model, has been proposed to complement the dual-sorption model [30, 66]. With two different diffusion modes, Fick's first law is rewritten as:

$$J_A = -\left(D_{DA} \frac{dC_{DA}}{dx} + D_{HA} \frac{dC_{HA}}{dx} \right) \quad (2.14)$$

where D_{DA} and D_{HA} are the diffusion coefficients of penetrant A in the Henry and Langmuir environments, respectively, and C_{DA} and C_{HA} correspond to the penetrant A concentration in the Henry and Langmuir environments, respectively. Since permeability is the product of solubility coefficient and diffusivity coefficient (Equation 2.3), the permeability of gas component A in glassy polymer membrane can be explained by dual-sorption model [67, 68]. In simplified manner, it can be expressed as:

$$P_A = K_{DA} D_{DA} + \frac{C'_{HA} b_A D_{HA}}{1 + b_A p_A} \quad (2.15)$$

2.2.3.2 Diffusion of Gas in Molecular Sieves Particles

Highly porous carbon materials such as activated carbons, wood charcoals, carbon molecular sieves, etc. are considered to have a random orientation structure, or called nongraphitizable. The basic constituents of these materials are randomly intermingled, forming either opened or closed pores between them. The structure of carbon molecular sieves (CMS) is considered to adapt the structure of activated carbons (ACs), because they were prepared from common precursors (coal, vegetable, polymer, etc.) and with similar processing. Activated carbons have a 'turbostratic' structure. This concept was coined to describe the graphite-like structure with a random orientation of layer planes along the a axis and a rotation of layer planes along the c axis. It is visualized as comprising by large cavities formed by the graphite planes which interconnected by constrictions approaching the dimensions of the diffusing molecules. The shape and size of the channel formed supports its molecular sieving ability. Early models used to describe the structure of ACs were described by the Franklin model (Figure 2.8(a)) and a ribbon-like structure which is similar to the Jenkins and Kawamura model (Figure 2.8(b)) for glass-like carbon [69].

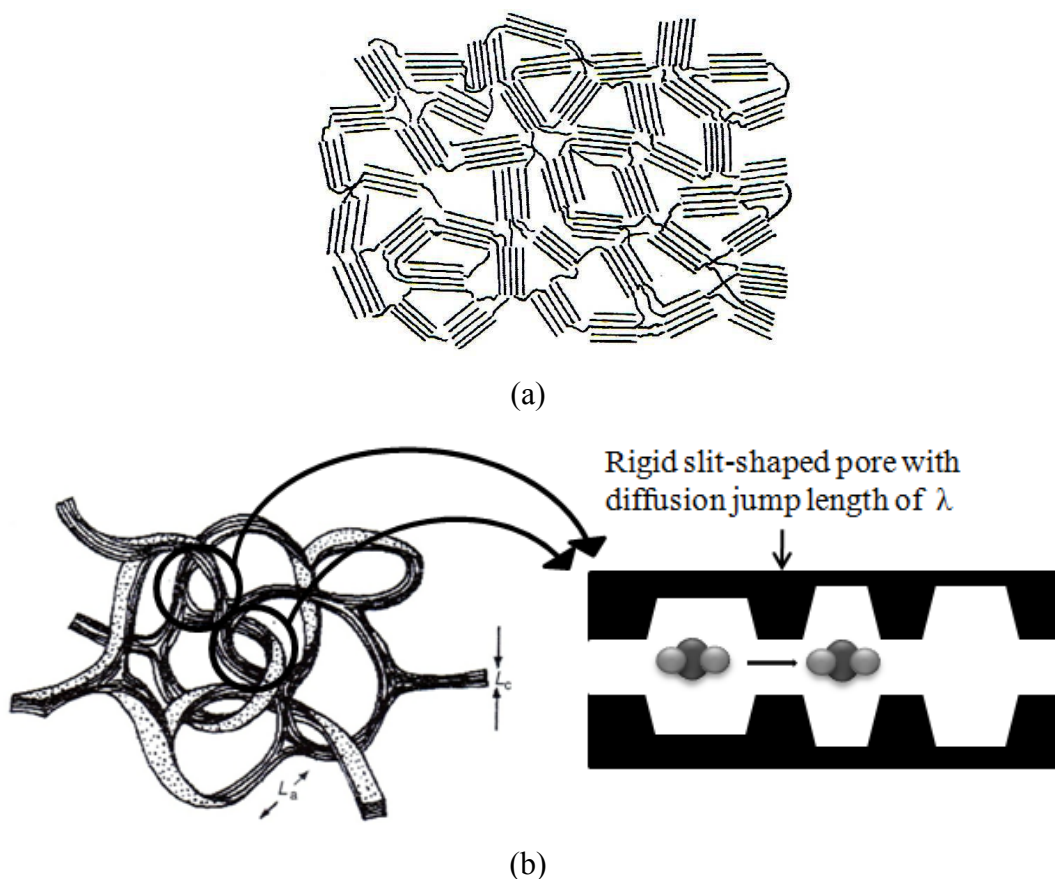


Figure 2.8: The structure models of carbon materials: (a) for a nongraphitizable carbons by Franklin and (b) ribbon model for glass-like carbon by Jenkins-Kawamura. Adapted from [69].

In molecular sieves, the diffusion process is envisioned to occur when a gas molecule makes a diffusive jump from one sorption cavity to another through the narrow pore opening, as depicted in Figure 2.8(b). The gas penetrant molecules require a characteristic activation energy which could overcome the net repulsive interaction with the pore wall. The net repulsive interaction of gas penetrant and adsorbent surface is explained as the sum of Lennard-Jones potential for each penetrant and surface adsorbent atom. The interactions are assumed to be pairwise additive. When a molecule is placed in slit-shaped pore (Figure 2.8(b)), it interacts with both top and bottom surface, and the repulsive potentials on the surfaces overlap. The extent of the overlap depends on the pore size, and the Van der Waals radii of the molecules. For a given pore, larger-sized penetrant will encounter a stronger repulsive

force than the smaller-sized one. Thus, the size discrimination process enables very high selectivities in molecular sieving materials. Therefore, a small difference in molecular penetrant dimension is very important to achieve the separation. The molecular dimensions of several gas penetrants are provided in Table 2.4.

Table 2.4: Molecular dimensions of gas penetrants.

Gas molecule	Molecular length (Å)	Molecular width (Å)	Lennard-Jones diameter (Å)	Kinetic diameter (Å)
CO ₂	5.10	3.70	4.42	3.30
O ₂	3.75	2.68	3.58	3.46
N ₂	4.07	3.09	3.69	3.64
CH ₄	-	4.20	4.01	3.80

Activated diffusion is typically described by an Arrhenius relationship:

$$D_A = D_{0A} e^{-E_{DA}/RT} \quad (2.16)$$

where D_A is the diffusion coefficient of gas component A , D_{0A} is the pre-exponential term, E_{DA} is the activation energy required for the gas molecule A to execute a diffusive jump from one cavity to another, R is the universal gas constant, and T is the absolute temperature.

CHAPTER 3

MATERIAL AND METHODOLOGY

This chapter covers the materials used in membranes preparation and modification of molecular sieve particles surface as well as the experimental procedures for the formation and characterization of these materials. Section 3.1 gives the details of the polymer (used to form dense homogeneous membrane), the molecular sieve material (used as the filler particle in mixed matrix membrane formation) and the material used to modify the sieve surface. The detailed experimental procedures used to form the homogeneous and mixed matrix membranes, and to modify the sieve surface are presented in Section 3.2 and 3.3, respectively. The detailed of material characterization techniques and the permeation experiments on the membrane materials are discussed in Section 3.4 and 3.5, respectively.

3.1 Material

3.1.1 Polysulfone

Polysulfone (PSU) was used to form dense homogeneous membrane film and as continuous matrix phase in the mixed matrix membrane formation. The tough, rigid, high-strength and thermal properties of PSU are the main reasons for the choice of PSU for membrane fabrication. P-1800 Udel[®] PSU was purchased from Solvay Advanced Polymers, L.L.C, U.S. The chemical structure and the physical properties of PSU are described in Figure 3.1 and Table 3.1, respectively. The density and glass transition temperature (T_g) were experimentally determined in this work (characterization techniques described later in Section 3.4). Prior to use in membrane

fabrication, polymer powder was dried in an oven by spreading the powder in a stainless steel tray to 1 cm depth for at least 12 hours at 110°C.

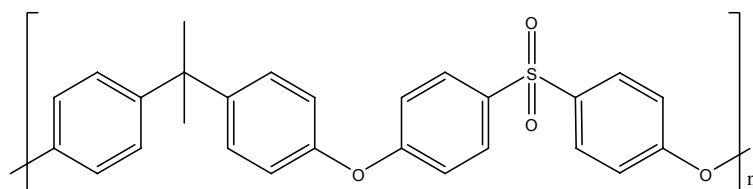


Figure 3.1: Chemical structure of PSU. Adapted from [70].

Table 3.1: Chemical and physical properties of PSU.

Properties	Value
Molecular weight of monomer	442.5 g/mol
Density	1.38 g/cm ³
Glass transition temperature	195.5°C
Solubility parameter	20.3 J ^{1/2} /cm ^{3/2}

3.1.2 Solvents

Dichloromethane (DCM, reagent grade, Merck[®]) was used as solvent in this study since it provides rapid evaporation (boiling point 40°C); however there are some other organic solvents such as N,N-dimethylacetamide (DMAc), N,N-dimethylformamide (DMF), 1-methyl-2-pyrrolidone (NMP), chloroform, tetrahydrofuran (THF) may as well be used. The selection of solvent may affect the permeation properties and the structure of the final film [30, 71]. Table 3.2 describes the properties of common organic solvents used to dissolve PSU. Solvent selection was based on the miscibility with the polymer, polymer-solvent interaction and the desired evaporation rate. Among the common organic solvents listed in Table 3.2. DCM provides the lowest boiling point and also the closest solubility parameter with PSU, hence DCM was selected as solvent to be used in membrane fabrication.

Table 3.2: Chemical and physical properties of typical organic solvents for PSU.

Solvent	MW (g/mole)	ρ (g/cm ³)	b.p. (at 20°C)	v.p. (at 20°C)	Solubility in water	δ (J ^{1/2} /cm ^{3/2})
DCM (CH ₂ Cl ₂)	84.94	1.336	39.8-40°C	46.5 kPa	Not soluble	19.9
DMAc (C ₄ H ₉ NO)	87.12	0.937	166°C	0.2 kPa	Soluble	22.1/22.8
DMF (C ₃ H ₇ NO)	73.09	0.949	153°C	0.3 kPa	Soluble	24.9
NMP (C ₅ H ₉ NO)	99.13	1.028	202°C	0 kPa	Soluble	22.9
Chloroform (CHCl ₃)	119.39	1.499	58-62°C	21.1 kPa	Not soluble	18.9-19.0
THF (C ₄ H ₈ O)	72.10	0.888	64-66°C	19.3 kPa	Soluble	19.5

MW: molecular weight; ρ : density; b.p.: boiling point; v.p.: vapour pressure; δ : solubility parameter

3.1.3 Carbon Molecular Sieve

Carbon molecular sieves (CMS) particles were used as inorganic filler in the mixed matrix membrane fabrication. Uniform pore size on the CMS surface allows selective adsorption of CO₂ over CH₄, which has kinetic diameter of 3.30 Å and 3.80 Å, respectively. For consistency, Shirasagi MSC-3K (type 161) purchased from Japan Enviro Chemical (Takeda) was used for mixed matrix membrane preparation and molecular sieves surface modification.

Prior to introducing into the polymer matrix, CMS pellets were crushed into a fine particle size. A pressure grinder (Rocklabs[®]) was used to crush the CMS pellets. CMS pellets were loaded into a stainless container together with a mill ball. The container was then placed inside a shaker which provides a rapid shaking, allowing the stainless steel ball to crush the pellets into fine particles. Every 5 grams of CMS pellets were grinded for 15, 30, 45, and 60 minutes. After grinding, the container was then allowed

to stand for 15 minutes to cool down and to let the airborne CMS particles to settle inside the container. CMS particles were then dried in a drying oven for at least 12 hours at 250°C to remove the adsorbed moisture. The particle size of the resulting CMS powder was then measured (Scirocco 2000 particle size analyzer from Malvern Instruments Ltd.) and the sample results are shown in Figure 3.2. From the particle size distribution obtained, 30 minutes of grinding period was chosen as the optimum grinding period. The selected grinding period gave a particle size of $0.964 \pm 0.588 \mu\text{m}$, with a density of 2.1664 g/cm^3 as measured by Ultracycrometer 1000 (characterization techniques described later in Section 3.4.6). In order to maintain the consistency, 30 minutes grinding period was used for further experiments. The properties of CMS powder is presented in Table 3.3.

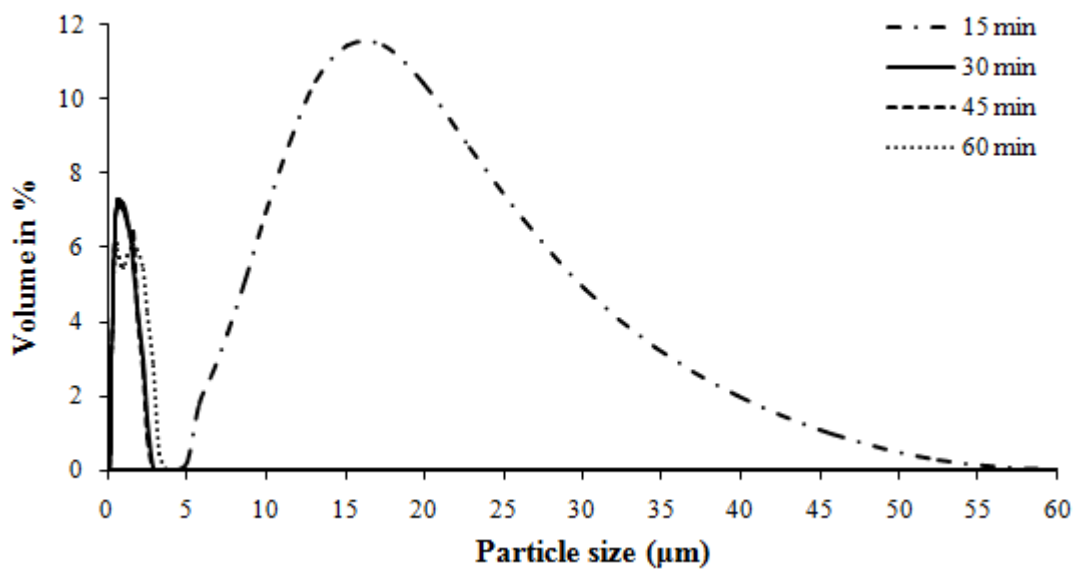


Figure 3.2: CMS particle size distribution for various grinding period.

Table 3.3: Carbon molecular sieve characteristics.

Properties	Shirasagi MSC-3K
Density	2.1664 g/cm^3
Particle size	$0.964 \pm 0.588 \mu\text{m}$
Mean pore size	3.8 \AA

3.2 Fabrication of Membranes

Two types of membranes, homogeneous and mixed matrix membranes, were prepared in this study. These membranes are prepared in two steps: (i) preparation of casting solution; (ii) casting process to form membrane thin film. During the preparation of mixed matrix membranes using the modified CMS, additional step to modify CMS surface was done by oxidation process to produce the oxidized-CMS (ox-CMS). The simplified methodology of the present study is depicted in Figure 3.3.

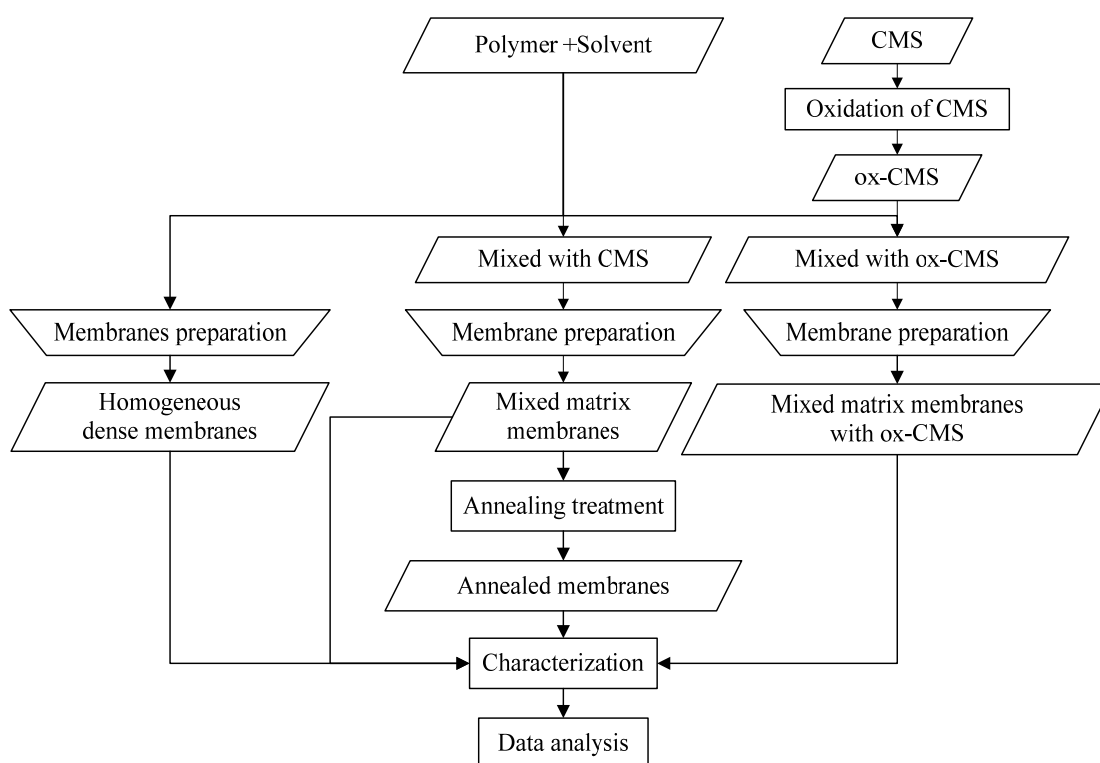


Figure 3.3: Experimental methodology of the study.

3.2.1 Fabrication of Homogeneous Polysulfone Membrane

All membranes used in this study were prepared by using solvent-evaporation technique. Dried polymer was slowly added into a 250 ml Duran[®] laboratory bottles containing the desired amount of organic solvent and stirred for 24 hours. After 24 hours mixing, a clear viscous solution was obtained. The solution was then allowed to stand for at least 12 hours to remove the air bubbles form during mixing. Presence of

bubbles in casting solution may form holes in the membrane films. A gentle stirring was used to minimize the formation of bubbles.

A flat, smooth, dry, and dust-free glass plate was used as casting template. Acetone was used to clean and remove moisture from the glass surface, and compressed air was used to remove dust particles. Casting knife was adjusted to 250 μm thickness. Casting solution was then poured across the glass plate edge. As the casting knife was pulled towards the user, a uniform wet film was drawn across the glass plate surface. Since DCM is a highly volatile solvent, a rapid evaporation should lead to the formation of film with wavy structure. Therefore, a glass cover was placed over the glass plate immediately to slow down the evaporation rate of the solvent and also to prevent dust or particulate contamination to stick on the wet membrane film. After 24 hours of evaporation, the dry film was carefully peeled off from the glass surface, sometimes a razor blade was used to initiate delaminating the film at the membrane edge. After peeling off from the glass plate, the film was then dried in an oven at 110°C for 24 hours to remove the residual solvent and moisture. The resulting dry films have a thickness of $\approx 100 \mu\text{m}$. These homogeneous PSU dense membranes were used as the bench marking in evaluating their physical and chemical properties as well as performance versus the mixed matrix membranes developed in Section 3.2.2. The illustration of casting process is depicted in Figure 3.4.

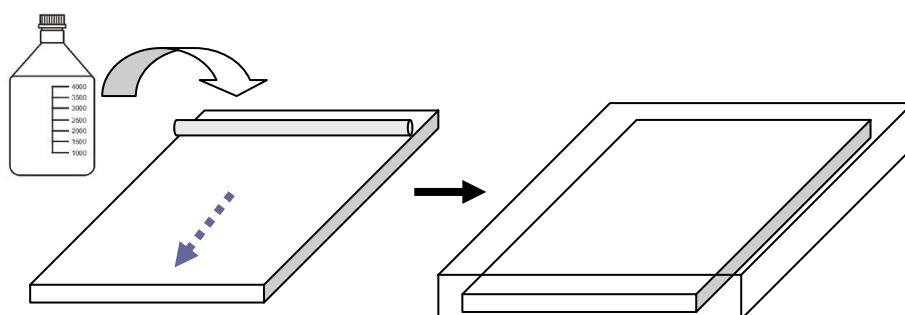


Figure 3.4: Casting steps of homogeneous dense membrane.

3.2.2 Mixed Matrix Membrane

The preparation of mixed matrix membrane was similar to the preparation of dense homogeneous membrane but several additional steps were introduced. Before being used as filler in the mixed matrix membrane preparation, the unmodified and modified CMS powder were prepared following the steps described in Section 3.1.3 and 3.3, respectively. In this study, mixed matrix membranes were prepared with several CMS loadings and the details of mixed matrix membrane composition are described in Table 3.4.

Table 3.4: Mixed matrix membranes composition.

Filler type	% CMS (w/w)	% PSU (w/w)
CMS ($\rho = 2.6114 \text{ g/cm}^3$)	10	
	20	15
	30	
Modified CMS ($\rho = 2.16 \text{ g/cm}^3$)	10	
	20	15
	30	

The casting solution was prepared by adding a desired amount of CMS into a 250 ml Duran[®] laboratory bottles containing the corresponding amount of solvent. The solution was sonicated in an ultrasonic bath (Transsonic Digital S, Elma[®]) using 100 Hz frequency for 10 minutes to break the aggregates of CMS to enhance the homogeneity of CMS dispersion in the solution.

Polymer was then introduced into the casting solution in two steps. Firstly, a small amount (10 wt.% of total polymer) was introduced as a sizing agent and stirred until it dissolves completely. Sizing technique was carried out to promote the compatibilization of the filler particles with the polymer matrix by sizing or undercoat the filler surface by a thin layer of polymer [30]. Secondly, after sizing the CMS particles, the remaining amount of polymer was introduced into the solution and the solution was again stirred for 24 hours. The preparation of mixed matrix membrane

casting solution is illustrated in Figure 3.5. After a black homogeneous viscous solution was obtained, the solution was allowed to stand for at least 15 minutes to remove the bubbles which formed during the solution mixing. The casting process is similar to the formation of dense homogeneous membrane. The solvent was evaporated for 24 hours. After the membranes were peeled off from the glass surface, it was then dried in an oven for 24 hours at 110°C.

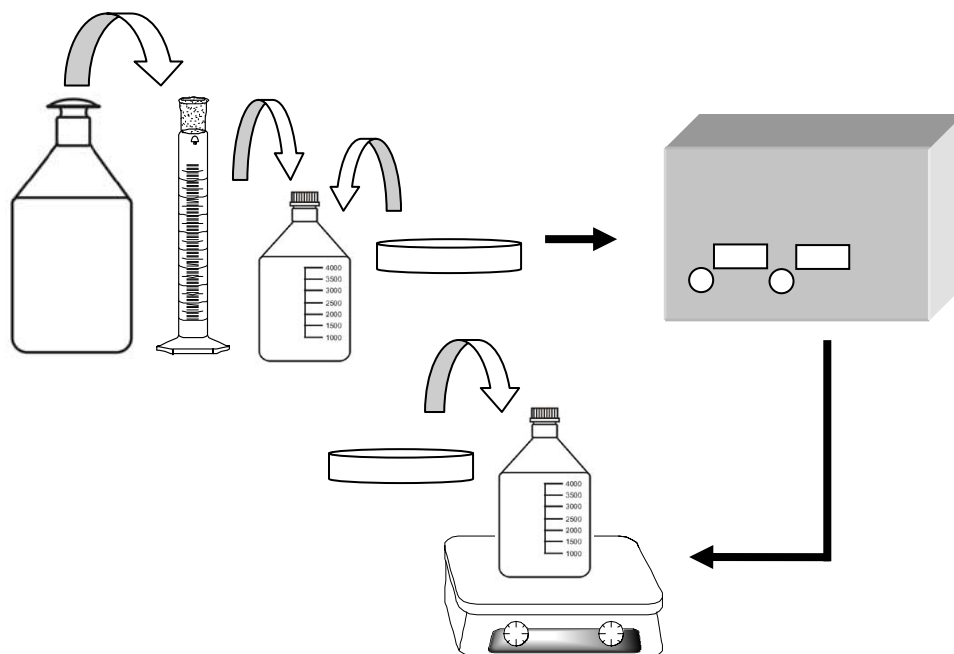


Figure 3.5: Preparation of casting solution to form mixed matrix membrane.

3.3 Nitric Acid Oxidation of Carbon Molecular Sieve

The main purpose of nitric acid (HNO_3) oxidation of CMS particles was to allow the surface of CMS to get functionalized by acidic functional groups [72]. For oxidative treatment, HNO_3 was reported to be the best known oxidation agent [73]. Oxidation with HNO_3 is often used because its oxidizing properties can be controlled by concentration and temperature [74]. In this study 2 M, 5 M, 8 M and 11 M of HNO_3 were applied for oxidation of CMS.

Predetermined quantities of CMS powder (30 grams) were added into HNO₃ solution (300 ml, Merck®) in a 500 ml two-neck round-bottomed flask. The solution was sonicated in an ultrasonic bath under 20 Hz frequency for 10 minutes, to break carbon aggregates within the solution. After sonication, the mixture was oxidized for 3 hours at 100°C. The configuration of the reflux set-up is shown in Figure 3.6.

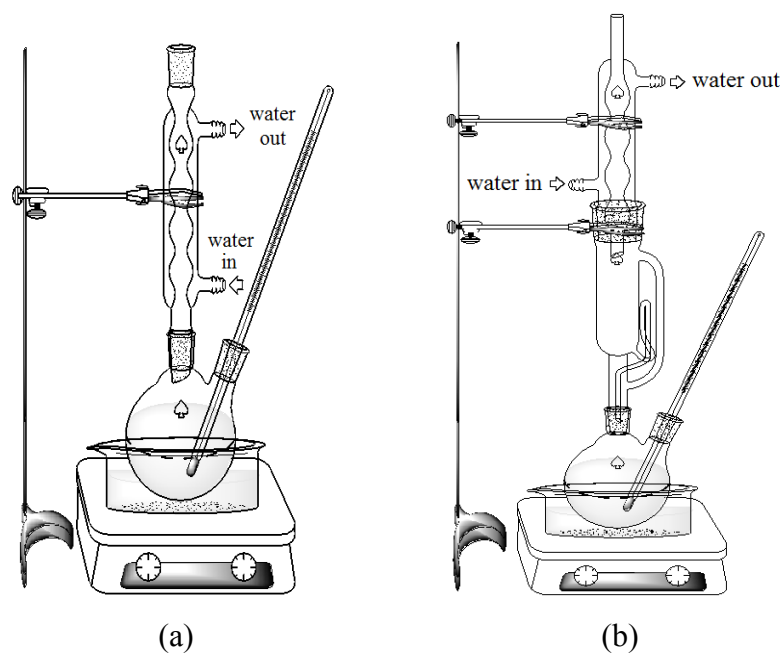


Figure 3.6: Experiment set-ups for: (a) reflux of CMS by HNO₃ and (b) Soxhlet extraction of CMS by distilled water.

The oxidized-CMS (ox-CMS) were then washed with 1 M sodium hydroxide (NaOH, 300 ml) to neutralize the HNO₃ on their surfaces [75] and also to quench the oxidation reaction. Filtration of ox-CMS was done by using a custom-made stirred filtration cell as shown in Figure 3.7. The cell consists of three main parts: cell base, reservoir, and cell cap. All contact surfaces of the cell are non-metallic. A PTFE membrane filter with a pore size of 0.45 μm and 47 mm in diameter was mounted on the Teflon® cell base by using 19 layers of filter paper (Whatman®) as support to prevent bending of the membrane that may cause breakage when a high pressure air is applied to the cell. On top of the PTFE membrane, a Teflon® O-ring was used to hold the membrane from shifting. As the reservoir, a clear acrylic cylinder with 6 cm diameter and 13 cm height, placed above the cell base, was then sealed by nitrile

butylene rubber (NBR) O-ring on the top and bottom of the cylinder. The transparency of the reservoir allows continuous observation of the solution level and condition. A long stick with magnetic stirrer bar attached on the edge was screwed to the cell cap allowing the bar to stir the solution near to the membrane surface and prevent fouling of the carbon particles on the membrane pores. The reservoir was then covered by the cap and locked using three bolts and nuts. Pressurized air, with pressure as high as 5 bar, was subjected to the filtration cell. Removal of residual nitric acid and oxidation byproduct was further done by refluxing the oxidized CMS with 1 M NaOH for 1 hour [75], and filtered. The ox-CMS was then purified by Soxhlet extraction with distilled water (150 ml) for 120 hours. The oxidized CMS was then dried at 55°C for 4 days.

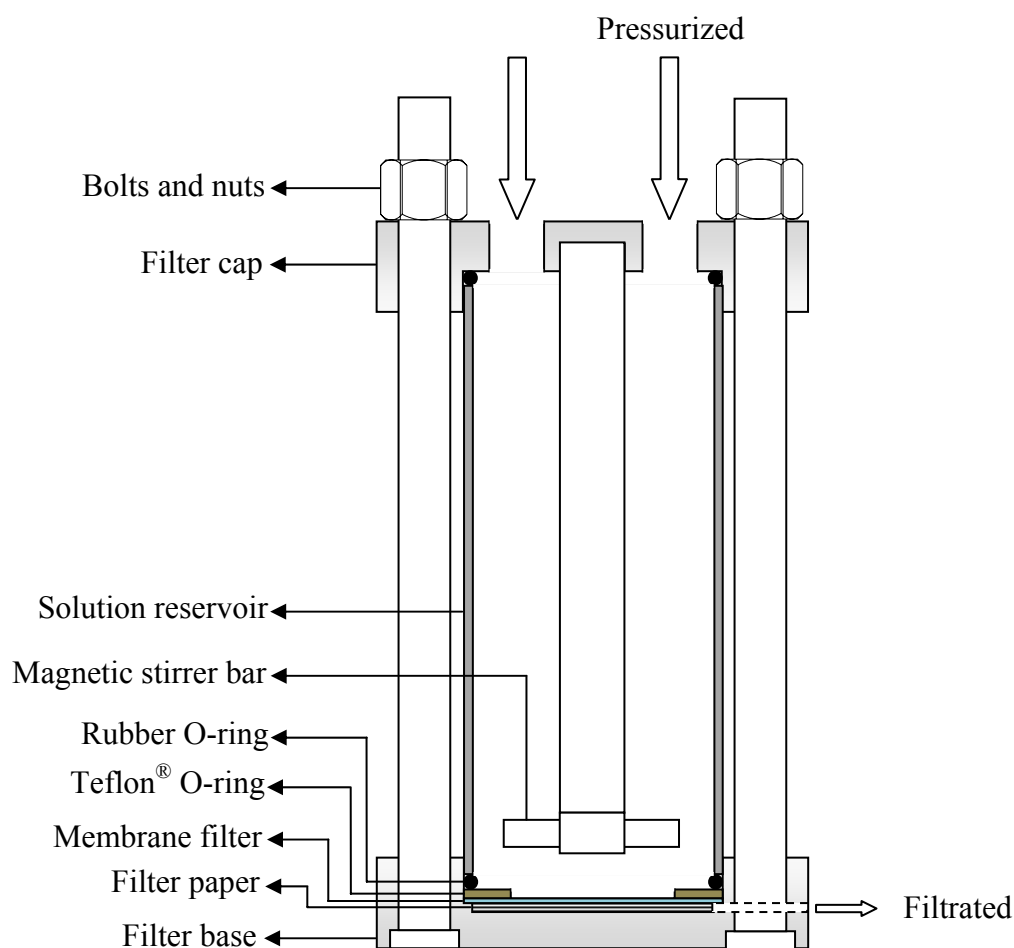


Figure 3.7: Schematic diagram of stirred filtration cell.

3.4 Characterization of Homogeneous Polysulfone and Mixed Matrix Membranes

Several characterization techniques were performed to verify the physical and chemical analysis of membranes and CMS used. The morphology of homogeneous and mixed matrix membranes, as well as the surface of CMS was verified by field emission scanning electron microscope (FESEM). Mechanical and dynamic mechanical analyses of the membranes were done by tensile test and dynamic mechanical analysis (DMA). The particle size, density, and structure were verified by particle size analyser, gas pycnometer, and X-ray diffraction (XRD). Functional groups attached to the CMS surface and the acidic capacity of CMS surface was verified by Fourier transform infrared (FTIR) spectroscopy and surface neutralization by NaOH, respectively.

3.4.1 Field Emission Scanning Electron Microscope

FESEM was used to characterize the morphology of membrane films and carbon particles. In FESEM instrument, electrons were used to form a detailed and magnified image of the sample. FESEM instrument consists of an electron emission gun placed at the top of the microscope to produce a stream of high energy electron beam. The electron beam follows a vertical path through the microscope, which is held under vacuum. The beam travels through a series of electromagnetic fields and lenses, which is designed to focus the beam down toward the sample. Once the beam hits the sample, secondary electrons are emitted from the sample surface. Detector collects these secondary electrons and converts them into a signal that is being sent to a screen to produce the final image. The schematic diagram of the electron pathway in a FESEM instrument is shown in Figure 3.8.

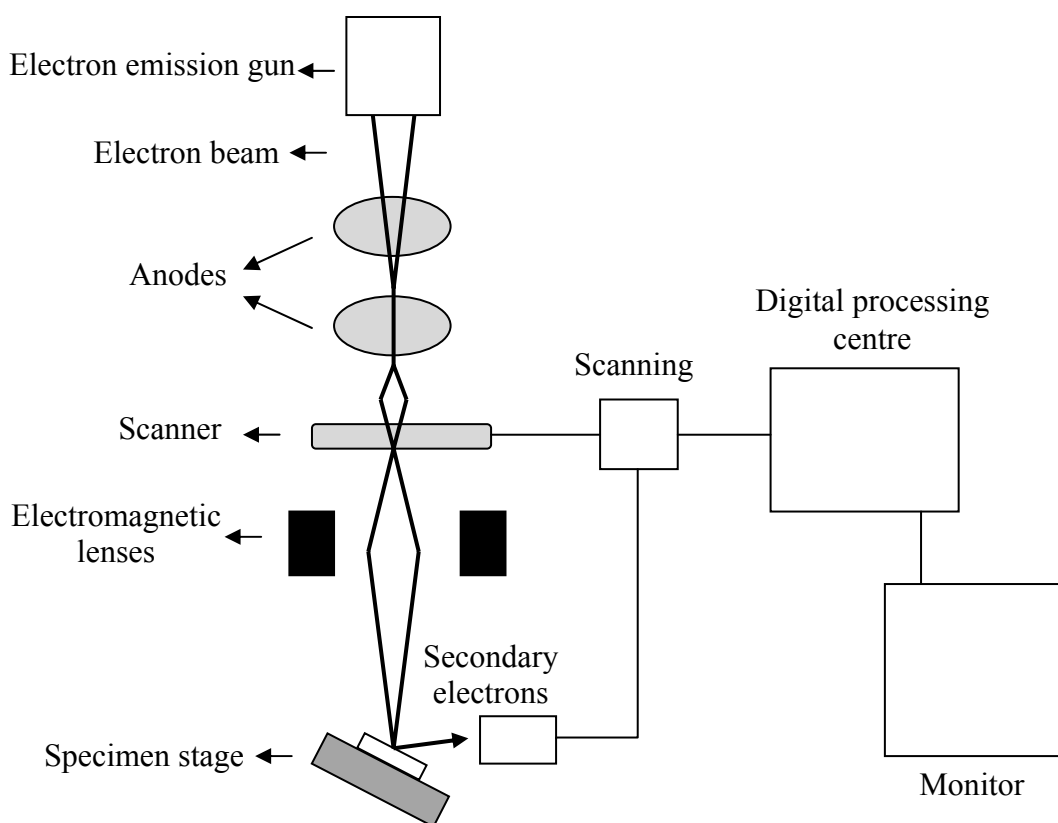


Figure 3.8: The schematic diagram of SEM instrument.

In this study, analysis using FESEM (ZEISS SUPRA™ 55VP) was done for pure polymer membrane film, mixed matrix membrane films, CMS and ox-CMS particles. For pure polymer and mixed matrix membrane films, FESEM micrographs provide a qualitative assessment on membrane morphology, polymer-sieve contact, and the homogeneity and distribution of CMS throughout the polymer matrix [30]. For the CMS and ox-CMS particles, SEM micrographs enabled a qualitative comparison on the surface porosity of CMS before and after oxidative treatment.

To characterize the membrane film, the films were initially fractured cryogenically in liquid nitrogen, to get a clear cut of the cross-section, and mounted on to a circular stainless steel sample holder with an electrically conductive double-sided tape. Immersing membrane film for several minutes in nitrogen liquid was necessary for the less brittle membrane. The samples were then sputter-coated by gold/palladium using Polaron Range SC7640 sputter coater to provide a conductive

coating that enhances the quality of images under FESEM. FESEM micrographs were examined using an accelerating voltage of 5 kV with a magnification range from 5,000 to 100,000 times.

3.4.2 Tensile Test

One of the techniques to observe mechanical properties of a material is by subjecting a known tension to a material and record the response in a stress-strain curve also known as tensile test. Although it is simple and inexpensive, tensile test is the best way of mechanical properties measurement and is very widely reported [76]. The typical stress-strain curve is illustrated in Figure 3.9. The engineering measures of stress (σ) and strain (ϵ) are determined from the measured the load (P) and deflection (δ') using original specimen cross-sectional area (A_o) and length (L_o) as:

$$\sigma = \frac{P}{A_o} \quad (3.1)$$

$$\epsilon = \frac{\delta'}{L_o} \quad (3.2)$$

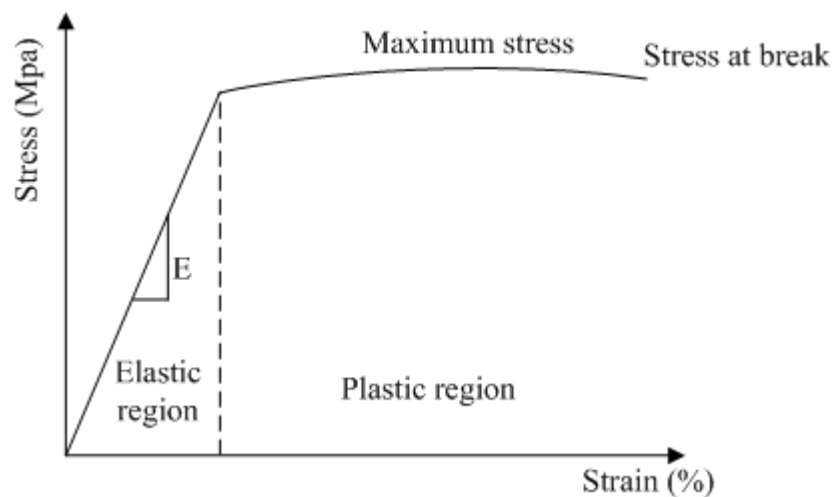


Figure 3.9: The stress-strain curve.

In early phase many material obey Hooke's law when subjected to a stress, which the stress is directly proportional to the strain and in reversible process. The constant

of the linear proportionality of stress-strain in elastic region is called the Young's modulus or the modulus of elasticity, denoted as E :

$$\sigma = E\varepsilon \quad (3.3)$$

Young's modulus value is related to the rigidity or stiffness of the material [77]. As the strain is increased the material eventually deviates from the linear proportionality and reaches the plastic region where the process is no longer reversible and end up by sample breakage. The maximum stress and strain is evaluated from this region [78]. Toughness of the material is evaluated from the area below the stress-strain curve. Toughness value indicates the maximum energy that can be absorbed by a material before rupturing.

Membrane tensile properties were determined by following standard tensile test method from ASTM D-882-02. Membrane film was clamped between grips and pulled in an opposite direction with a constant grip separation rate. The illustration of tensile test is depicted in Figure 3.10. The sample area was 100 mm×7 mm, and minimum five samples were tested. Before tested, membrane thickness and width was measured by a digital micrometer (Fowler[®]) for 10 repetitions. The tests were carried by using universal testing machine LR 5K from Lloyd Instruments at 1 mm/min grip separation rate.

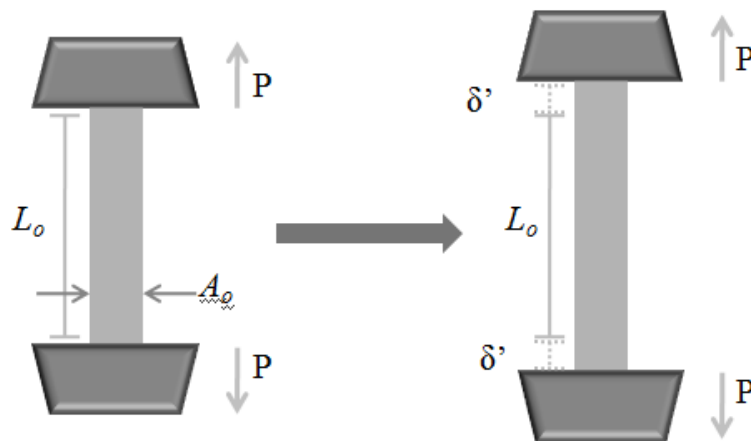


Figure 3.10: The illustration of tensile test.

3.4.3 Dynamic Mechanical Analysis

DMA technique was used to study the viscoelastic properties of a material. DMA can be simply described as applying an oscillatory force (stress, σ) to a sample and analyzing the material's response (strain, γ) to that force [79]. The stress is applied sinusoidally with a defined frequency, which generates a sinusoidal strain. In DMA, a complex modulus (E^*), an elastic (storage) modulus (E'), and viscous (loss) modulus (E'') are calculated from the material response to the sin wave. The phase lag between stress and strain sine waves is used to calculate the $\tan \delta$. The ratio of loss modulus and storage modulus is the value of $\tan \delta$, which indicate the ability of the material to dissipate energy in the form of heat [79]. The illustration of the stress-strain sine waves are shown in Figure 3.11.

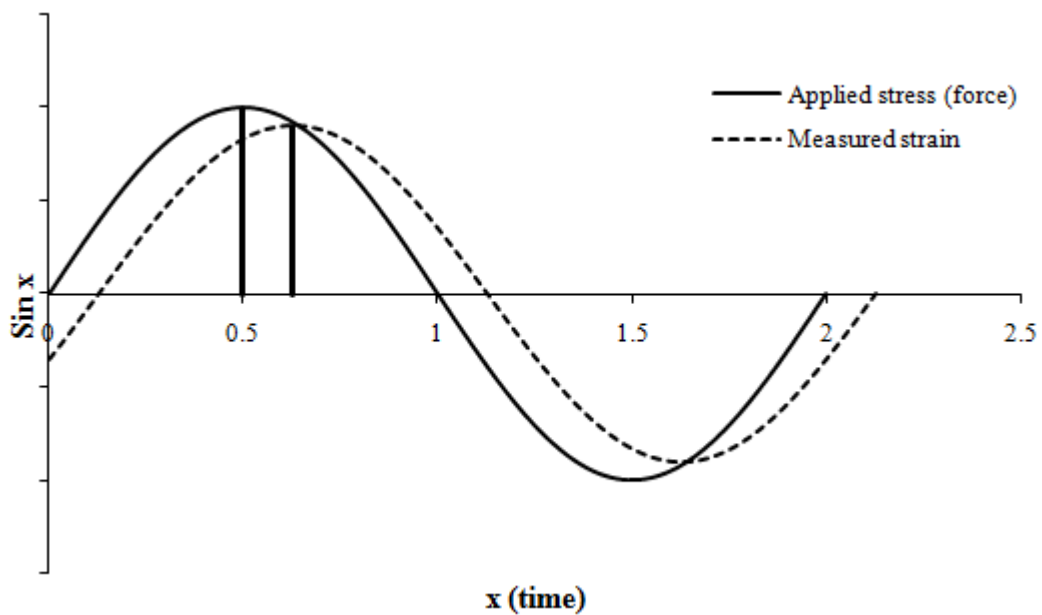


Figure 3.11: The sinusoidal wave of stress and strain in DMA.

In this study, Mettler Toledo DMTA 862 was used to characterize the viscoelastic properties of the membrane films. All measurements were done in Universiti Sains Malaysia, Penang. According to ASTM D 4065-01, the analysis was carried out with oscillatory mode, forced constant amplitude, fixed frequency, and tensile oscillation. Samples were cut into 10×5 mm rectangular shape with a thickness of 100 μm , For

consistency, all experiment were performed with 1 Hz frequency, 0.1 % strain, and a 2°C/min heating rate with an operational temperature range of 30-220°C. The maximum of the $\tan \delta$ peak was considered as the T_g of the film [80].

3.4.4 Particle Size Analysis

The particle size analysis was performed by using Mastersizer-Scirocco 2000 from Malvern Instrument. The measurement was carried out by laser diffraction technique. The samples were passed through a focused laser beam, and the lights scatters at an angle that is inversely proportional to their size. The angular intensity of the scattering lights was then measured by a series of photosensitive detectors.

3.4.5 X-Ray Diffraction

XRD is a versatile, non-destructive analytical technique that reveals the detailed information about chemical composition and the crystallographic structure of materials. The technique is based by observing the pattern of scattered reflected beam from a monochromatic X-ray beam that projected onto a material. Based on the arrangement of the atoms, solid material can be described as amorphous or crystalline. The atoms in amorphous material are arranged in a random way; on the other hand the atoms are arranged in a regular pattern in crystalline material. When an X-ray beam hits an atom, the electrons around the atom will oscillate with the same frequency as the incoming beam and interfere in both destructive as well as constructive direction with the beam from nearby atoms, as illustrated in Figure 3.12. According to Bragg's law, constructive interference only happens when the path difference of the waves ($2d \sin\theta$) is equal to an integer (n) multiple of the wavelength (λ), written as:

$$2d \sin \theta = n\lambda \quad (3.4)$$

The constructive interferences are recorded to construct the diffraction pattern of the material. XRD spectra are plotted as intensity of XRD spectra (Cps) against diffraction angle (2θ).

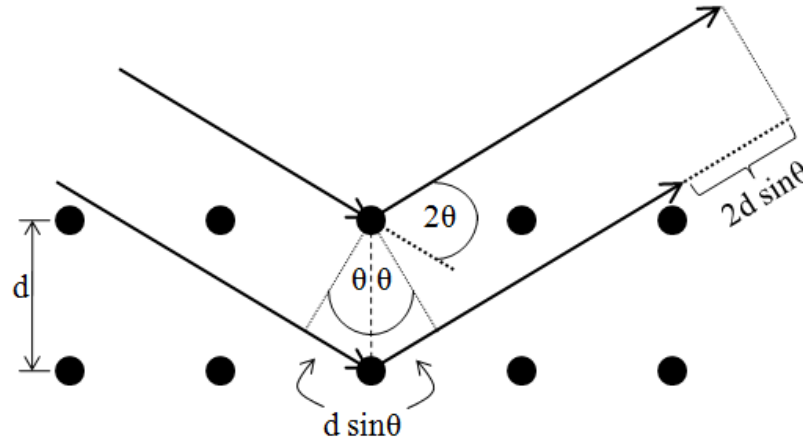


Figure 3.12: Bragg's diffraction.

In this study the average d-spacing of CMS was determined by using XRD technique with graphite as the reference. The value of d-spacing indicates the spacing between the adjacent carbon atoms within the graphitic plane. Bruker A&S D8 advanced diffractometer equipped with a $\text{CuK}\alpha$ radiation source (at 4 kV and 30 mA, in the scanning angle (2θ) range of 2-60°C at scanning speed of 1.2°C/min) was used for the present analysis.

3.4.6 Density Measurement

The density of the carbon particles was measured by gas pycnometer. The true volume was measured by employing Archimedes's principle of fluid displacement and gas expansion. Helium was chosen due to its small kinetic diameter of 2.6 Å, therefore it could access all porosity with diameter less than 2.6 Å. The density was measured by comparing the volume of gas in the empty sample cell with the filled cell. The density measurement was performed by using Ultrapycnometer 1000 from Quantachrome Instrument. The schematic of the instrument is shown in Figure 3.13.

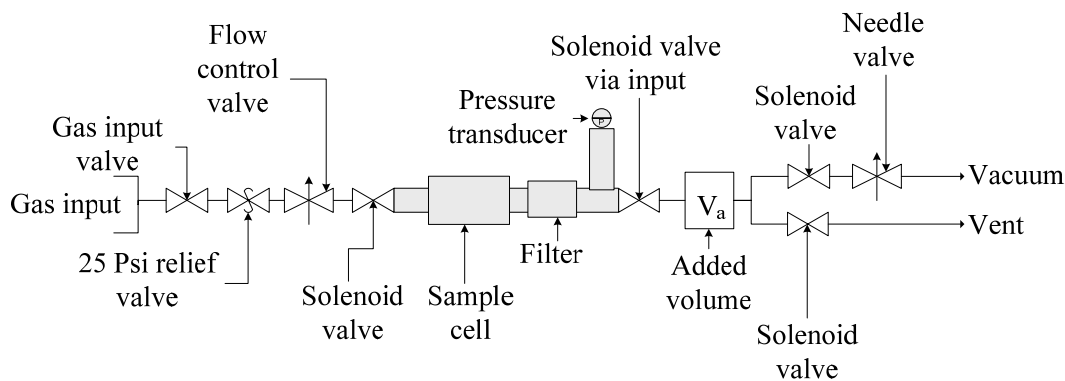


Figure 3.13: Schematic of a gas pycnometer.

A certain weight of samples were loaded in a micro sample cell and allowed to settle in the cell holder. Before each measurement the sample was purged to remove contaminants if any and the trapped air. The cell was vented to ambient until the stable pressure was reached. Subsequently, the system was pressurized to the target pressure of 19 psi. When the pressure has stabilized, the true density was obtained. For each sample the measurement were made for 10 times to maintain higher accuracy and reproducibility.

3.4.7 Fourier Transform Infrared Spectroscopy

Infrared spectroscopy is a technique used to identify the presence of a certain functional group in a molecule by observing the specific absorption of radiation by each molecule in the sample. The practical use of infrared radiation in organic chemistry is limited to the portion between $4000\text{-}400\text{ cm}^{-1}$. In this region the infrared radiation is converted by the organic molecular into its vibrational and rotational energy. The frequency or the wavelength of absorption depends on the relative mass of the atoms, the force constant of the bonds, and the geometry of the atoms [81].

FTIR instrument is equipped with infrared source, interferometer, detector and computer. Infrared radiation from the source are send to the interferometer, where the light will passes through a beam splitter and send into two direction which are at right angles. One beam goes to the stationary mirror and sends back to the beam splitter,

and the other beam goes to the moving mirror. The motion of the moving mirror makes the total path length of the beam vary versus that taken by the stationary mirror, and when they recombine at the beam splitter it creates an interferogram. The recombined beam passes through the sample where it is absorbed at different wavelength and constructs its specific spectrum. Finally the intensity of the beam is detected by a detector and then digitized to construct the intensity vs. frequency spectrum. The schematic of FTIR instrument is depicted in Figure 3.14.

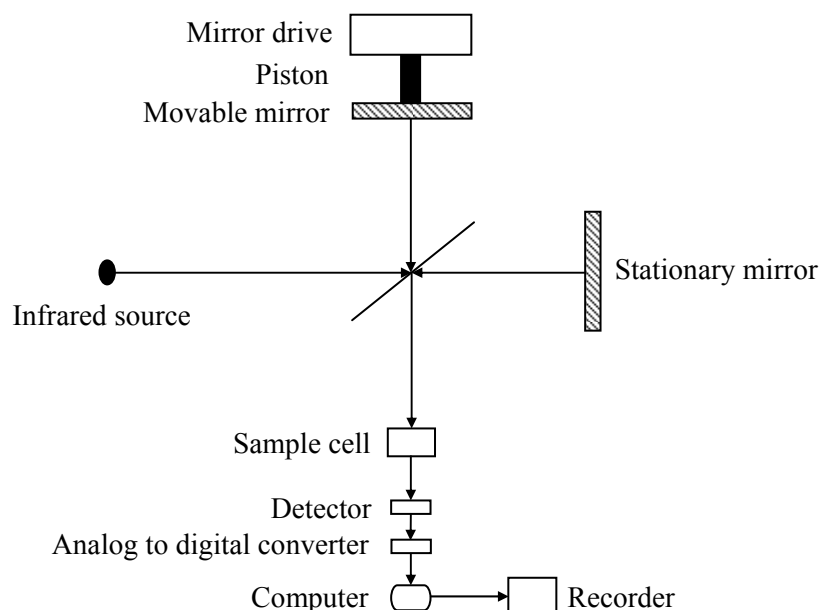


Figure 3.14: Schematic of FTIR instrument.

In the present work, all of infrared spectrums were recorded by using Perkin-Elmer[®] infrared instrument and analyzed by using Spectra One[®] software. Spectrums were obtained by co-addition of 200 scans at a resolution of 4 cm^{-1} in the range of $400\text{-}4000\text{ cm}^{-1}$. The sample pellets were prepared by mixing 6 gram of CMS powder with 600 mg of potassium bromide (KBr) and by adding 20 mg aliquot of this mixture to 200 mg of KBr. The samples were dried overnight at 110°C and pressed just before the measurement.

3.4.8 Determination of Acidic Functionality on Carbon Molecular Sieves Surface

The traditional Boehm's titration method [74] was employed to determine the acidic properties of the ox-CMS. The amount of carboxylic group attached to the surface of the ox-CMS was determined by its neutralization with sodium hydroxide (NaOH, R&M Chemicals[®]) and then followed by titration using hydrochloric acid (HCl, Merck[®]). This was achieved by contacting 1 g of ox-CMS with 50 ml of 0.5 M NaOH in a 125 ml polyethylene bottle. A control solution was prepared by adding 50 ml of the 0.5 M NaOH into an empty bottle. Both the sample and the blank solution were allowed to equilibrate in an orbital shaker for 72 hours. A 20 ml aliquot of the mixture was pipetted into a 250 ml Erlenmeyer flask and titrated against standardized 0.5 M HCl. Phenophtalein was used as the indicator. All titrations were done in duplicate and the average values are reported. The concentration difference of the control and the sample solution was assumed to be equal to the number of moles of NaOH neutralized by the acidic functional groups on the surface of 1 gram of the ox-CMS powder.

3.5 Gas Permeation Study

The performance of flat membranes was evaluated by using a gas membrane permeation unit, as depicted in Figure 3.15. The permeation testing depends on maintaining both the pressure on the feed phase and measures the gas flux across a known thickness and area of membrane on the permeate phase. Pure CO₂ and CH₄ were employed as the test gases with different feed pressure of 2, 4, 6, 8 and 10 bars. All tests were carried out at room temperature (25°C) condition.

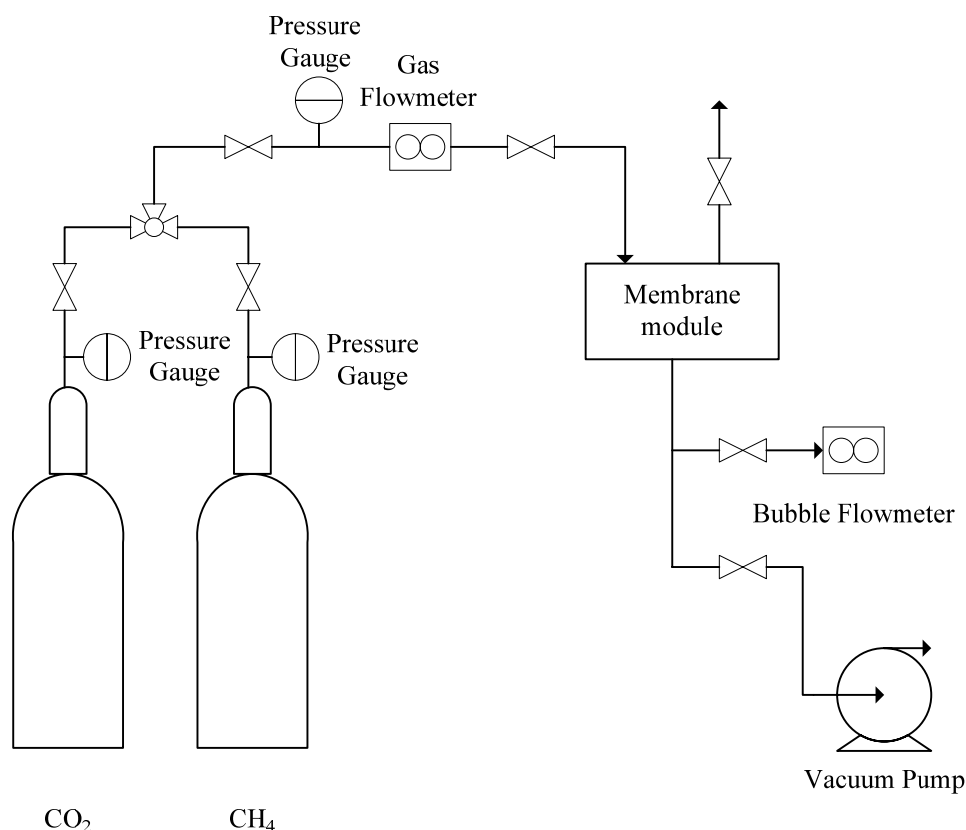


Figure 3.15: Schematic of gas membrane permeation test unit.

The permeation test system is equipped with a feed gas tank (CO_2 and CH_4), pressure gauges, gas flowmeter, dead-end membrane test module, bubble flowmeter and vacuum pump. Swagelok[®] fittings and valves are used in the test system. Bubble flowmeter was used to measure the permeate gas flowrate because of its ability to measure accurately at low flowrates ($< 100 \text{ ml/min}$) of gas into compared to the electronic flowmeter [25].

A circular membrane was cut into a 5 cm diameter and dried at 110°C for one hour to remove any adsorbed moisture. Before being placed in the membrane module, the membrane was measured for 10 repetitions using digital micrometer (Fowler[®]). Underneath the membrane, a circular perforated thick polypropylene sheet (PP) and mesh were placed as the support. Two O-ring seals were used to prevent any gas leakage from the membrane module. The top half of the membrane module was attached to the upstream of the system and the lower half was attached to the

downstream of the system. The retentate valve was closed during the test. The upper half and the bottom half was coupled together by using five bolts and nuts. The schematic diagram of the membrane module is shown in Figure 3.16.

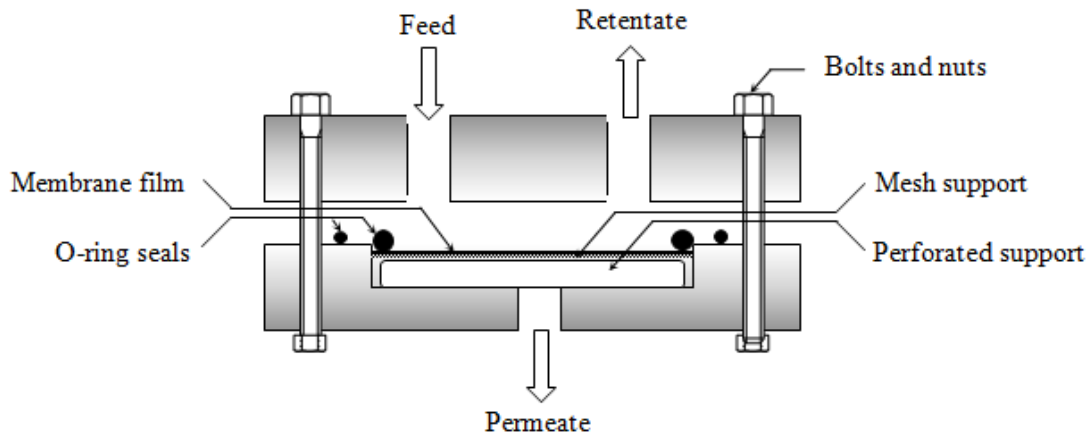


Figure 3.16: Schematic of the membrane module.

Before the start of the experiment, the system was vacuumed for 10 minutes to remove residual gases remaining in the system. The feed gas was directly supplied from the gas cylinder, equipped by a pressure gauge. A three-way valve was attached as the entry point of the system allowing only one pure gas stream can enter the system at a time. Before entering the membrane module, the feed stream pressure was measured by a pressure gauge. Each run was conducted at required feed stream pressure i.e. 2, 4, 6, 8, and 10 bars. The flow rate of the permeate stream was measured by a bubble flowmeter, and the permeate stream was assumed to be at atmospheric conditions. The permeate flowrate was recorded every 20 minutes for 3 to 4 times, until the difference is not greater than 5%. The permeability (P_i) of each gas was determined by the following expression:

$$P_i = \frac{Q_i \cdot 273 \cdot \ell}{T_i \cdot A \cdot \Delta p_i} \quad (3.5)$$

where Q_i is the volumetric flowrate (cm^3/s) of the permeated gas, ℓ is the thickness of the membrane film (cm), T_i is the absolute temperature (K), A is the effective area of the membrane (cm^2), and Δp_i is the partial pressure driving force of the gas component's (cmHg). Permeability of the membranes were reported in the unit of

Barrer (1 Barrer = 10^{-10} cm³ (STP) cm/cm² s cmHg). The ideal selectivity (α_{CO_2/CH_4}) of the membrane with respect to CO₂ and CH₄ was determined as the ratio of CO₂ permeability over CH₄ defined as,

$$\alpha_{CO_2/CH_4} = \frac{P_{CO_2}}{P_{CH_4}} \quad (3.6)$$

Plots of the pure gas permeability of CO₂ and CH₄ as well as the membrane ideal selectivity against operating pressures were drawn and presented in Chapter 4.

CHAPTER 4

RESULTS AND DISCUSSIONS

In this study, mixed matrix membranes were fabricated using polysulfone (PSU) and carbon molecular sieves (CMS) particles as the filler. Further modification to enhance the adhesion of polymer matrix and the sieves surface were carried out by annealing treatment of mixed matrix membranes and by using surface functionalized molecular sieves. In Section 4.1 the physical characterization of pure PSU membranes are discussed. The characteristics of mixed matrix membranes and CMS particles used, as well as the effect of annealing treatment to the membranes are discussed in Section 4.2, whereas modification of the CMS surface by oxidation process and its effects on the membrane characteristics are discussed in Section 4.3. Section 4.4 deals with discussion on separation performance of each membrane.

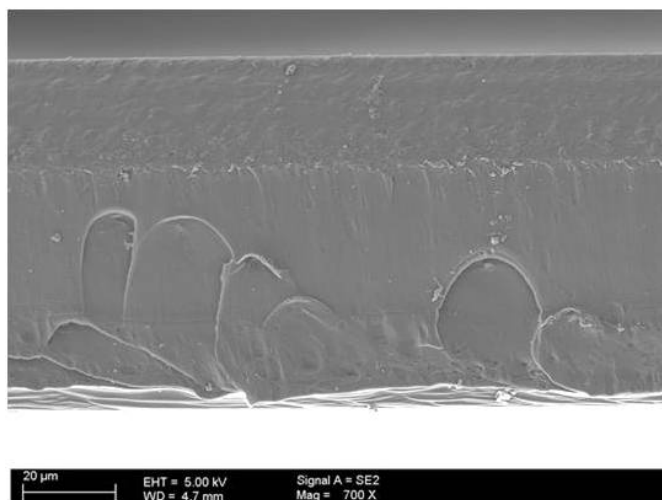
4.1 Formation of Homogeneous Polysulfone Membranes

During the elementary step of pure PSU membranes fabrication, the casting solutions were prepared in three different polymer concentrations, of 10, 15, and 20 wt.% PSU, in order to choose the suitable polymer concentration for the subsequent fabrication process. The morphology, mechanical, and viscoelastic properties of the membranes were analyzed by field emission scanning electron microscope (FESEM), tensile test, and dynamic mechanical analysis (DMA).

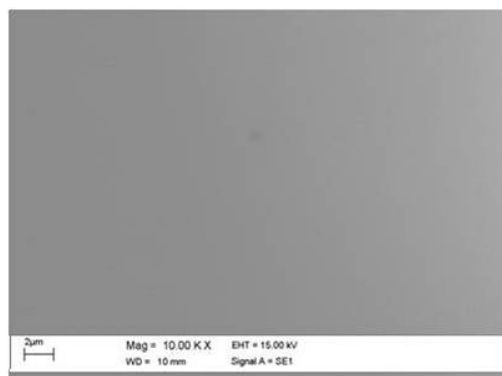
4.1.1 Effect of Polysulfone Concentration

Figure 4.1 shows FESEM micrographs of PSU dense homogeneous membranes. With increase in polymer concentration no change in the morphology was observed,

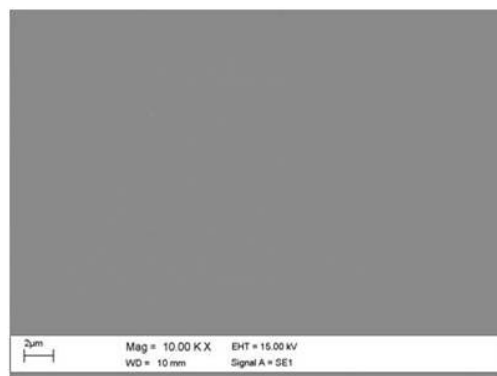
whereas increase in polymer concentration leads to an increase in viscosity of the casting solution, which can be seen visually through the formation of gel-like solution at higher polymer concentration. Consequently, the membranes thickness increases with polymer concentration. When a 250 μm casting gap was used, dry membrane film with polymer concentration of 10, 15, and 20 wt.% was resulted in 38, 53, and 87 μm in average thickness respectively.



(a)



(b)



(c)

Figure 4.1: Field emission scanning electron micrographs of 15 wt.% polysulfone membrane: (a) cross-section (700 \times); (b) top section (10K \times); (c) bottom section (10K \times).

A dense homogeneous polymeric membrane was found to be the simplest morphology, with a nonporous, dense, single polymer that was homogeneous in all

directions. Therefore, it is the most suitable structure to investigate the chemical and structure modification of the membrane [82]. Since PSU backbone possesses the polar $\text{—SO}_2\text{—}$ groups and rigid aromatic rings, it had caused the structure very rigid and coagulative leading to higher viscosity of casting solution when higher PSU concentration were used [83].

Although the morphology of the membrane remains the same for different polymer concentrations, the mechanical properties of the membrane were found to vary depending on the percentage of polymer used. Figure 4.2 shows the stress-strain curve of the homogeneous PSU membranes and the corresponding mechanical properties are listed in Table 4.1. The strain-stress curve shows that in early strain, all samples were obey the Hooke's law, where stress is proportionate to the strain. But as stress was increased, it started deviate from the linear proportionality. Here the material was undergoing rearrangement on its intermolecular structure towards its new equilibrium structure [78]. The profile of the curve indicated a ductile material behaviour, where the stress continued to rise beyond the proportional limit, until it was finally ruptured.

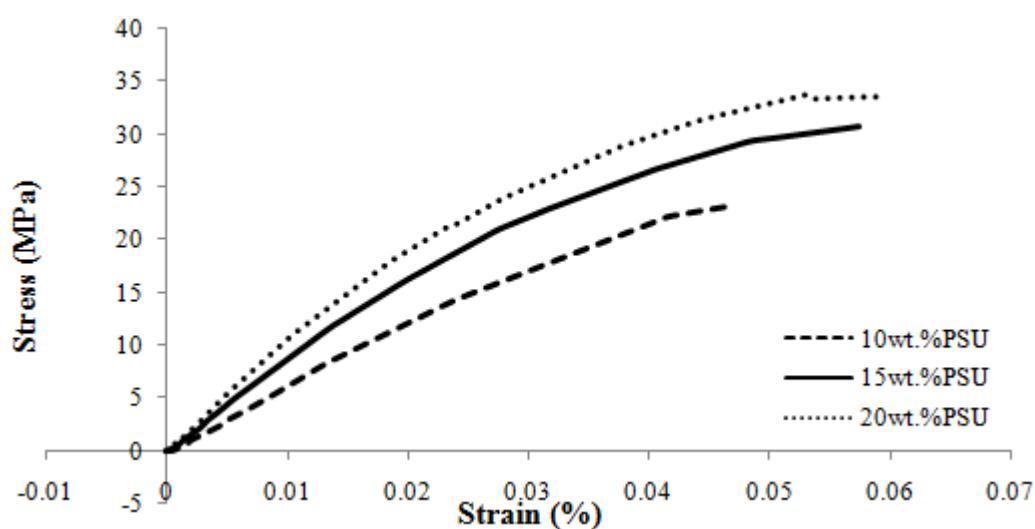


Figure 4.2: Stress-strain curve of homogeneous PSU membranes in different polymer concentrations.

Table 4.1: Effect of polymer concentration to the mechanical properties of the membrane films.

Mechanical properties	Polymer concentration (wt.%)		
	10	15	20
Young's modulus (MPa)	1636	1786	1770
Tensile strength (MPa)	23.17	33.68	33.29
Strain (mm/mm)	0.0464	0.0573	0.0594
Toughness (J/m ³)	0.5252	0.5809	0.5954

Table 4.1 shows that all mechanical properties including Young's modulus, maximum tensile stress, strain at maximum stress, and toughness of the membranes were found to significantly increased with increasing polymer concentration from 10 to 15 wt.%, however the properties of 20 wt.% polymer does not significantly differ from the 15 wt.%. This is due to the increase in polymer chain entanglement with polymer concentration lead to constrain the polymer chain mobility resulting in a stiffer film. This is further strengthen by the presence of polar —SO₂— groups and rigid aromatic rings in the PSU backbone [83], hence the Young's modulus of the film showed an increasing trend when increasing polymer concentration. Following the Young's modulus, the tensile strength and the toughness of the films show an increasing trend. The toughness of the membrane was calculated from the area of the stress-strain curve, which shows an increment with increasing polymer concentration. In line with tensile stress, by increasing polymer concentration tensile strain at maximum stress also shows an increasing trend. Increase in the number of chain entanglement in the film enables the membrane to have longer elongation.

Table 4.1 is also shown that the change in the properties are minimum or negligible for 15 and 20 wt.% polymer films, yet an increase in viscosity of the solution was noticed. High viscosity solution could led to an aggregation of filler particles as has been reported by Vu [20] and Vankelecom et al. [40] in CMS-polyimide and zeolite-polyimide system, respectively. Therefore, to minimize the agglomeration of CMS particles in highly viscous solution, 15 wt.% of polymer was maintained as the bench mark for further membrane fabrication processes. Hence, the

dynamic mechanical analysis for homogeneous PSU membrane was carried out for 15 wt.% polymer only.

Figure 4.3 shows the $\tan \delta$ and storage modulus (E') profile of homogeneous PSU membrane plotted against temperature. $\tan \delta$ indicates the damping ability of the membrane, while storage modulus indicates the stiffness of the membrane. Between the initial temperature and 180°C, both $\tan \delta$ and storage modulus maintain a plateau, indicates an elastic behaviour of PSU on its glassy state. As the temperature increased the storage modulus drops sharply, whereas $\tan \delta$ increases sharply, indicates the movement of the polymer chains has begun which transformed the polymer to its rubbery state. The T_g value for the homogeneous PSU membrane was observed at 195.5°C, measured from the peak of the $\tan \delta$ curve. A single peak of $\tan \delta$ shows a homogeneous distribution of polymer chain within the membrane film.

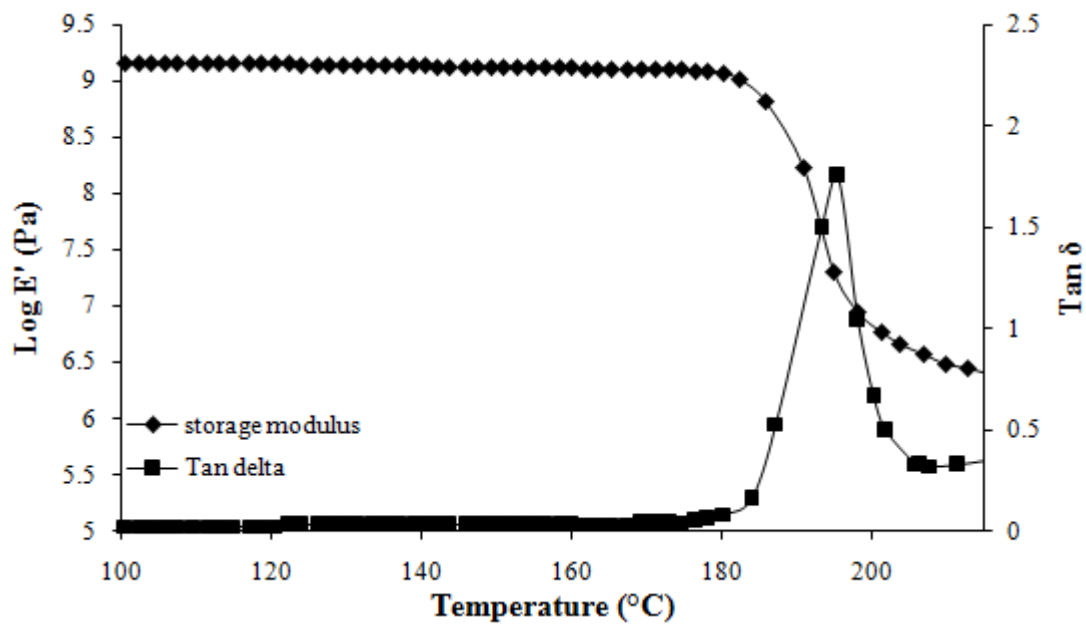


Figure 4.3: $\tan \delta$ and storage modulus profile of homogeneous PSU membrane.

4.2 Formation of Mixed Matrix Membranes with Carbon Molecular Sieves

Mixed matrix membranes comprised of PSU and CMS were fabricated in various CMS loadings. CMS particles properties were evaluated by FESEM, X-ray diffraction (XRD), gas pycnometer, and adsorption study. The effect of filler loading and annealing treatment to the morphology, viscoelastic, and mechanical properties of the membranes were discussed.

4.2.1 Characterization of Carbon Molecular Sieves

Figure 4.4 shows the field emission scanning electron micrograph of CMS powder. The micrograph confirmed that CMS powder has a wide range of particle size distribution. The particle size distribution of the powder was found within the range of 0.20 to 4.00 μm with an average size of $0.964 \pm 0.588 \mu\text{m}$. Rough surface and non-uniform shape of CMS shown in Figure 4.4 was due to the grinding process.

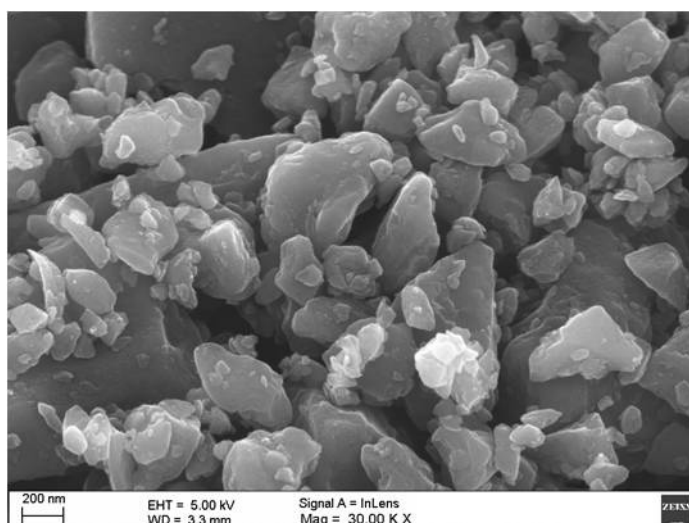


Figure 4.4: Field emission scanning electron micrograph of CMS powder (30K \times).

X-ray diffraction (XRD) characterization gives the average d-spacing in a material, which is visualized as the average spacing between the centers of chains in the molecular matrix. The XRD spectra of CMS particles, shown in Figure 4.5, gave a broad peak at $2\theta = 22.35^\circ$ with d-spacing value of 3.65 \AA , scattered-like spectra

shows an amorphous structure of CMS. A single crystalline peak for graphite is observed at 3.35 \AA , as reported by Steel [46]. Higher d-spacing from the CMS particle used is due to the less ordered structure in CMS compared to the standard graphite structure. A peak also appeared at $2\Theta = 43.35^\circ$ with d-spacing of 2.09 \AA , approximate with the d-spacing of 100 plane in graphite (2.1 \AA), this phenomena indicates the conjugate aromatic graphitic planes without the long range order formed in the structure of CMS, which are similar to graphite [30, 46].

The density of CMS particles were measured by gas pycnometer (Ultracycrometer 1000, Quantachrome Instruments) and resulted in the value of 2.1664 g/cm^3 , where the density value of graphite without pores is 2.3 g/cm^3 [30]. Lower value of density indicates a less packed and ordered structure of CMS compared to graphite. Amorphous state of CMS is responsible for the disordered structure of CMS.

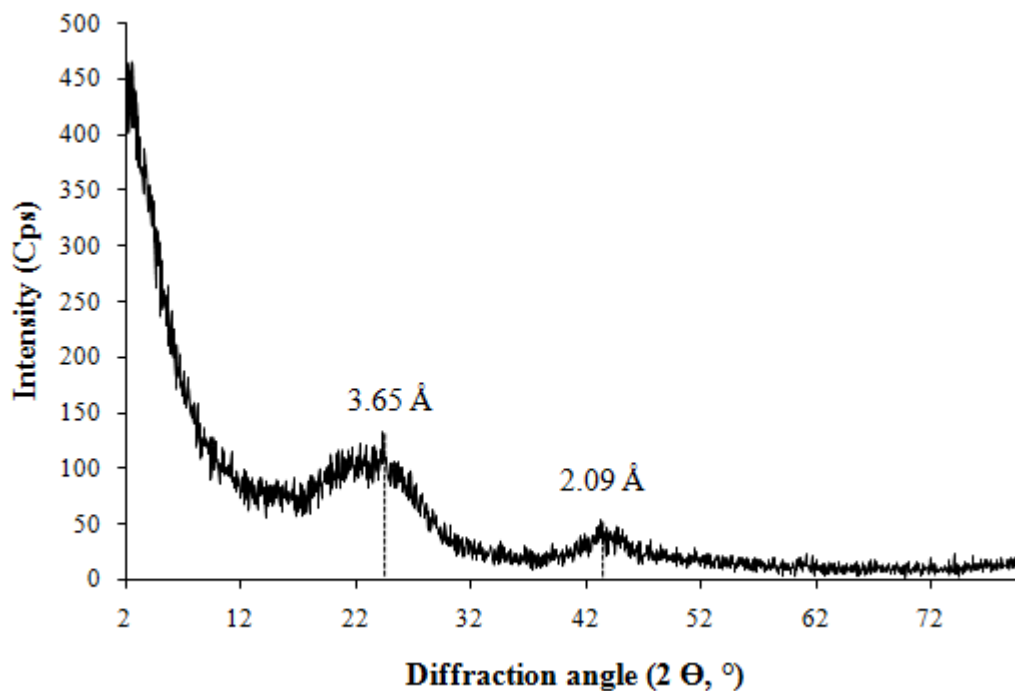


Figure 4.5: XRD spectra of CMS particle.

The equilibrium based adsorption study on CMS used (Alhamid [84]) showed its higher capability for CO₂ adsorption compared to CH₄. It has been proved that CMS showed a relatively slower adsorption of CH₄ compared to CO₂. The diffusivity ratio of CO₂ and CH₄ (D_{CO_2} / D_{CH_4}) on CMS were calculated as 68.77, therefore it is feasible to separate CO₂ from CH₄ by using CMS [84]. Since CO₂ has a smaller kinetic diameter than CH₄, 3.3 Å and 3.8 Å, respectively, CO₂ is more strongly adsorbed on CMS compared to CH₄. A similar kinetic diameter of CH₄ and the CMS pore size (3.8 Å) were responsible for the slow adsorption of CH₄ onto the CMS surface.

4.2.2 Characterization of Mixed Matrix Membranes

Mixed matrix membranes comprised of PSU and CMS particles were made using three different CMS loading, of 10, 20, and 30 wt.%. Higher loading as high as 40 wt.% were attempted in earlier fabrication stage, however, the membranes formed were brittle and could not be handled without a support layer, which made it impossible to used in further characterization process. Annealing treatment above its T_g were subjected to improve the polymer-filler adhesion. The behaviour of CMS particles within the polymer matrix were evaluated by FESEM, DMA, and tensile test.

4.2.2.1 Effect of Carbon Molecular Sieves Loading

Homogeneous distribution of CMS particles (10 & 20 wt.%) in the polymer matrix are shown in Figure 4.6(a)-(b). However, with increasing CMS loading, not all particles distributed homogeneously in PSU matrix, dense CMS regions started to appear, as shown in Figure 4.6(c) for 30 wt.% of CMS content. The formation of CMS clusters due to the nature of carbon materials which have a hydrophobic surface and thus readily agglomerate under aqueous conditions [85].

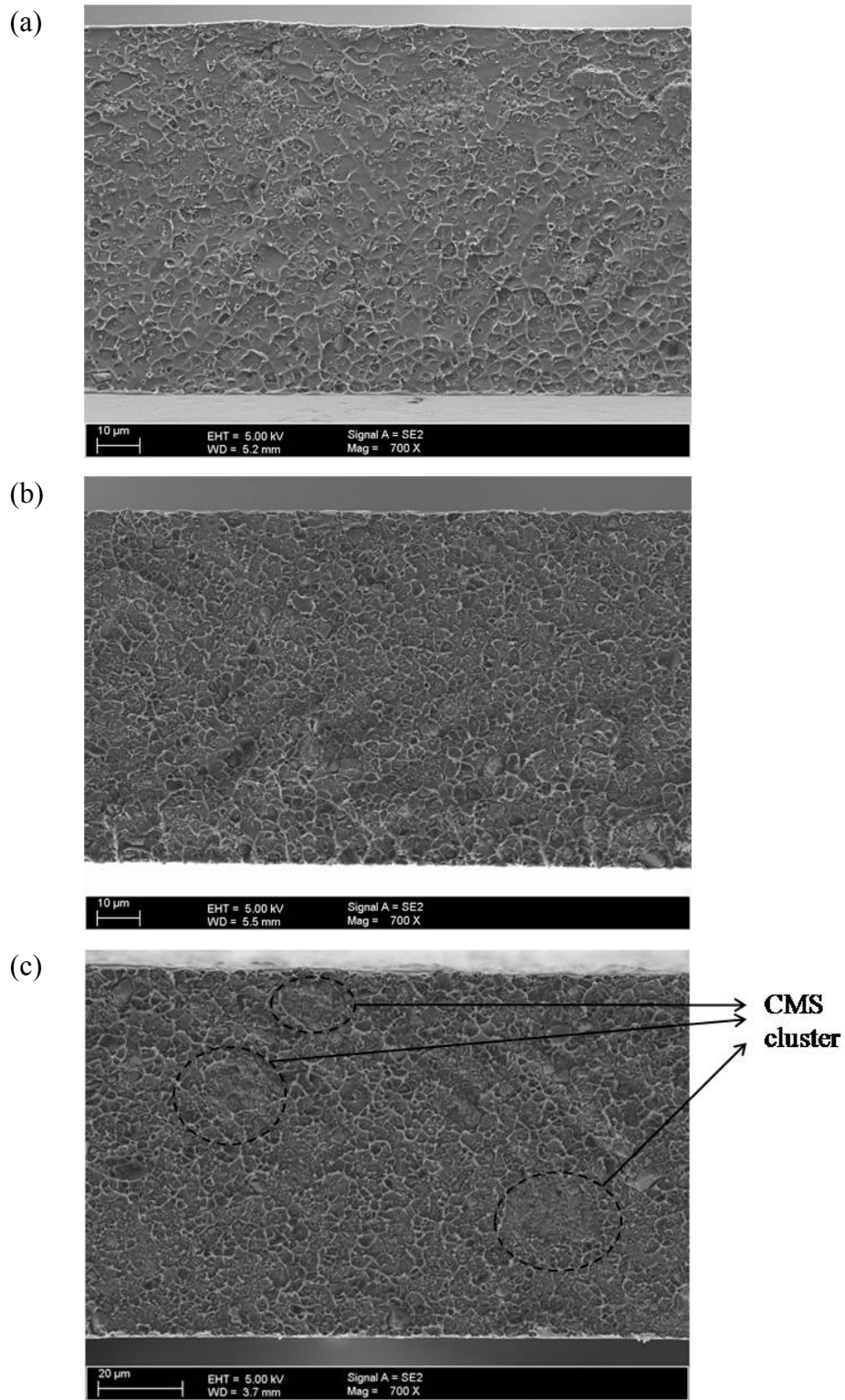


Figure 4.6: Field emission scanning electron micrograph of mixed matrix membrane using CMS in different loadings: (a) 10 (700 \times); (b) 20 (700 \times); and (c) 30 wt.% (700 \times).

In the dispersion of carbon powder in aqueous solution, there is a competition between the shearing forces that applied to break the agglomeration and the cohesive force which keep the agglomerate to resist dispersion [86]. In higher loading CMS clusters were formed by the smaller particles. Dispersion is more difficult to achieve in higher loading since van der Waals interparticles attractions between CMS particles are more dominant compared to other interactions in the solution [52]. But despite the agglomeration of CMS, areas with well-dispersed CMS in high loading of CMS still exist. Some modifications in the fabrication process were then applied such as sonication and sieving of molecular sieve particles to enhance the homogeneity of CMS distribution within the polymer matrix. Higher magnification (25K ×) of FESEM in Figure 4.7 shows a good adhesion between CMS and PSU matrix. A good polymer-CMS adhesion also reported by Vu [20], when working with self-pyrolyzed CMS and polyimide (Matrimid[®] 5218 and Ultem[®] 1000) systems.

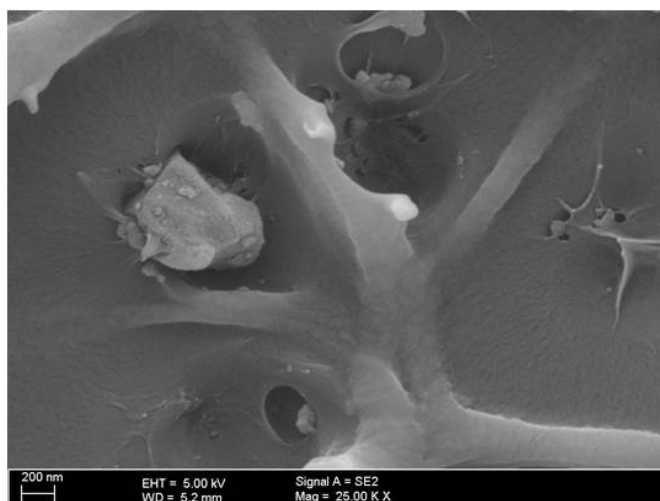


Figure 4.7: Field scanning electron micrograph of CMS and PSU interaction (25K ×).

The results obtained from DMA shows that mixed matrix membrane exhibited two $\tan \delta$ peaks, reflecting the presence of two glass transition temperatures (T_g). The $\tan \delta$ profile for each mixed matrix membranes are depicted in Figure 4.8 and the corresponding results are presented in Table 4.2. The first peak assigned to the T_g of unfilled polymer. While, the second peak assigned to the T_g of polymer chain experiencing mobility restrictions due to its interaction with the filler particles [87].

The position of the maximum in the first $\tan \delta$ peak is slightly shifted to a lower temperature by increasing filler content, while the peak appear to be broader and decreases in area. Located in 33-37°C higher than the first $\tan \delta$ peak, the second peak appears. Compared to the first peak, the second peak is broader and the peak size decreases as its maximum shift to a lower temperature with increasing filler content.

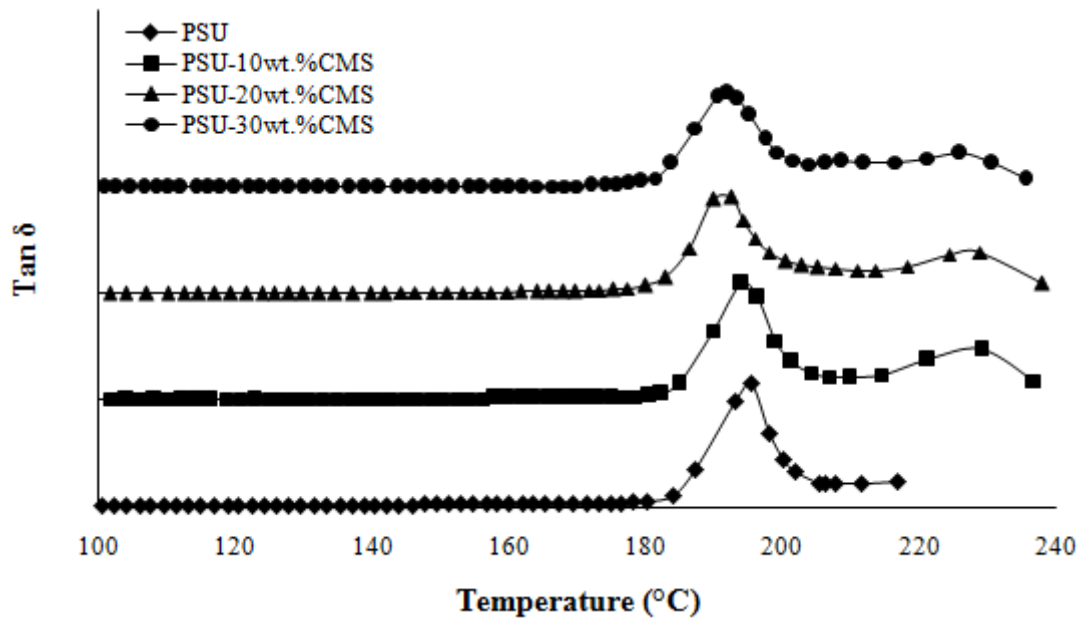


Figure 4.8: $\tan \delta$ profile for mixed matrix membranes with different CMS loadings.

Table 4.2: $\tan \delta$ curve properties of mixed matrix membranes with different CMS loadings.

Membrane	$\tan \delta_1$	$\tan \delta_2$	T_{g1} (°C)	T_{g2} (°C)	Area ₁	Area ₂
PSU	1.75	-	195.50	-	23.23	-
PSU-10wt.%CMS	1.65	0.73	194.15	229.08	20.41	14.87
PSU-20wt.%CMS	1.37	0.60	192.53	229.00	18.42	13.72
PSU-30wt.%CMS	1.34	0.49	192.09	225.96	17.69	11.68

Figure 4.9 shows the storage modulus (E') vs temperature also showing a dual drop profile corresponds to the $\tan \delta$ profile. A sharp drop in storage modulus appears at the first T_g for all samples. The magnitude of the drop depends on the filler content,

and it becomes smaller with increasing the filler content. The drop magnitude of storage modulus indicates the reinforcement or stiffness of membrane with the addition of CMS. The smallest drop observed at 30 wt.% of CMS content showing the largest reinforcement by CMS. The second drop appears at higher temperature, signifying the second T_g . A plateau-like region appears between the first and the second T_g for all samples. The region is broader for higher filler content.

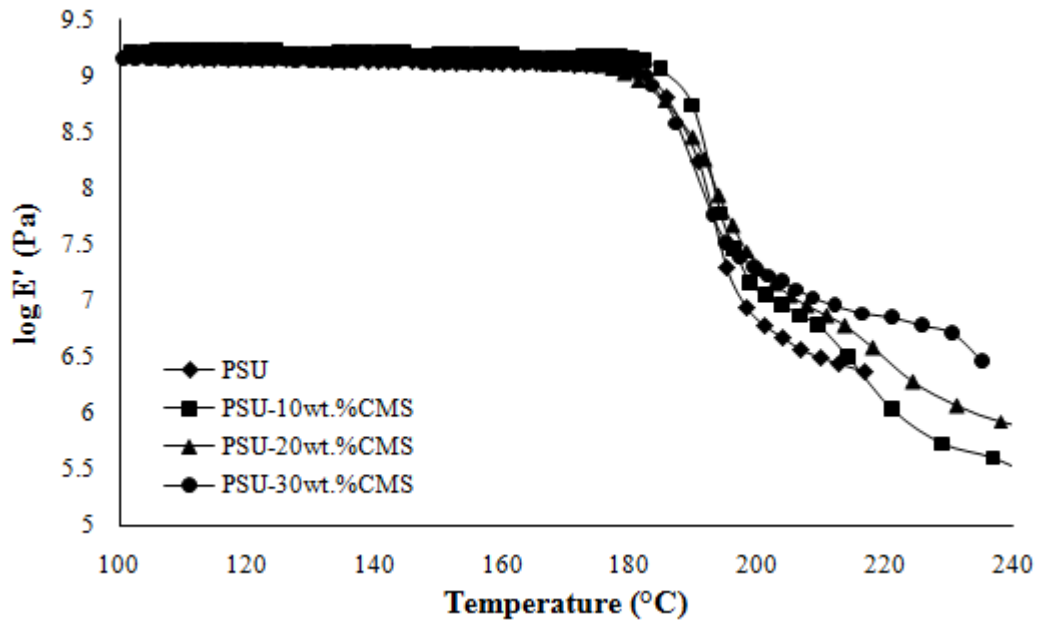


Figure 4.9: Storage modulus profile for mixed matrix membranes with different CMS loadings.

The presence of dual T_g in composite materials indicate the existence of interphase between the filler surface and the polymer. According to Kim [88], dual T_g appear only when the fine particles are used as filler, and the interaction between the filler surface and polymer are strong enough. A dramatic reduction in chain mobility is experienced by the segment of the polymer interacting with the solid surface. This may be due to the entropy effects, local ordering or crowding at the interphase [88]. The properties of the polymer chains forming the interphase deviate significantly from their corresponding value in the bulk phase. The morphological transformation in filled polymer model proposed by Tsagaropoulos and Eisenberg [87] (illustrated in Figure 4.10) is used to understand these phenomena. In their study, they observed

dual $\tan \delta$ peak of silica filled polymers, with different molecular weights (MW), heat treatment, and acid-base treated silica.

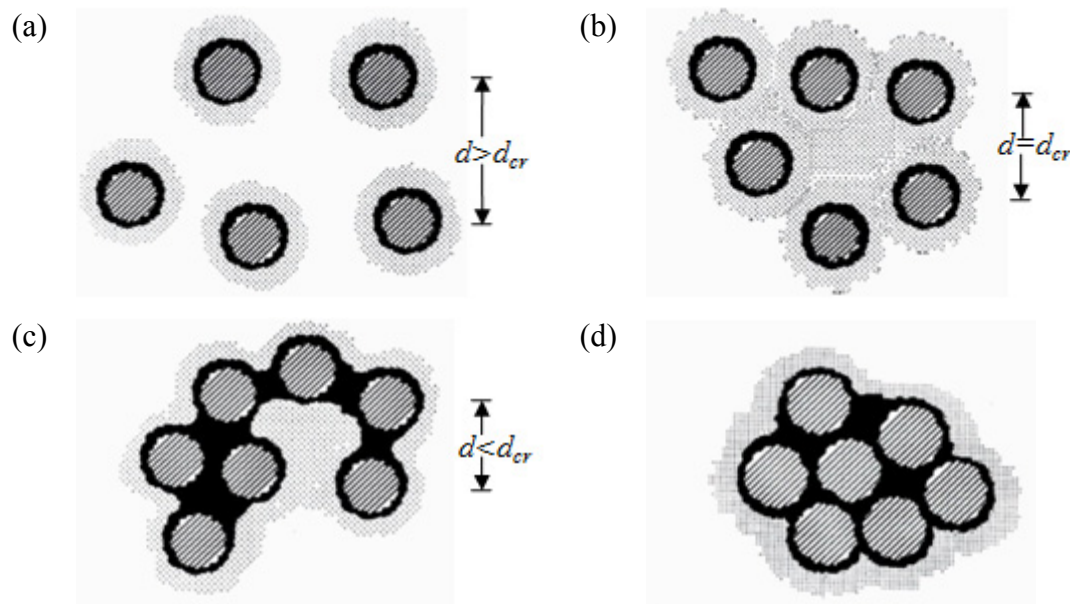


Figure 4.10: Schematic model of the morphological transformation in filled polymer by Tsagaropoulos and Eisenberg [87].

The building units of the morphological transformation in filled polymer model are the filler particle (line shaded) surrounded by a layer of polymer (black areas), designated as immobilized or tightly bound polymer which does not participate in either of the two T_g . The second area (grey area) is capable of participating in the second T_g , called as reduced mobility or loosely bound polymer. The average of interparticle distance has a critical value denoted as d_{cr} . When the distance is larger than its critical value, the mobility of the polymer chains surrounded the tightly bound polymer is not significantly affected, therefore the second T_g does not appear (Figure 4.10(a)). By the addition of filler content the distance between particles is reduced, overlaps between the regions of loosely bound polymer are large enough to exhibit their own T_g (Figure 4.10(b)). With the addition of more filler, the reduction of mobility decreases further, causing loosely bound polymer gradually transformed into tightly bound polymer (Figure 4.10(c)). Since the volume fraction of loosely bound polymer decreases, leads to a decrease in the area of second $\tan \delta$ peak. In parallel, a

further drop of the total area the two $\tan \delta$ peaks appear. As more filler is added to the matrix, more polymer chains get immobilized, and the distance between the particles become much smaller than d_{cr} (Figure 4.10(d)).

Results from the present study are in good agreement with the above model (Figure 4.10). By the addition of 10 wt.% of CMS the second T_g appears, which contribute to the shifting and reduction of the first $\tan \delta$ peak area (Table 4.2), signifying a good interaction between polymer-filler and the formation of loosely bound polymer regions. Further addition of CMS particles contribute to the reduction of the total area of the two $\tan \delta$ peaks (Table 4.2), representing the formation of more tightly bound polymer regions. The first T_g also appears in the storage modulus profiles, shown by a sharp drop of modulus, and the second T_g appears as the second drop of storage modulus in higher temperature. Reinforcement of the membrane film by the incorporation of CMS particle is indicated by a lesser drop of storage modulus in higher CMS content.

Mechanical properties of the membrane films were evaluated by tensile test, the stress-strain curve from the tensile tests is shown in Figure 4.11 and the corresponding results obtained are presented in Table 4.3. The profile of stress-strain curve shows that when CMS particles incorporated into the PSU matrix, the membrane become more rigid as indicated by increasing Young's modulus value with CMS loading. Since CMS particle itself is a rigid material, incorporated it into a ductile material will increases the overall material rigidity [89]. Similar to the trend of Young's modulus, tensile strength of the membrane increases with the concentration of CMS added to the polymer matrix, and hence it could withstand a higher stress. However, the ability of the membrane to elongate was reduced, shown by the decreasing trend of tensile strain. From visual observations, membranes with higher CMS content are more fragile compared with the lower CMS content, and this fact is supported by the value of toughness as it decreases with the addition of CMS.

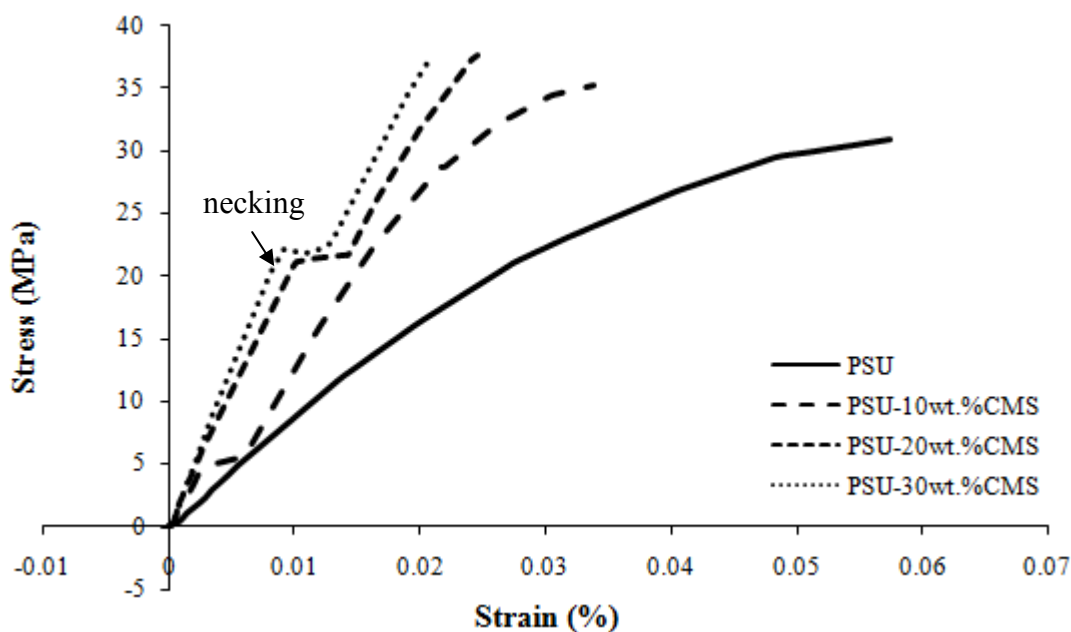


Figure 4.11: Stress-strain curve of mixed matrix membranes in different CMS loadings.

Table 4.3: Effect of CMS loading to the mechanical properties of mixed matrix membranes.

Mechanical properties	CMS loading (wt.%)			
	0	10	20	30
Young's modulus (MPa)	1786	1811	2259	2450
Tensile strength (MPa)	33.68	34.41	35.22	37.25
Strain (mm/mm)	0.0573	0.0313	0.0246	0.0217
Toughness (J/m ³)	0.5809	0.5859	0.5127	0.4233

Unique phenomena observed during the experiments, a plateau of yield elongation observed at the stress-strain curve when CMS particles were incorporated into PSU matrix indicated a necking process, made it clearly distinguishable between the elastic and the plastic region. In the elastic region, an increase in stress produced a proportionate increase in the strain, and at the yield point, an increase in strain occurred with a smaller increase in stress. Subsequently, the strain continued rising with the increase of stress until the specimen gets ruptured. A similar phenomena was

also observed by Gou et al. [90] in multi-walled carbon nanotubes (MWCNT)/epoxy composite. Lauke [89] suggested that the incorporation of particles into a matrix causes stress concentrations in the neighbourhood of the particle when the material subjected to a certain load. In the model, Lauke used the two particles arrangement as illustrated in Figure 4.10, where the particles are assumed to have a mean diameter of ' d ' and a centre-to-centre distance of ' r ' which behave elastically. During loading, the particle and matrix is deformed with displacement of ' u '. When the gap between the particles is under maximum deformation and finally reaches a critical value of stress, ε , debonding process starts. The initiated debonding crack extends all around the particle at this applied load. Subsequently, the matrix yielding takes place until rupturing of the specimen.

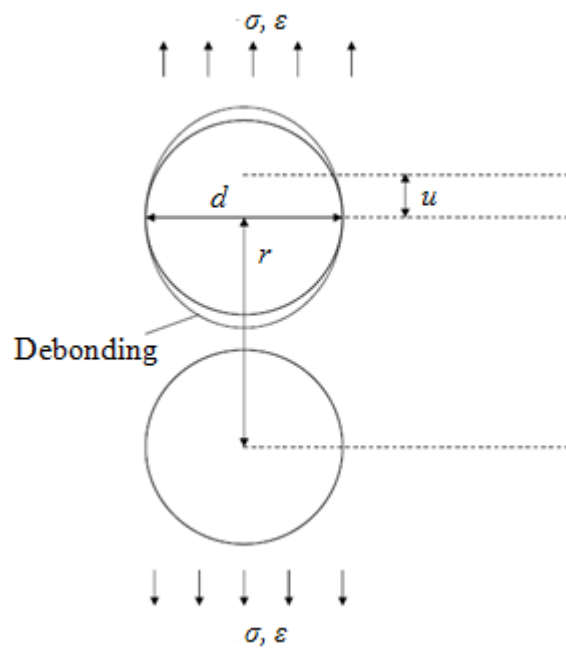


Figure 4.12: Schematic illustration of debonding mechanism of one particle in a pair by Lauke [89].

The gap between the particles is assumed to be the same as the restricted mobility region explained by Tsagaropoulos and Eisenberg [87] (Figure 4.10). From the stress-strain curve depicted in Figure 4.11, it can be explained as the initiated debonding crack took place at the maximum stress in the elastic region, and at the neck region

debonding process continues to occur, later followed by yielding matrix process. Since the restricted mobility polymer regions were stiffer than the bulk phase of polymer, the stress needed to unfold the polymer chains in this region were higher, and increases with increasing population of this region. Therefore, at the yielding elongation region, the strain continues to rise as the load continuously applied to the membrane. With increasing strain the polymer chains can slide each other breaking and forming weak bonds, and when nearly all chains are unfolded then the membrane rupture. From the DMA and tensile test results it is believed that CMS particles and PSU matrix has a favourable interfacial interaction.

4.2.2.2 Effect of Annealing Treatment

Annealing treatment of mixed matrix membranes were done by subjecting heat at 200°C for 1 hour, and cooled slowly to room temperature. After annealing, extended polymer appear at the protruding part, (denoted by the arrow in Figure 4.13(a)) was reduced significantly, membrane without annealing is presented as comparison (Figure 4.13(b)). The protruding part existed due to the high elasticity of polymer matrix, since annealing treatment increase the brittleness of the material (later confirmed by results from tensile test) polymer chains surrounded the filler particles become more brittle and lost its ability to elongate when drawn. From Figure 4.13, it can be seen that in membrane with annealing treatment, polymer is well-surrounded the filler particles, indicates a better polymer-filler adhesion compared to membrane without annealing treatment.

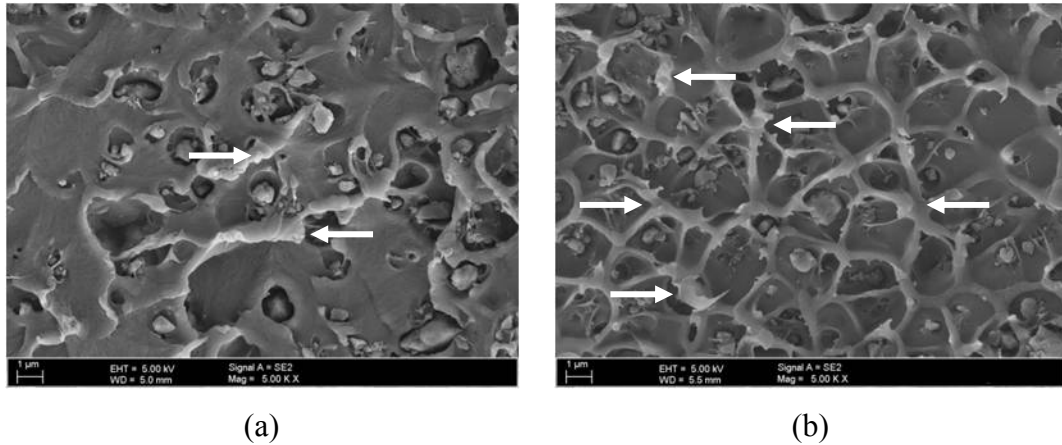


Figure 4.13: Comparison of mixed matrix membranes: (a) with annealing (5K ×) and (b) without annealing treatment (5K ×).

The effects of annealing treatment to the viscoelastic properties of mixed matrix membranes are shown in Figure 4.14, and the corresponding results of membranes with annealing treatment are presented in Table 4.4. Following the trend of the membranes without annealing treatment, membranes with annealing treatment show a dual $\tan \delta$ peak shape. It is observed that as annealing treatment subjected to mixed matrix membrane with 10 wt.% CMS content, the area of the first $\tan \delta$ peak become smaller (Figure 4.14(a-1)). The reduction of the first $\tan \delta$ area indicates that the fraction of polymer which participate in the first T_g become smaller. The position of the maximum of the first $\tan \delta$ has slightly shifts to a lower temperature, while the second $\tan \delta$ peak shifts to a higher temperature. The effect of annealing treatment also seen in the 20 wt.% CMS content (Figure 4.14(a-2)). However, the effect of annealing treatment on the $\tan \delta$ profile become weaker with increasing CMS content, as depicted in Figure 4.14(a-3) where there is no significant change observed in $\tan \delta$ profile of membrane with 30 wt.% of CMS. Similar behaviour can be seen in the storage modulus profile for 10 wt.% of CMS, the drop in storage modulus is less in the annealed membranes, indicating the higher reinforcement of the material by the filler (Figure 4.14(b-1)). As the filler content increased, the effect due to heat treatment become weaker, as shown in Figure 4.14(b-3), where there is no significant change due to annealing treatment.

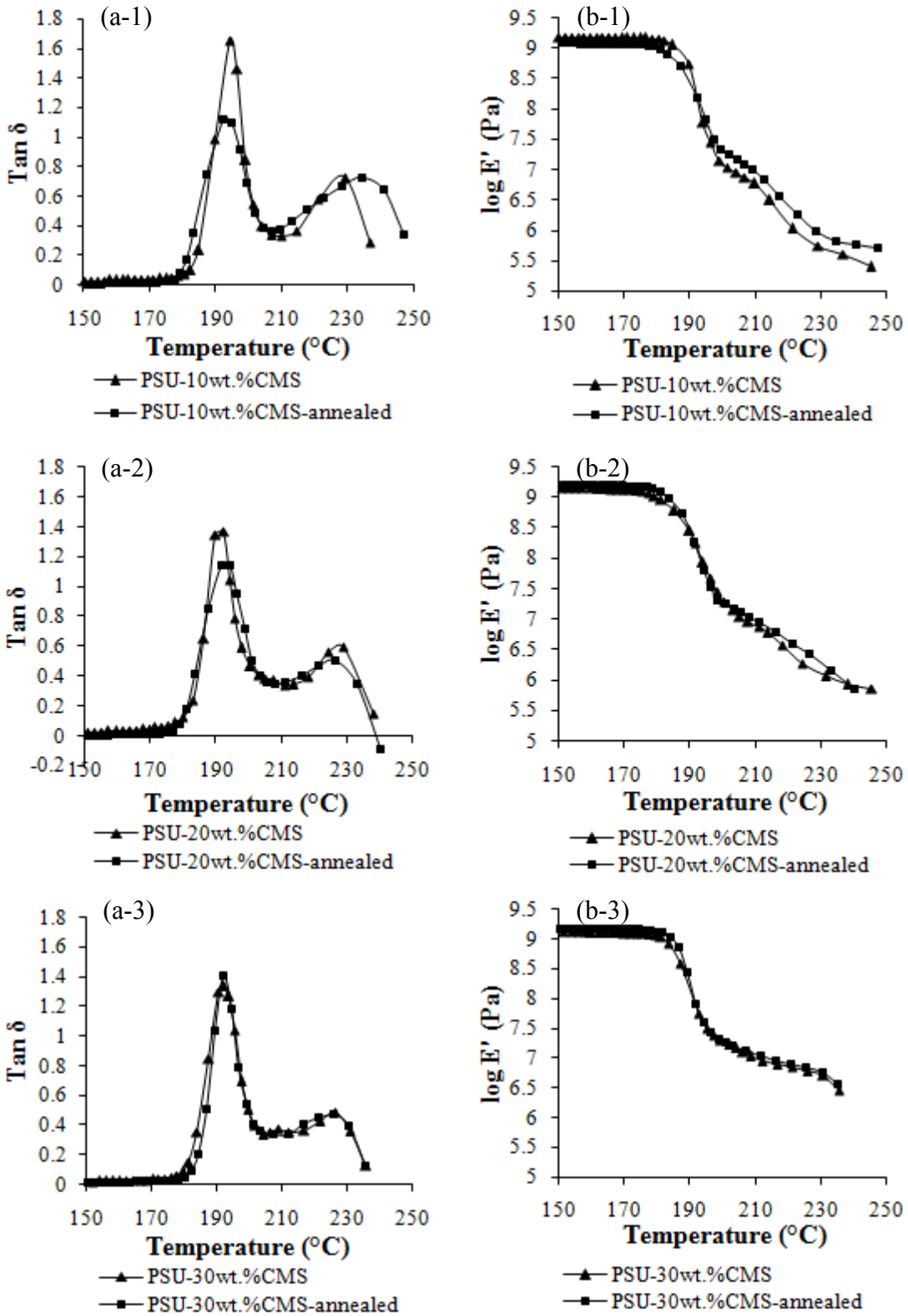


Figure 4.14: Comparisons of: (a) $\tan \delta$ and (b) storage modulus profile of mixed matrix membranes with and without annealing treatment in different CMS loadings.

Table 4.4: Tan δ curve properties of mixed matrix membranes with annealing treatment.

Membrane	Tan δ_1	Tan δ_2	T_{g1} ($^{\circ}\text{C}$)	T_{g2} ($^{\circ}\text{C}$)	Area ₁	Area ₂
PSU-CMS10wt.-%-annealed	1.12	0.73	192.43	234.55	18.38	15.28
PSU-CMS20wt.-%-annealed	1.14	0.50	191.59	226.54	17.82	12.41
PSU-CMS30wt.-%-annealed	1.41	0.47	192.00	225.63	14.85	12.04

According to Ito and co-workers [91], during annealing process loosely bound polymer is formed and continuously transformed into tightly bound polymer during prolonged heat treatment. This phenomena would leave the fraction of polymer participate to to the first and second T_g reduces after the treatment. The results of the present study agreed with the above observation. The area of the first and second tan δ peak is reduced by annealing treatment, since tightly bound polymer which formed during annealing treatment does not participate in either of the two glass transitions. The shifting of the second tan δ peak to a higher temperature in low filler content (10 wt.%) might be due to the formation of a more packed loosely bound polymer regions. By increasing filler content within the matrix, the polymer in the loosely bound polymer would start to overlap and loosely bound polymer located in the space between the particles would transformed to tightly bound polymer, since it experiences mobility restrictions from different particles, as illustrated in Figure 4.10(c). Hence, the annealing effect become significant for membrane with CMS content less than 20 wt.% where polymer chains still have significant movement during annealing. For membrane with CMS content more than 20 wt.%, it is believed that the main constituent is tightly bound polymer therefore no significant change appear in tan δ peaks and storage modulus profile after annealing treatment.

Correspond to the DMA results, tensile test results of membranes with annealing treatment presented in Figure 4.15 and Table 4.5 show that annealing treatment significantly changed the shape of the stress-strain curve of mixed matrix membrane with 10 wt.% of CMS content, and the effect of annealing treatment become weaker with increasing CMS content, similar to the DMA results.

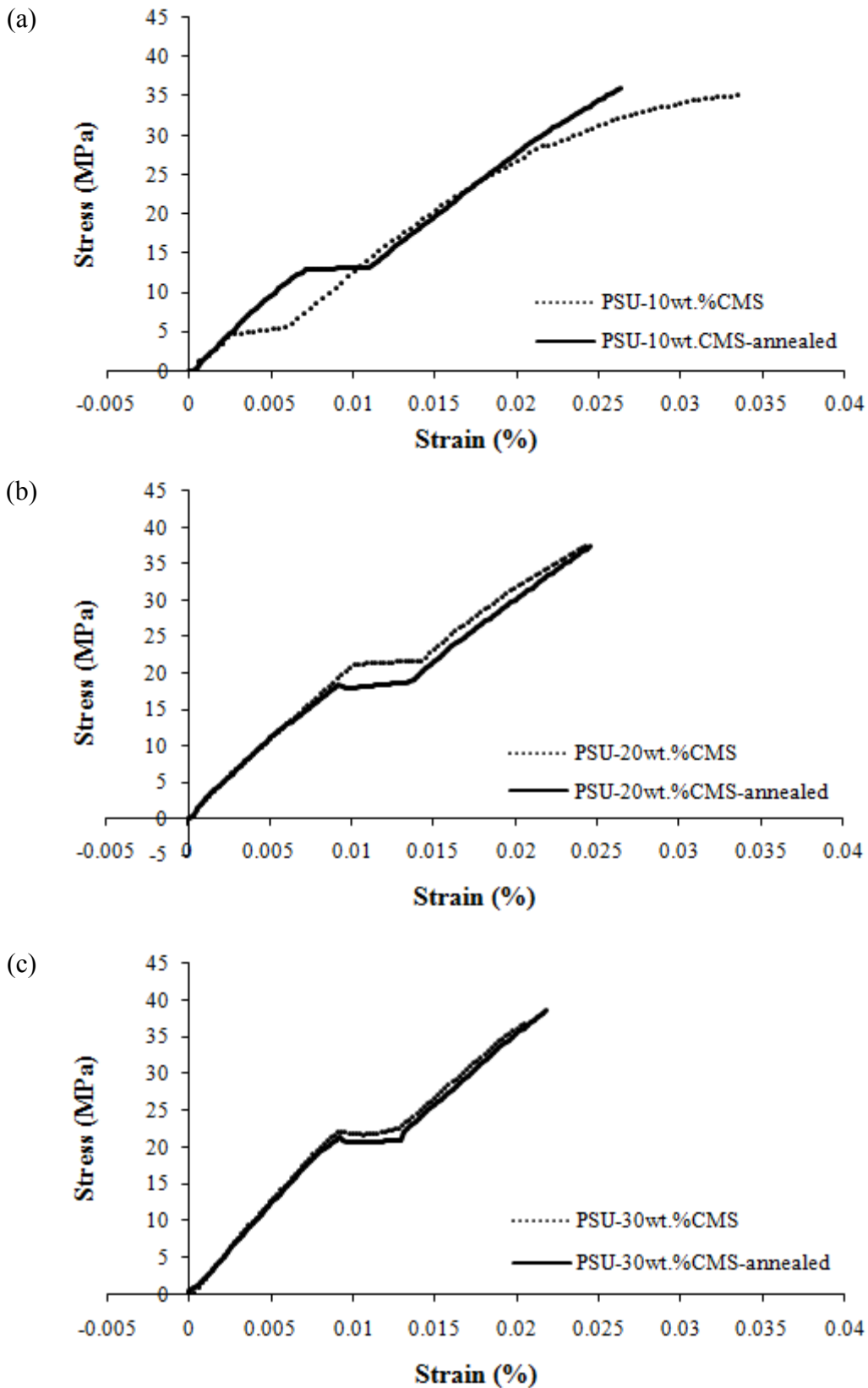


Figure 4.15: Comparisons of stress-strain curve of mixed matrix membranes with and without annealing treatment: (a) 10 wt.%; (b) 20 wt.%; and (c) 30 wt.% CMS.

From Figure 4.15(a), it can be seen that membrane transformed from a relatively ductile membrane into a more brittle membrane, supported by the increasing of Young's modulus value. After treatment, the membrane could resist a higher stress, but it partially lost its ability to elongate. The resulting material has a higher toughness value, indicate that it can absorb a higher energy before rupturing compared to the membrane without annealing. In Figure 4.15(b), the effect of annealing treatment still noticed by the increase in Young's modulus, and the decreasing of yield point to a lower stress as annealing treatment subjected to the membrane. While in Figure 4.15(c), the profile of stress-strain curve for the respected membrane does not show any significant change. It can be concluded that annealing treatment is seen as a potential strategy to enhance the adhesion between filler and polymer phase, however its effects gets reduced with filler content.

Table 4.5: Effect of annealing treatment to the mechanical properties of mixed matrix membranes.

Mechanical properties	CMS loading (wt.%)		
	10	20	30
Young's modulus (MPa)	2201	2275	2468
Tensile strength (MPa)	36.14	37.47	38.57
Strain (mm/mm)	0.0264	0.0246	0.0218
Toughness (J/m ³)	0.6210	0.5299	0.4259

4.3 Formation of Mixed Matrix Membranes using Oxidized-Carbon Molecular Sieves

Surface of CMS were modified by nitric acid oxidation to functionalize the surface of CMS particles with acidic functional groups and increase the polarity of the surface, which further used to enhance its interaction with polymer matrix. The effect of oxidation of CMS to the morphology, viscoelastic, and mechanical properties of the membranes are discussed.

4.3.1 Nitric Acid Oxidation of Carbon Molecular Sieves

In order to observe the effect of nitric acid (HNO_3) to the CMS surface, it was oxidized in 2, 5, 8, and 11 M HNO_3 . After oxidation process, the oxidized-CMS (later referred as ox-CMS) was then refluxed by NaOH. The formation of functional groups on CMS surface by different concentration of HNO_3 determined by FTIR spectra is shown in Figure 4.16. The FTIR spectra of ox-CMS show some pronounced peaks at about 1714, 1580, 1400, 1385, and 1260 cm^{-1} wave numbers. All the samples showed a similar peak, only differ on its intensity, indicating that all sample went through a similar process. The peak at 1714 cm^{-1} is attributed to the stretching vibrations of C=O in carboxylic or carbonyl group [74, 92-95] which mainly involve in aromatic rings, this peak appears only on the ox-CMS. On the other hand the peak appears at 1580 cm^{-1} may be attributed to the quinone structure [73, 92, 96], which also appears in the CMS without oxidation only it is less pronounced. Peak at 1400 cm^{-1} could be attributed to the vibrations of carboxylic —OH group [94], whereas peak at 1385 cm^{-1} confirm the carboxylic structure [94]. Peak at 1260 cm^{-1} could be assigned tentatively to C-O-C vibrations in ether structure or other single bonded oxo group C-O-R [97]. The structures of the possible acidic groups attached to the CMS surface are shown in Figure 4.17.

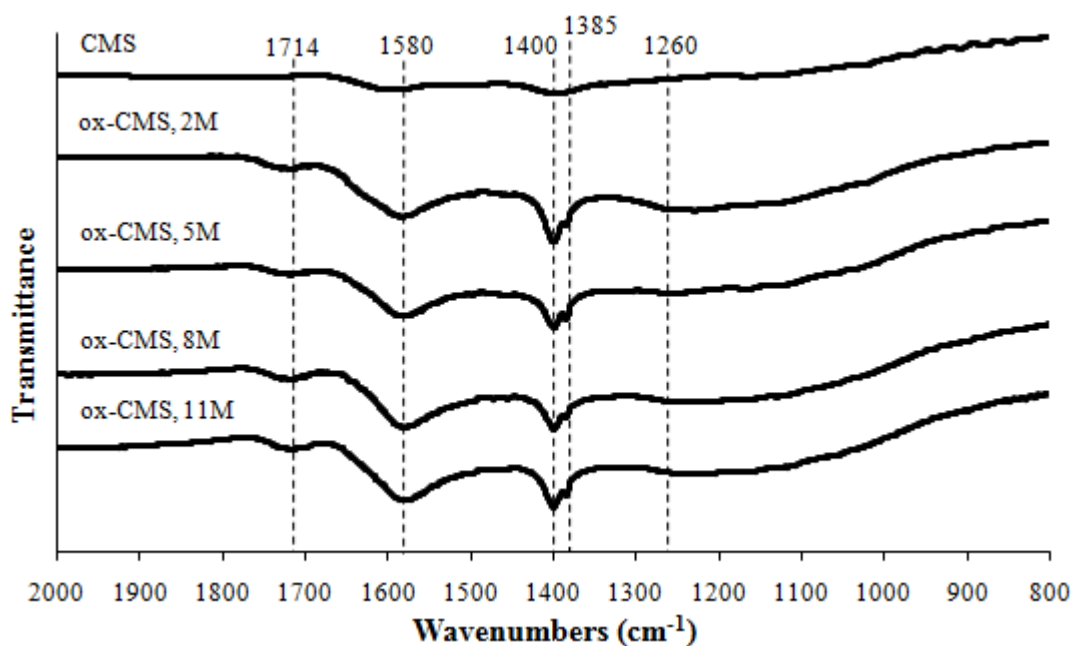


Figure 4.16: FTIR spectra of surface CMS treated with various HNO_3 concentrations.

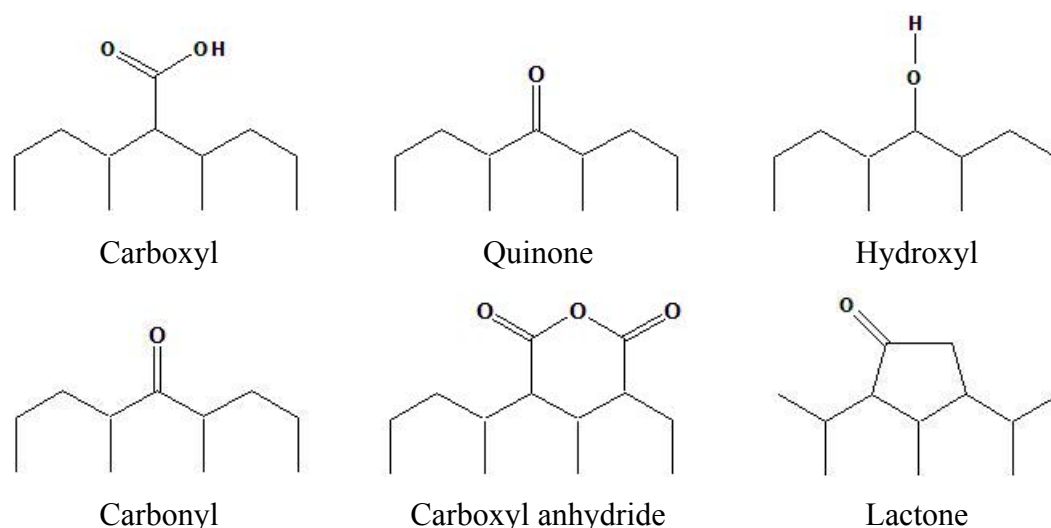


Figure 4.17: Possible acidic groups attached to the CMS surface [98].

Since carbonaceous materials such as activated carbon and CMS consist of condensed aromatic structures, its oxidation has some analogies to the oxidation of aromatic hydrocarbons. As described by Vinke et al. [73], the reaction site most likely to occur on the aliphatic side chains of the carbon because such sites are highly susceptible to oxidation. If the side chains of more than one carbon atom are present, the reaction may initiated by the splitting of the C—C bond at the α -position of the benzylic carbon atom. This scheme of reaction, is similar to the oxidation of 9,10-dihydrophenanthrene, results in formations of dicarboxylic acid Figure 4.18(a). When only one methylene (CH_2) present between two aromatic chains, such as in diphenylmethane, the reaction is expected to stop at the formation of ketone as shown in Figure 4.18(b).

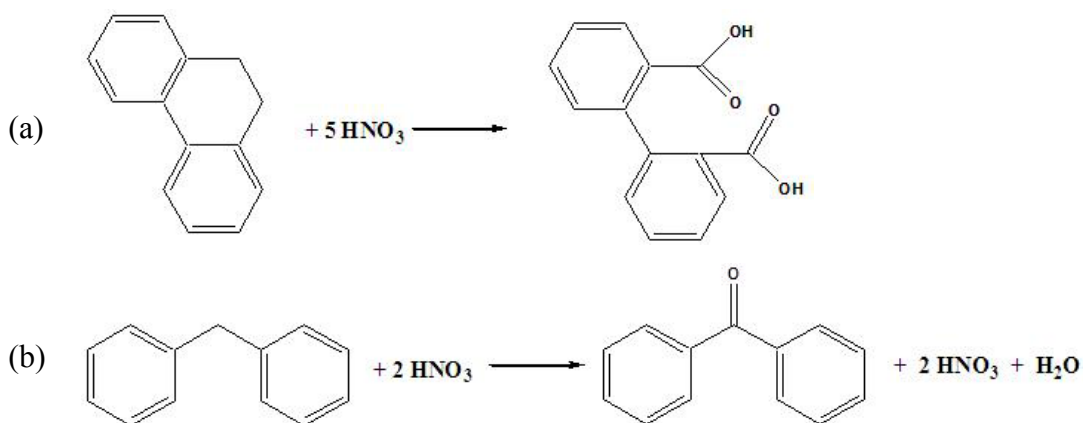


Figure 4.18: Nitric acid oxidation of 9,10-dihydrophenanthrene (a) and diphenylmethane (b). Adapted from Vinke et al. [73].

Figure 4.19 shows the total acidic capacity (TAC) of the ox-CMS in various HNO_3 concentrations. Since carboxylic group attached to the CMS surface, its neutralization reaction towards NaOH were used to determine the acidic capacity of CMS surface. The acidic capacity of ox-CMS increases with the HNO_3 concentration used. A significant increment was observed in 8 M of HNO_3 . The creation of large functional group is expected to improve the interaction between ox-CMS and polymer in mixed matrix membrane preparation.

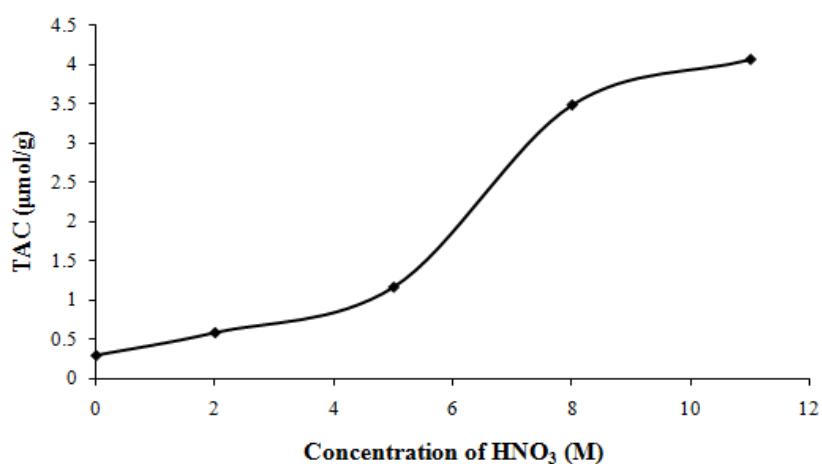


Figure 4.19: Acidic capacity of oxidized CMS treated with several HNO_3 concentrations.

After the oxidation process, ox-CMS particles were washed by refluxing in NaOH to remove the oxidized graphitic fragment, considered as byproducts which could cause pore blockage. The oxidized graphitic fragment is highly hydrophilic, therefore it is easily soluble in NaOH solution. The photograph of the filtered NaOH solution is shown in Figure 4.20. The transparent NaOH solution turned into a black brownish solution after the treatment, while the blank solution remains transparent since no byproducts was extracted. As reported by Wu et al. [75] on their study in carbon fibers oxidation with nitric acid, subsequent treatment by refluxing with NaOH did not affect the structure of the fibers. In their study, similar brownish black solution was observed after the treatment. A possible structure of oxidized graphitic fragment proposed by Wu et al. [75], is illustrated in Figure 4.21. In the present study, the intensity of the color increases with increasing HNO₃ concentration indicates that more oxidized graphitic fragment were extracted and removed from the ox-CMS surface leaving pits and cavities at the surface. The comparison of CMS surface with and without oxidation treatment is shown in Figure 4.22.

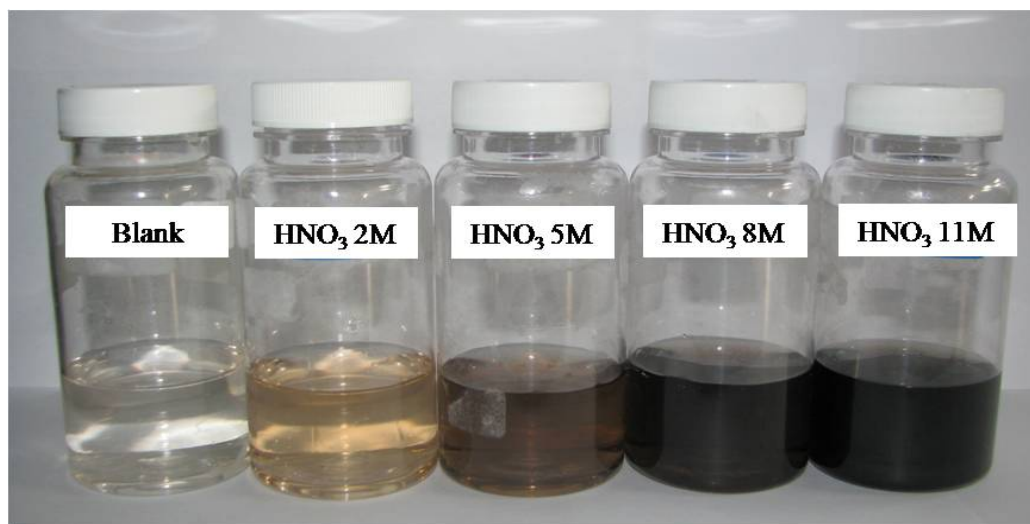


Figure 4.20: Filtered NaOH solution after reflux treatment.

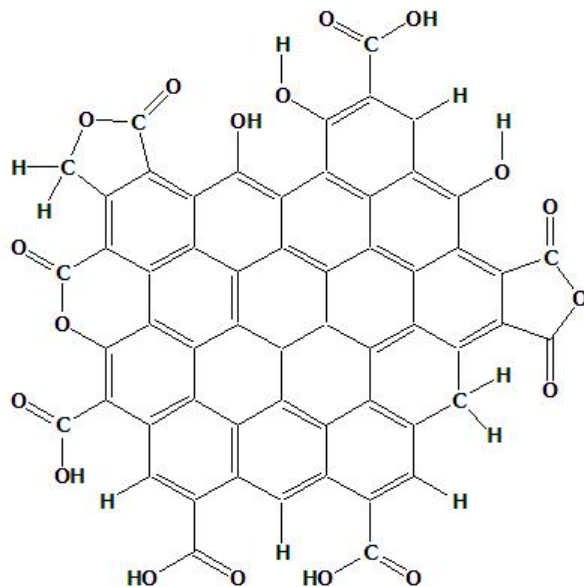


Figure 4.21: Possible structure of oxidized graphitic fragment. Adapted from Wu et al. [75].

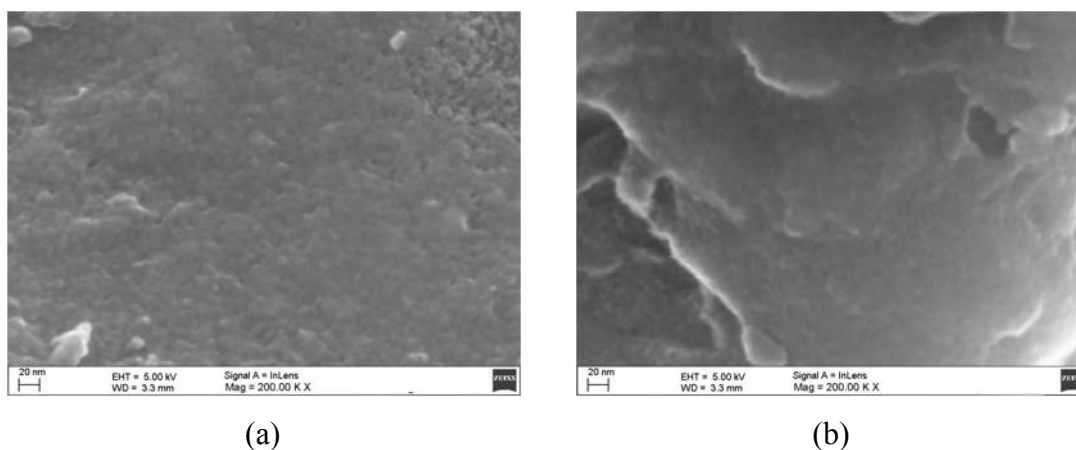


Figure 4.22: The comparison of CMS surface: a) without oxidation (200K ×) and b) with oxidation treatment using 11 M of HNO₃ (200K ×).

The XRD spectrums for both CMS with and without oxidation treatment are shown in Figure 4.23. Compared to CMS without oxidation treatment, ox-CMS exhibit a sharper peak at $2\theta = 25.1^\circ$, indicating an increase in regularity and order of packing around d-spacing 3.41 Å. During the oxidation process, the amorphous phase of CMS particles is oxidized, which contribute on the rise of regularity in its structure.

The structure become more close to the structure of graphite which has a single crystalline peak with d-spacing of 3.35 Å, as reported by Steel [46]. Lower d-spacing in the ox-CMS is attributed to the formation of functional group layer on its surface, which made the distance of atoms closer. Furthermore, both samples exhibit peak at $2\Theta = 43.35^\circ$ with d-spacing of 2.09 Å, which is generally represent the carbon-carbon spacing on graphitic planes. Increase in structure regularity also confirmed by the density of ox-CMS of 2.2179 g/cm^3 , where the density of CMS without oxidation is 2.1664 g/cm^3 . For comparison, the skeletal density of graphite in extreme condition without the presence of pore is 2.3 g/cm^3 . The increase in skeletal density of ox-CMS indicates that its structure become more close and packed as there is more atom per unit volume.

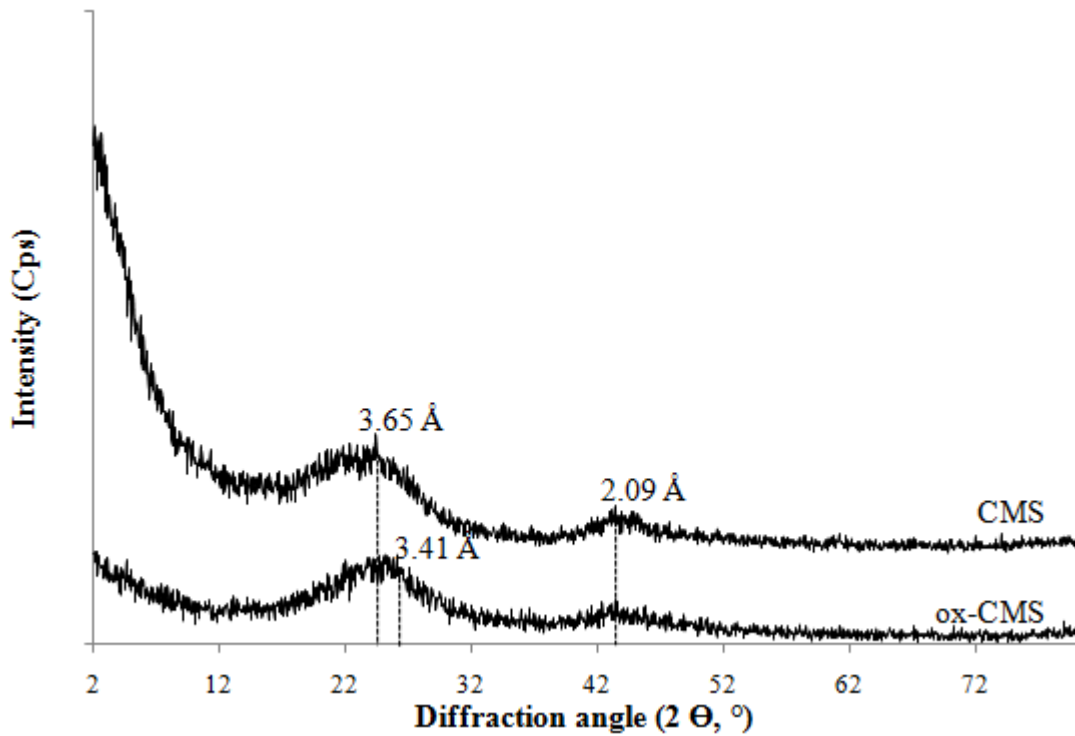


Figure 4.23: XRD spectra of CMS particle before and after oxidation process.

4.3.2 Characterization of Mixed Matrix Membranes with Oxidized-Carbon Molecular Sieves

Mixed matrix membranes were prepared by using ox-CMS treated in 11 M HNO₃ due to its high acidic capacity. Field emission scanning electron micrographs of the membranes are shown in Figure 4.24. The micrographs reveal that in the low loading of ox-CMS (10 wt.%), filler particles were distributed homogeneously throughout the matrix. As increasing ox-CMS loading, dense ox-CMS regions were formed within the matrix. The formation of these regions is assumed due to maintaining DCM, which is non-polar, as solvent during the fabrication process. Since ox-CMS has a highly hydrophilic character, during its introduction to DCM it is readily agglomerate with each other via intermolecular forces. Only after PSU powder was added to the solution, ox-CMS interact with PSU chains due to the polar —SO₂— groups possessed by PSU backbone. In higher magnification micrograph, shown in Figure 4.25, it is observed that the polymer chains cover the filler particles indicate a better adhesion between ox-CMS and PSU compared to CMS without oxidation treatment.

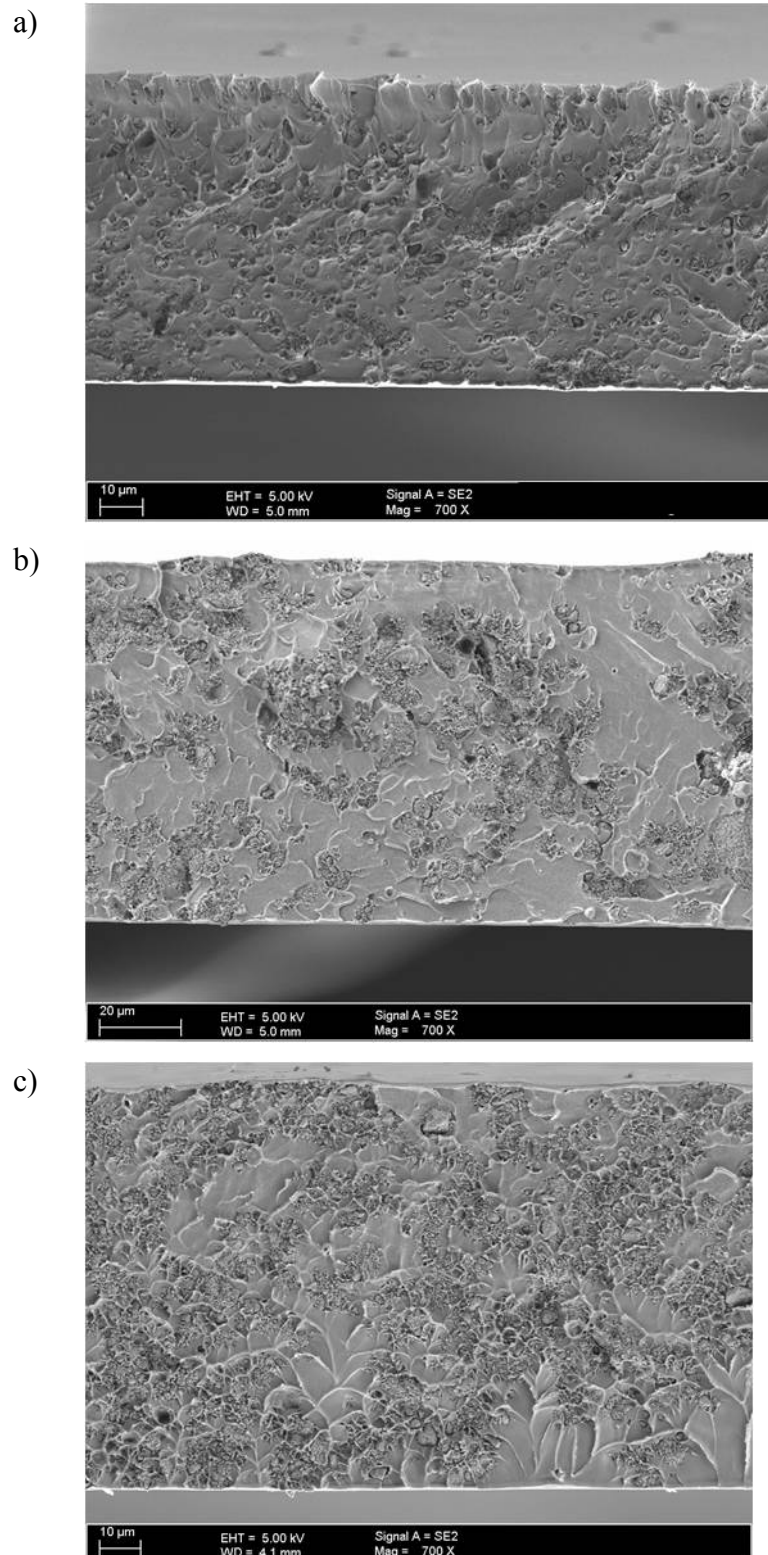


Figure 4.24: Field emission scanning electron micrographs of mixed matrix membranes using ox-CMS in different loadings: (a) 10 (700 ×); (b) 20 (700 ×); and (c) 30 wt.% (700 ×).

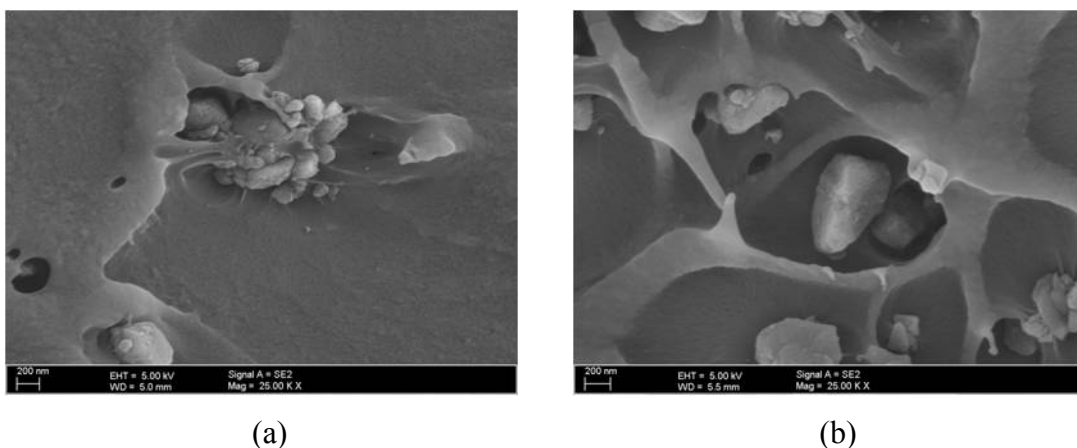


Figure 4.25: Comparison of mixed matrix membranes using: (a) ox-CMS (25K \times) and (b) CMS (25K \times).

The comparison of $\tan \delta$ peaks and storage modulus profile between membrane using CMS and ox-CMS in different CMS loadings are presented in Figure 4.26 and the corresponding results of membranes using ox-CMS are presented in Table 4.6. Figure 4.26 (a1)-(a3) show that the position of the first $\tan \delta$ peak of membranes using ox-CMS is hardly moved compared to CMS, since it is responsible for the T_g of the bulk polymer phase. However, the peak is broadened as ox-CMS used as filler. Similar observation has been made for various carbon nanotubes/polymer systems [35, 99-102]. The broadening of $\tan \delta$ peak indicates the favourable interaction between ox-CMS and PSU creates an interfacial zone of polymer segments with distribution in mobility [99-102]. Lower area of the first $\tan \delta$ peak compared to the PSU membrane indicates smaller fraction of polymer contribute to the first T_g due to the formation of loosely and tightly bound polymer surrounding the ox-CMS particles. The attraction of polar functional group to the polymer chain is considered to be responsible for this movement. The maximum of the second $\tan \delta$ peak is shifted to a higher temperature compared to mixed matrix membranes using CMS, due the denser loosely bound polymer regions formation correspond to the mutual ox-CMS and PSU interaction. As more ox-CMS added, less loosely bound polymer were formed due to the formation of more tightly bound polymer. Since tightly bound polymer does not participate to either the first or second T_g , its formation consequently caused less polymer participate in the first and second T_g , indicates by

the reduction of the first and second $\tan \delta$ peak area. Figure 4.26 (a-3) show that the effect of oxidized CMS become weaker (in 30 wt.%), as the constituent is mainly tightly bound polymer, although the effect is still noticeable compared to membranes with annealing treatment.

The storage modulus profiles of membrane with various loading of oxidized CMS are shown in Figure 4.26 (b1)-(b3). Similar to the trend of mixed matrix with CMS, a sharp drop of modulus occurs at the first T_g for all the samples with decreasing magnitude with CMS loading, indicates higher reinforcement yield. Differ from membranes with annealing treatment reinforcement effect of ox-CMS is still noticeable in high loading of ox-CMS (30 wt.%) due to the mutual interaction between ox-CMS and PSU.

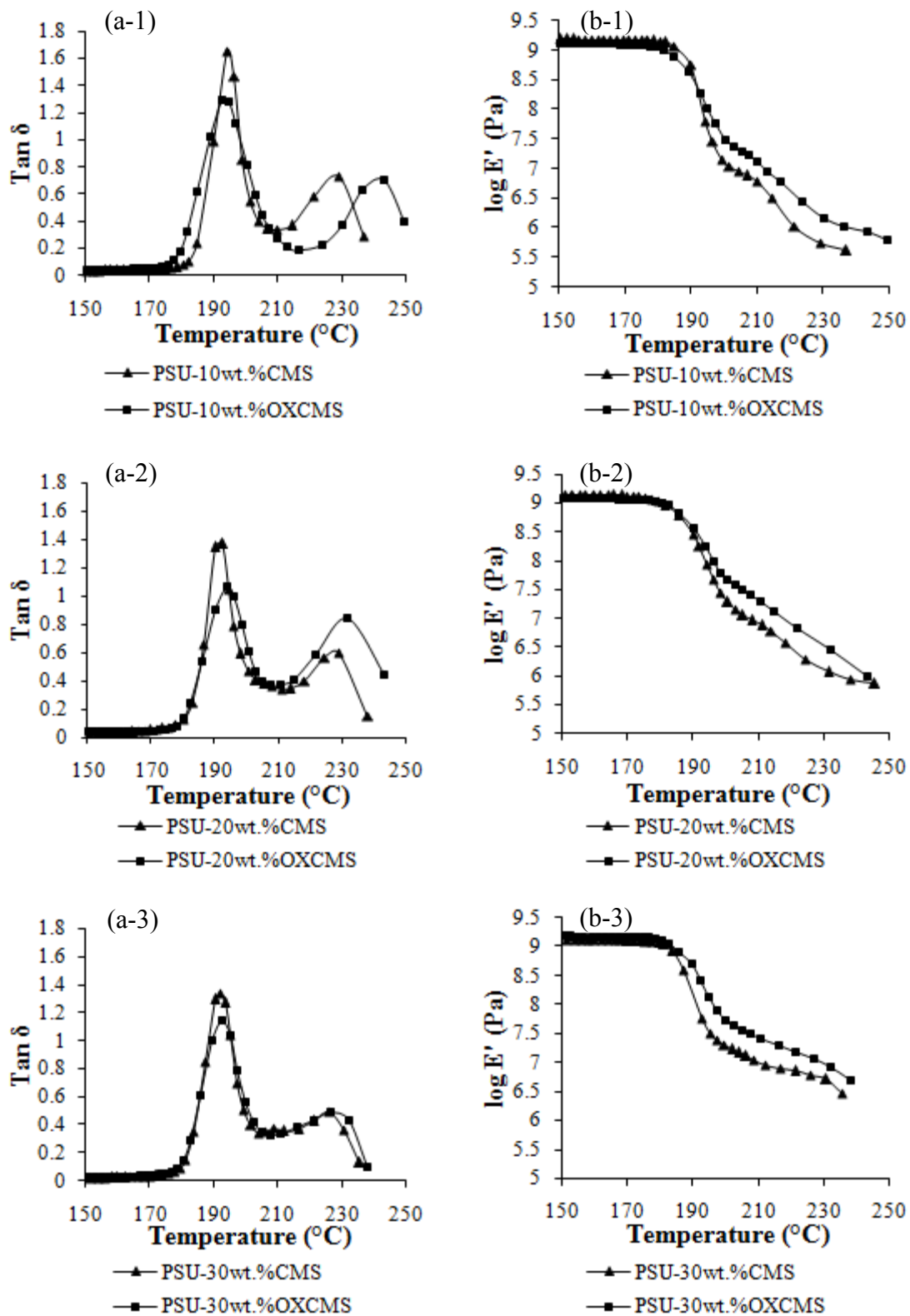


Figure 4.26: Comparisons of $\tan \delta$ (a) and storage modulus (b) profile of mixed matrix membranes using CMS and ox-CMS in different loadings.

Table 4.6: Tan δ curve properties of mixed matrix membranes with different loadings of oxidized-CMS.

Membrane	Tan δ_1	Tan δ_2	T_{g1} ($^{\circ}\text{C}$)	T_{g2} ($^{\circ}\text{C}$)	Area ₁	Area ₂
PSU-10wt.%OXCMS	1.29	0.70	192.74	243.38	23.17	16.52
PSU-20wt.%OXCMS	1.07	0.84	193.78	231.72	18.22	13.30
PSU-30wt.%OXCMS	1.14	0.49	192.44	226.84	17.31	12.48

4.4 Permeability Studies

Gas permeability studies of PSU and mixed matrix membranes were evaluated using pure gas CO₂ and CH₄ at five different feed pressures of 2, 4, 6, 8, and 10 bars with constant temperature at 25 $^{\circ}\text{C}$. The effect of CMS loading, annealing treatment, and surface modification of CMS are discussed in the following Sections.

4.4.1 Effect of Carbon Molecular Sieves Loading

The permeability of CO₂ and CH₄ versus operating pressure across the PSU and mixed matrix membranes are presented in Figure 4.27 and Figure 4.28. Permeability of PSU membrane was used as comparison. It is observed that there was a simultaneous increment of gas permeability and ideal selectivity by increasing the percentage of CMS loading within the matrix. As desired, the addition of CMS increases the CO₂ (fast gas) permeability and the CO₂/CH₄ ideal selectivity, while decreases the permeability of CH₄ (slow gas).

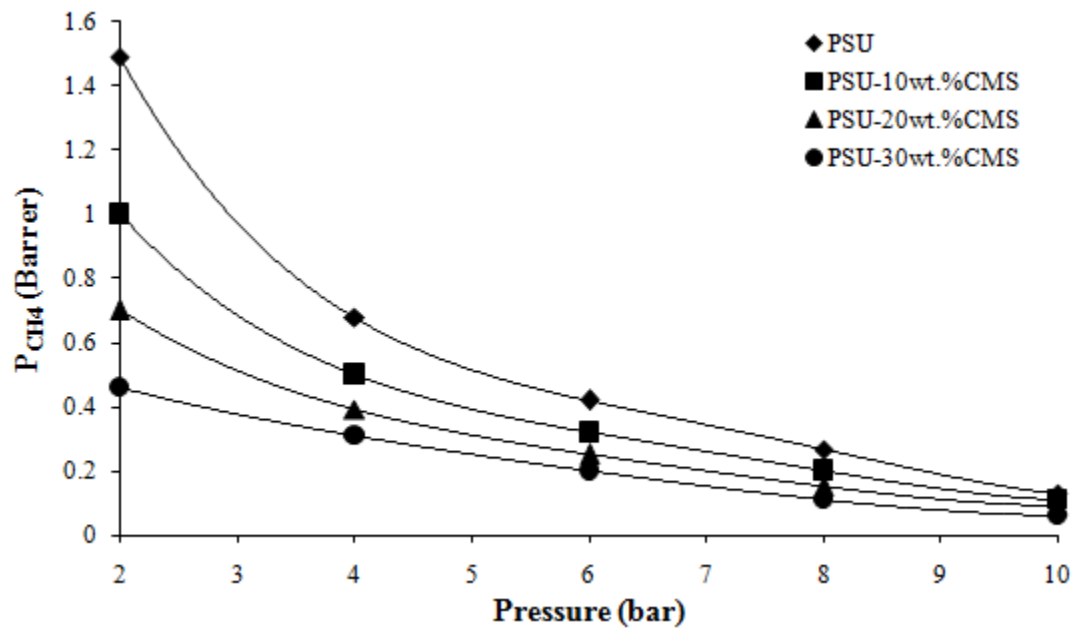
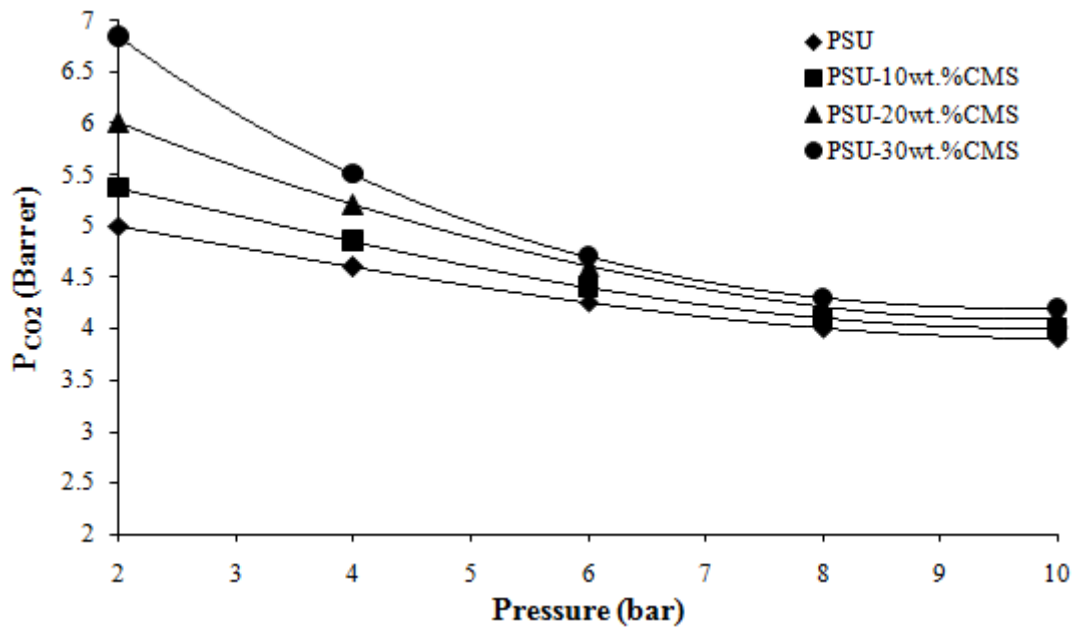


Figure 4.27: CO_2 and CH_4 permeabilities of mixed matrix membranes with different CMS loading in various feed pressures.

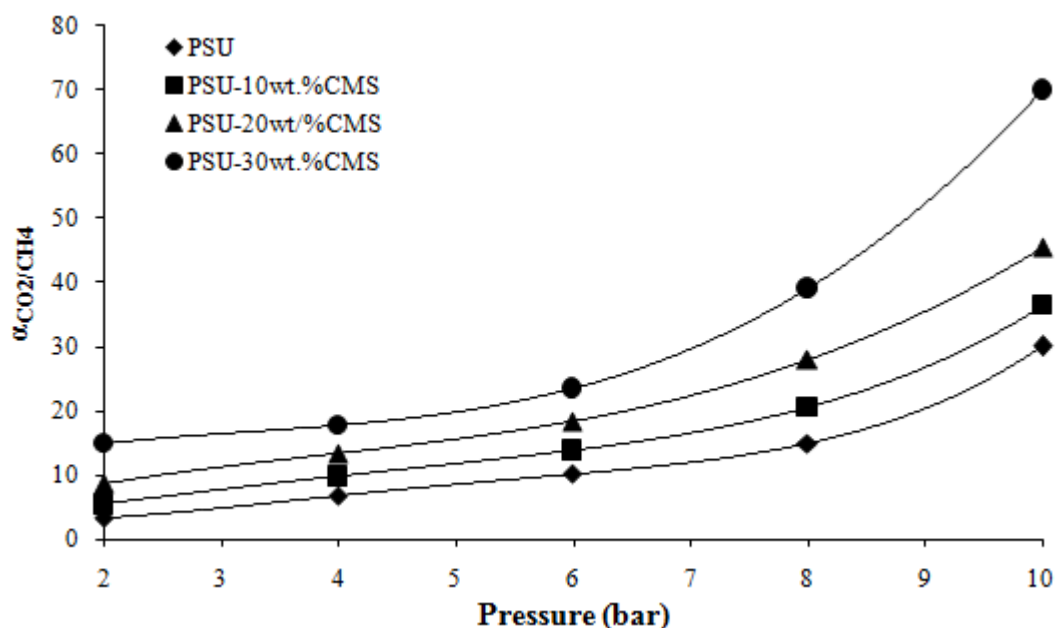


Figure 4.28: CO₂/CH₄ ideal selectivities of mixed matrix membranes with different CMS loading in various feed pressures.

Figure 4.27 shows that within the pressure range, all membranes showed decreasing trend of permeability with increasing feed pressure. The nonlinear correlation between pressure and permeability indicates the characteristics of dual sorption modes of gas in glassy polymer system, as described in Equation 2.15, when the diffusion coefficient in Henry and Langmuir environments are constant, the permeability is declined by feed pressure [68]. These results are also in good agreement with dual sorption model explained by Paul and Koros [103], and its extended form by Vieth et al. [104] which explain that the permeability coefficient decreases monotonically with the partial pressure differential across the membrane due to the different immobilization experiences by gas penetrant within the glassy polymer matrix. Similar results were observed by Kapantaidakis et al. [44] in pure PSU membrane, Huvard et al. [105] in poly(acronitrile) membrane, as well as by Paul and Kemp [47] in molecular sieves loaded PDMS membrane.

Inverse trends were observed for the permeabilities of CO₂ and CH₄. The relatively polar characteristic of PSU enhance its affinity towards CO₂ higher than CH₄, therefore CO₂ is readily permeated faster than CH₄ in PSU and mixed matrix

membrane. The permeability of CO₂ increased with CMS loading. The CO₂ selective pore size of CMS might be responsible for this occurrence. XRD analysis shows the d-spacing of CSM used is 3.65 Å (Figure 4.5) which is higher than CO₂ kinetic diameter (3.3 Å), even though the value of d-spacing does not explicitly correlate to the pore dimensions, but it indicates the distances between side-group atoms and skeletal atom or the distances between atom centers in neighboring planes. The smaller distance between atoms could promote a steric hindrance to the bigger molecular size of gases passing through the pore channel of CMS, therefore it could hinder CH₄ molecules (with kinetic diameter of 3.8 Å) to pass through the membrane.

The highest increase in CO₂ permeability and CO₂/CH₄ ideal selectivity was achieved by the addition of 30 wt.% CMS. The permeability of CO₂ increased from 8% at 8 bar to 37% at 2 bar. Whereas the CO₂/CH₄ ideal selectivity was 14.87 (2 bar), 17.74 (4 bar), 23.50 (6 bar), 39.09 (8 bar), and 70 (10 bar) representing the increments of 343, 162, 132, 162, and 133%, respectively, over the pure PSU membrane. From the permeability studies, it can be said that CMS particles have a good interaction with PSU matrix, since there is no reduction in selectivity, indicating the absence of unselective-gap formation between these two phases.

The objective of the development of gas separation membrane is to surpass the upper-bound limit of polymeric membrane, the gas separation properties obtained in this study is plotted to the CO₂/CH₄ ideal selectivity against CO₂ permeability as shown in Figure 4.29. The upper-bound limit showed in Figure 4.29 was plotted from Robeson et al. [26]. The membrane performance was enhanced by the addition of CMS, 30 wt.% CMS exhibit the highest performance in all pressures. Even though the upper-bound limit has not been exceeded, the performance of membrane is moving towards the upper-bound limit. The effort to exceed the upper-bound limit of polymeric membrane continued by annealing treatment and using surface functionalized CMS discussed in the following Sections.

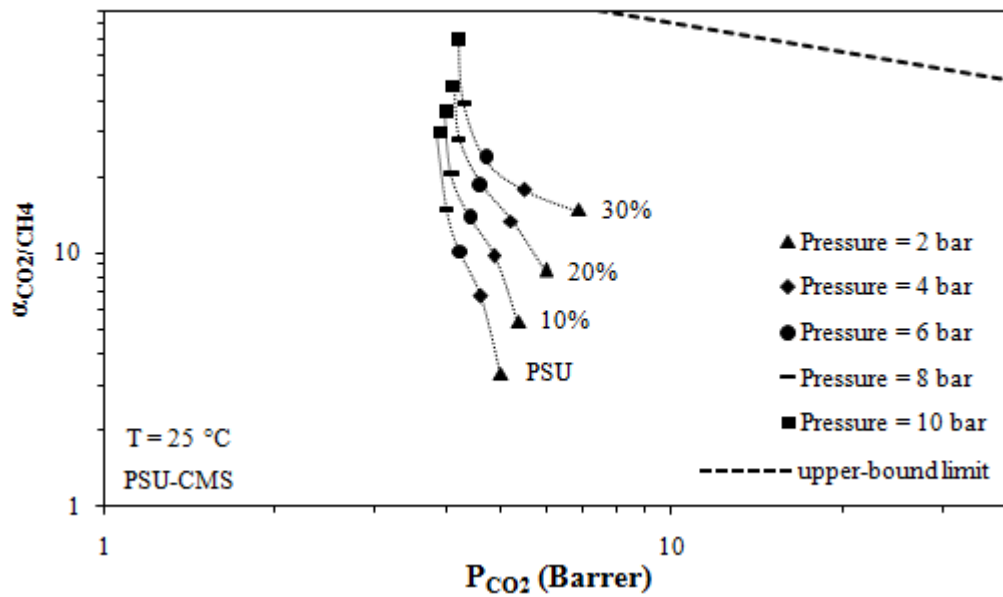


Figure 4.29: CO₂/CH₄ ideal selectivity vs CO₂ permeability for mixed matrix membranes using CMS in various feed pressures.

4.4.2 Effect of Annealing Treatment

The permeabilities of CO₂ and CH₄ of mixed matrix membranes with annealing treatment, as well as the ideal selectivity of CO₂/CH₄ are shown in Figure 4.30 and Figure 4.31, respectively. Mixed matrix membranes with annealing showed similar behaviour as membranes without annealing treatment, whereas the permeability of CO₂ and ideal selectivity of CO₂/CH₄ increases with CMS loading, while the permeability of CH₄ showed an opposite trend, sieving mechanism of CMS might be responsible for these phenomena.

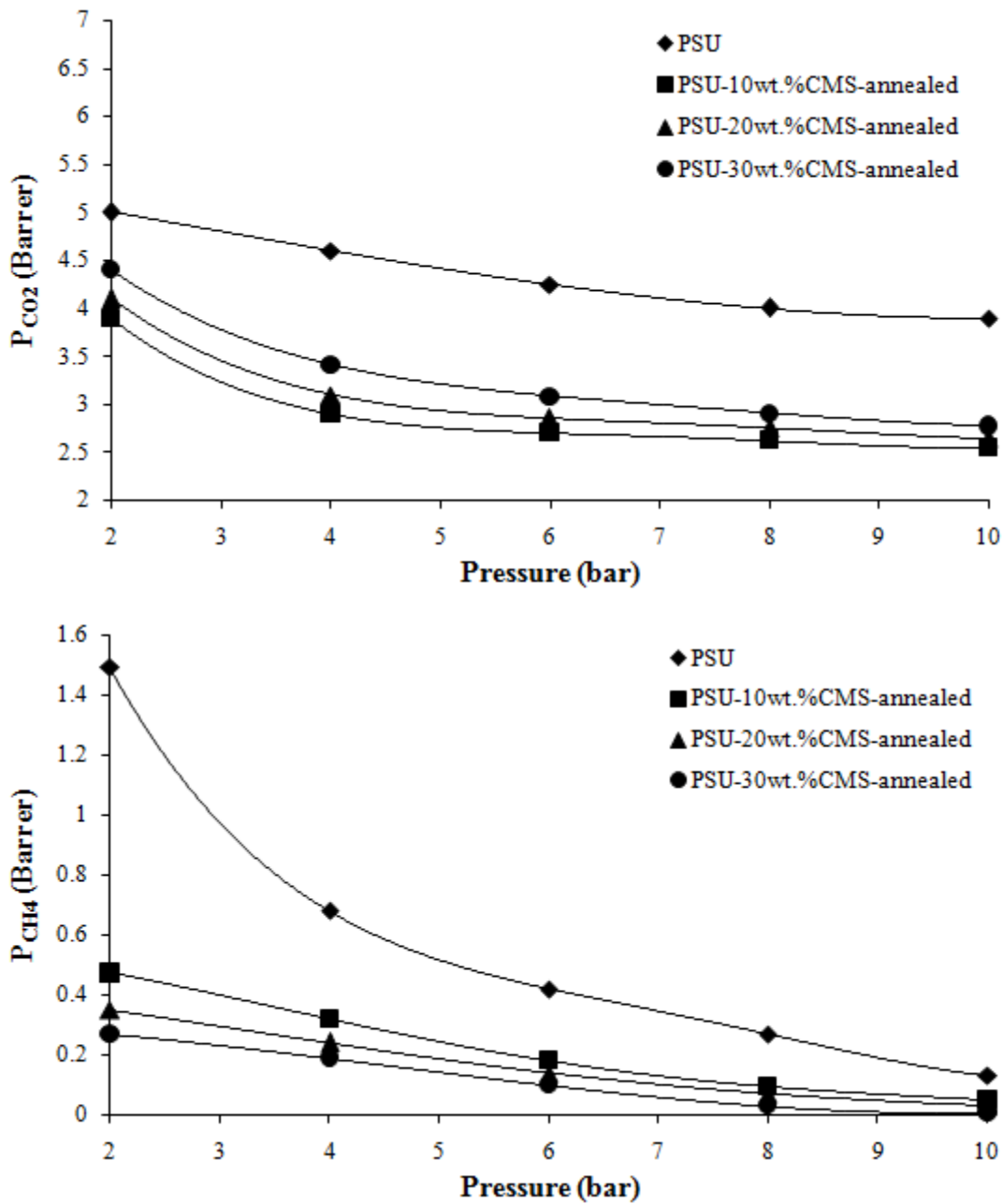


Figure 4.30: CO₂ and CH₄ permeabilities of mixed matrix membranes using CMS with annealing treatment in various feed pressures.

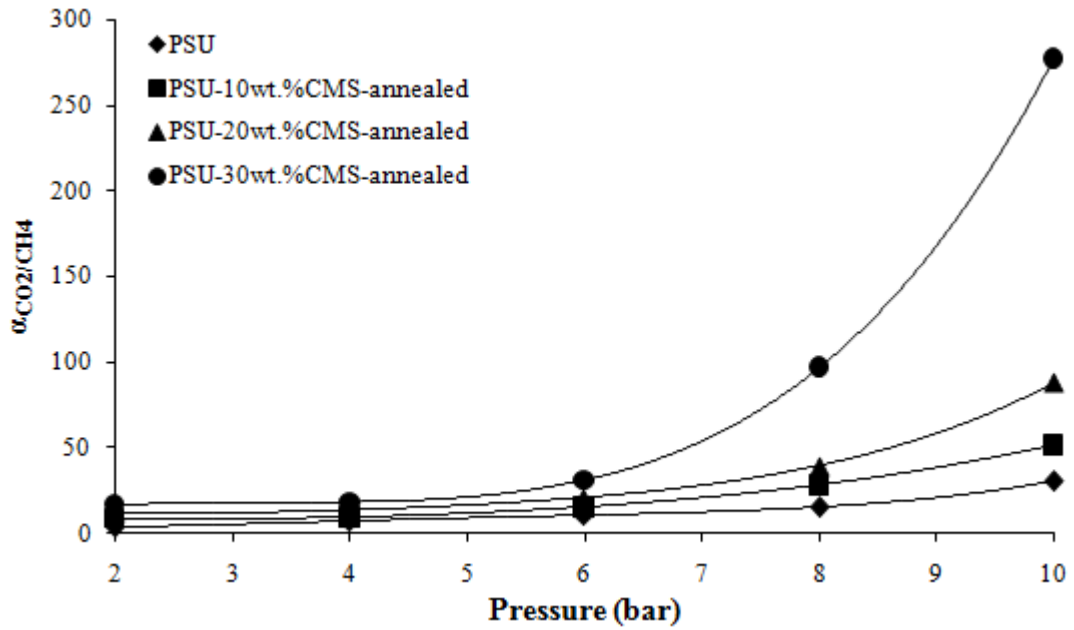


Figure 4.31: CO₂/CH₄ ideal selectivities of mixed matrix membranes using CMS with annealing treatment in various feed pressures.

On the other hand, in contrast to mixed matrix membranes without annealing treatment, membranes with annealing treatment shows lower permeabilities of CO₂ compared to the PSU membrane by 11-33% for CO₂ and 53-92% for CH₄ within the pressure range. However, the ideal selectivity of the membranes were increased, with 30 wt.% CMS the CO₂/CH₄ ideal selectivity of the membrane achieved the value of 16.3 (2 bar), 17.95 (4 bar), 30.8 (6 bar), 96.67 (8 bar), and 277 (10 bar). The same phenomena was observed by Vu et al. [20, 30] when Ultem-CMS (35 wt.%) membrane was subjected to annealing treatment above T_g , its CO₂ permeability decreased by 68%, while CO₂/CH₄ selectivity increased by 71%. The increasing rigidity of membrane, as confirmed by results from tensile test and dynamic mechanical analysis, is believed to responsible for this occurrence. As mentioned earlier, according to the model proposed by Tsagaropoulos and Eisenberg [87], the formation of loosely bound polymer and tightly bound polymer is initiated by the addition of filler particles to the polymer matrix and during annealing treatment more regions of these polymers were formed. It is also describe by Equation 2.16, when higher activation energy to make a diffusive jump is higher results in lower diffusion coefficient, which lead to lower permeability.

The diffusion of gas molecules through the polymer matrix is an activated process, as described in Section 2.2.3.2, when the gas molecules penetrate through a rigid polymer matrix higher energy is needed, since the operating condition is same for all permeation tests (i.e. the energy supplied is same) which results in lower diffusion rate of respected gas molecules. Consequently, permeability of the respected gas molecules is decreased (Equation 2.3) in higher rigidity polymer matrix. Besides the formation of reduced mobility regions, partial pore blockage of the CMS particles by polymer chains might be responsible for the reduced permeability [30]. Despite the reduced permeabilities, annealing treatment could be viewed as a potential way to enhance mixed matrix membranes performance, as shown in Figure 4.32, where the performance of membrane containing 30 wt.% CMS exceeded the upper-bound limit with 10 bar feed pressure.

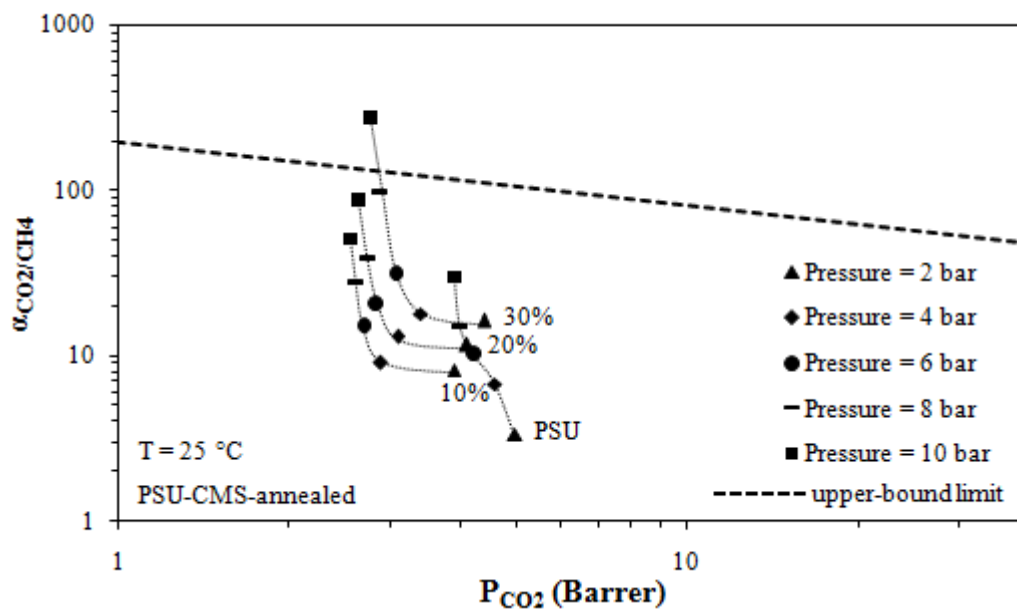


Figure 4.32: CO₂/CH₄ ideal selectivity vs CO₂ permeability for mixed matrix membranes using CMS with annealing treatment in various feed pressures.

4.4.3 Effect of using Oxidized-Carbon Molecular Sieves

Gas separation properties of mixed matrix membranes with ox-CMS are shown in Figure 4.33 and Figure 4.34. Same trend as membranes without and with annealing treatment were observed. The permeability of CO₂ and ideal selectivity of CO₂/CH₄

increases with CMS loading, while the permeability of CH₄ showing the opposite trend.

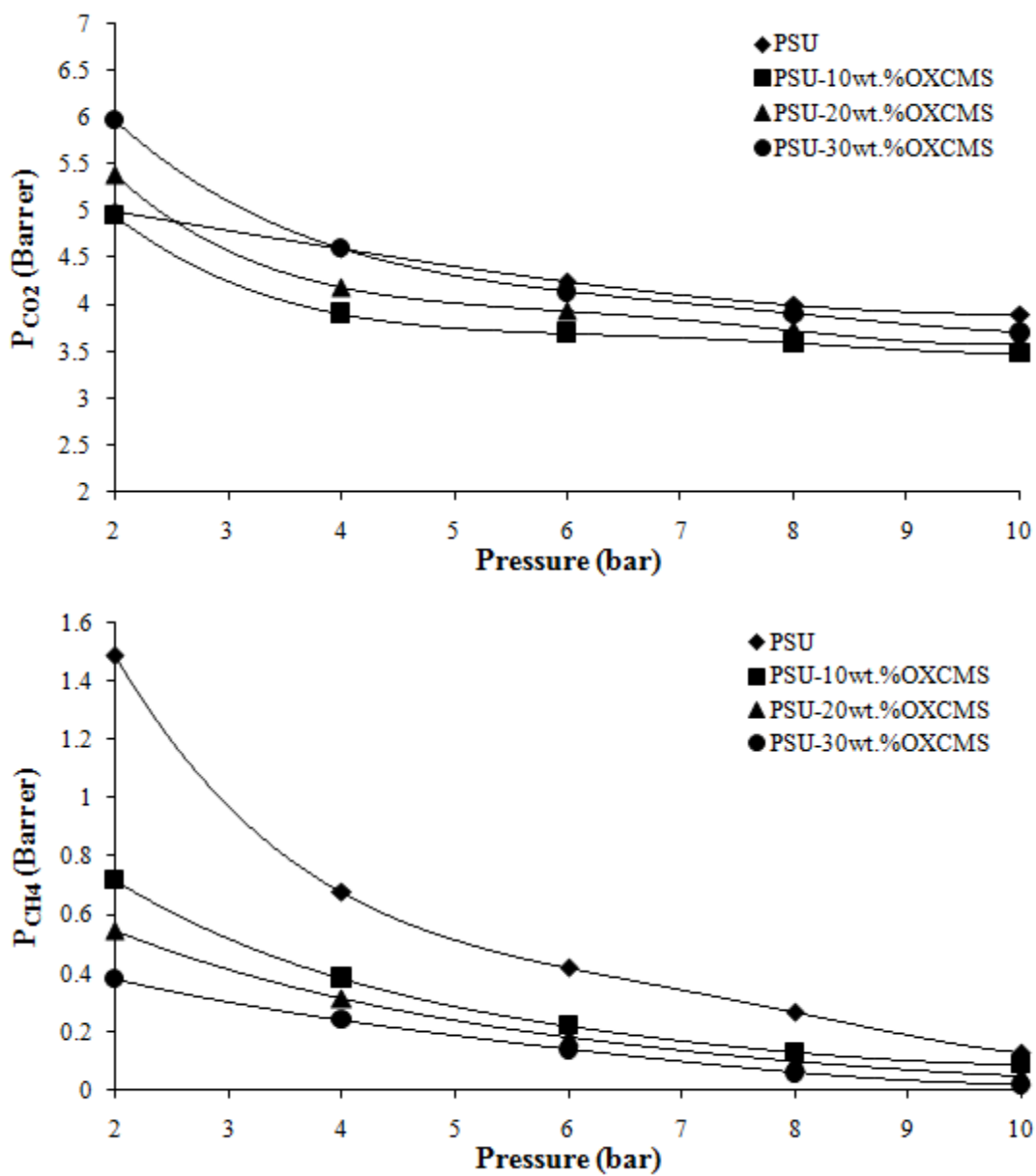


Figure 4.33: CO₂ and CH₄ permeabilities of mixed matrix membranes using oxidized-CMS in various feed pressures.

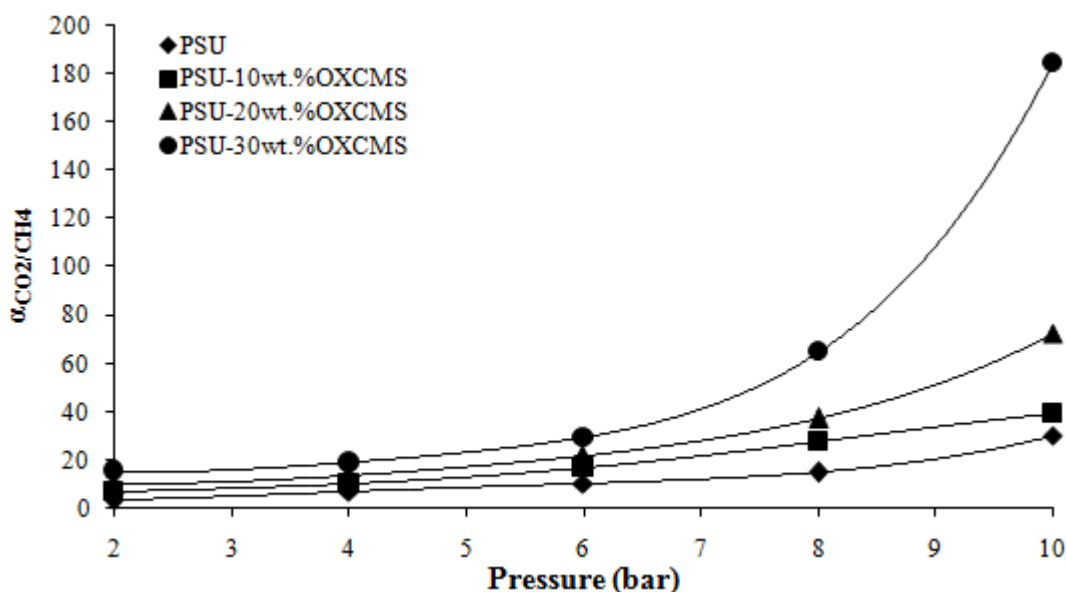


Figure 4.34: CO₂/CH₄ ideal selectivities of mixed matrix membranes using oxidized-CMS in various feed pressures.

Figure 4.33 shows that the permeabilities of CO₂ are decreased by the introduction of polar functional groups to CMS surface compared to PSU membrane, and consequently lower than mixed matrix membrane with non-functionalized CMS (Figure 4.27). Only in low feed pressure (2 bar) its CO₂ permeability exceed the pure PSU membrane, even though still lower compared to mixed matrix membranes with non-functionalized CMS by 7-19% for CO₂ and 19-67% for CH₄. Despite the reduced permeability, Figure 4.34 show the enhancement of CO₂/CH₄ ideal selectivities of mixed matrix membranes, the highest selectivity was achieved by 30 wt.% CMS at 15.67 (2 bar), 19.17 (4 bar), 29.57 (6 bar), 65 (8 bar), and 185 (10 bar). These results are similar to the membranes with annealing treatment, only the magnitude of decrement is lower when surface functionalized CMS are used. DMA results imply that there are mutual interaction between functionalized CMS with PSU since it shifted the second T_g to higher temperature compared to non-functionalized CMS, implicates stronger interaction between the two phases. Tightly and loosely bound polymers formed at CMS-PSU interface could led to counter the permeation of gas molecules through the polymer chains, due to the restricted mobility in these regions. Besides the mobility restriction of polymer chain, result from XRD analysis shows a

decrement of d-spacing from 3.65 Å to 3.41 Å due to the formation of functional groups, which can lead to block the channel to the internal structure of CMS. The map of CO₂ permeability vs CO₂/CH₄ ideal selectivity is shown in Figure 4.35. The use of 30 wt.% ox-CMS achieve the highest performance in all pressure range, and exceeded the upper-bound limit with 10 bar feed pressure.

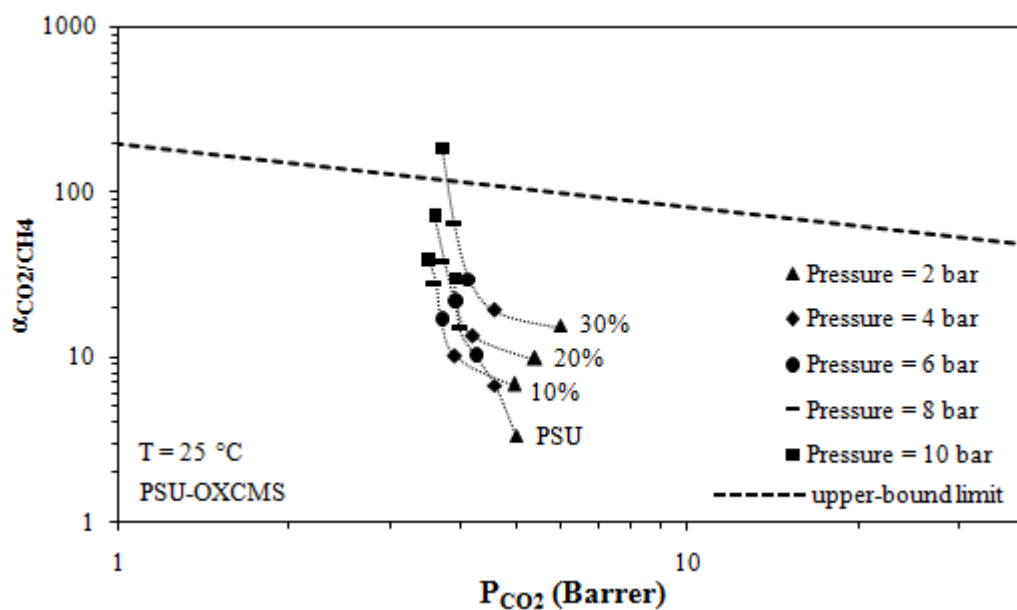


Figure 4.35: CO₂/CH₄ selectivity vs CO₂ permeability for mixed matrix membranes using oxidized-CMS in various feed pressures.

CHAPTER 5

CONCLUSIONS AND RECCOMENDATIONS

5.1 Conclusions

The development of new mixed matrix membranes has very promising future for gas separation, since it improves its physical and chemical properties as compared with the other organic and inorganic membranes. Furthermore, its performance in terms of permeability and selectivity has also been improved. The main objective of the present study was to develop mixed matrix membranes by incorporating carbon molecular sieves (CMS) particles within polysulfone (PSU) matrix. Three different CMS loadings of 10, 20, and 30 wt.% were used. Annealing of mixed matrix membranes and surface modification of CMS were done to improve PSU-CMS adhesion. The effect of CMS loading and modification in fabrication process to its morphology, mechanical, and viscoelastic properties has been studied. Gas separation properties of the present developed membranes were evaluated towards the permeability studies using CO₂ and CH₄ in several feed pressures, namely 2, 4, 6, 8, and 10 bars.

During the elementary fabrication process, mixed matrix membranes were prepared without modification on the fabrication step. It was found that the developed membranes showed homogenous distribution of CMS, however, dense CMS regions started to appear when CMS loading were increased. Dynamic mechanical analysis (DMA) of the membranes revealed the existence of dual glass transition temperatures (T_g) when incorporated with CMS in the PSU matrix, indicating the formation of restricted polymer chain regions due to the mutual interaction of the two phases. By increasing the CMS loading, the overall membrane rigidity was found to increase.

Annealing treatment subjected to mixed matrix membranes has improved the polymer-filler adhesion, shown by its morphology and the reduction of $\tan \delta$ peaks area with the shifting of the second T_g to a lower temperature. Annealing treatment has caused the brittleness of the membranes to increase, shown by its higher storage modulus, and the occurrence of necking process. However, the effect of annealing treatment appeared weaker with CMS loading, as most of the matrix constituents were thought to be tightly bound polymers.

Surface modification of CMS by nitric acid (HNO_3) oxidation formed oxidized CMS (ox-CMS) was found to improve polymer-filler adhesion due to formation of acidic functional groups on CMS surface. More orderly CMS structure was yielded after oxidation treatment as confirmed by X-ray diffraction (XRD) spectra and increasing density of CMS. Field emission scanning electron micrographs and DMA results has proved that ox-CMS shown better PSU-CMS adhesion.

Gas permeability studies of mixed matrix membranes showed a better gas separation performance over the homogeneous polymer membrane. The addition of CMS increased the CO_2 permeability and the CO_2/CH_4 ideal selectivity, while decreased the permeability of CH_4 . Within the pressure range of CO_2 2-10 bar, the addition of 30 wt.% loading of CMS increases the permeability of CO_2 up to 7-37%, and the ideal selectivity of CO_2/CH_4 up to 132-344%. On the other hand, annealing treatment had decreased the permeability of CO_2 as much as 12-29%, but increased its ideal selectivity as much as 165-823%. Similar observation were noted for the membranes with ox-CMS, the permeability of CO_2 was found to decreased down to 2-5% and increased its ideal selectivity up to 183-516%. Mixed matrix membranes modified by annealing treatment and by employing surface functionalized filler found to successfully surpass the upper-bound trade-off limit of polymeric membranes.

In conclusion, mixed matrix membranes fabricated in present study has shown a very promising potential to be used in CO_2 and CH_4 separation application. However, more research is needed before its commercial application.

5.2 Recommendations

The present study has demonstrated that mixed matrix membranes prepared could achieve significant improvement in performance. However, further work is needed to understand the characteristics of mixed matrix membranes in the effect of carbon molecular sieves used, characterize its performance under different process conditions, and the effect of membrane morphology to its performance.

Investigate alternative carbon molecular sieves

The present work could be extended by incorporate self-pyrolyze carbon molecular sieves, derived from polymeric membrane or powder. CMS derived from similar properties of continuous polymer phase are predicted to improve the adhesion between the two phases. The effect of pyrolysis conditions, such as precursor materials, temperature profiles, and pyrolysis durations to the structure of carbon molecular sieves yielded and the physical and separation properties of mixed matrix membranes could be investigated.

Permeation studies of mixed gas and different process conditions

Mixed matrix membranes fabricated in this study has revealed its separation behaviour towards pure gas (CO_2 and CH_4) in various pressures. Since the industrial application of membrane will not be in ideal conditions, further investigation on the feed gas composition and process temperature are necessary. The non-ideal environment of the mixed gas will provide information on the effect of feed gas composition to the separation mechanism and properties. The effect of feed composition will provide the information on the competition between CO_2 and CH_4 within the membrane, and its effect to membrane selectivity. Different process temperature will provide better understanding in membrane stability in various process conditions.

Fabrication of asymmetric mixed matrix membranes

In the present study flat dense mixed matrix membranes were prepared. Another strategy to improve separation properties could be done by fabricates asymmetric membrane. Asymmetric membrane structure are viewed to have better separation

properties as it combines high selectivity and high permeability due to its thin permselective layer which supported by porous substrate. Polymer, solvent, and non-solvent pair and composition may be studied to achieve membrane with greater performance. The parameter study on fabrication process such as casting rate, evaporation time, and coagulation bath composition could provide better understanding on the membrane formation mechanism.

Development of computational modelling of gas transport within the membrane

The present study could be further extended by develop a computational model of gas transport within the membrane. This computational model could later be used to predict the separation efficiency of a mixed matrix membrane. To construct the model more study such as CO₂ and CH₄ permeation in CMS particle, as well as pore size distribution of CMS would be necessary.

REFERENCES

- [1] A. Rojey, C. Jaffret, S. Cornot-Gandolphe, B. Durand, S. Jullian, and M. Valais, *Natural gas: production, processing, transport*. Paris: Editions TECHNIP, 1997.
- [2] B. Petroleum, "BP Statistical review of world energy June 2008," British Petroleum, 2008.
- [3] "Natural gas at a glance 2006," in *Secondary energy infobook: The Need Project*, 2008, pp. 28-31.
- [4] E. I. Administration, "Natural gas: Issues and trends 1998," U.S. Department of Energy, 1999.
- [5] "Natural gas - Formation and composition of natural gas, history of the discovery and use of natural gas, liquefied natural gas," in *Science encyclopedia - Volume 4*: Net Industries, 2009.
- [6] E. I. Administration, "International energy outlook 2009," U.S. Department of Energy, 2009.
- [7] E. I. Administrations, "Annual Energy Review 2008," U.S. Department of Energy, 2009.
- [8] B. Petroleum, "BP statistical review of world energy 2009," British Petroleum, 2009.
- [9] E. I. Administration, "Malaysia energy data," U.S. Department of Energy, 2008.
- [10] R.W. Baker, *Membrane technology and applications*, 2nd ed.: John Wiley & Sons Ltd., 2004.
- [11] D. Dortmund and K. Doshi, "Recent developments in CO₂ removal membrane technology," UOP LLC, Des Plaines 1999.
- [12] U. G. Limited, "Chemical composition of natural gas," Union Gas Limited, 2009.
- [13] K. Scott, *Handbook of industrial membranes*, 1st ed. Oxford: Elsevier Advanced Technology, 1995.
- [14] G. Sartori and D. W. Savage, "Sterically hindered amines for CO₂ removal from gases," *Ind. Eng. Chem. Fundam.*, vol. 22, pp. 239-249, 1983.

- [15] R.H. Perry and D. W. Green, *Perry's Chemical Engineer's Handbook*, 7th ed.: McGraw-Hill, 1997.
- [16] R. T. Yang, *Adsorbents: fundamentals and applications*: John Wiley & Sons, Inc., 2003.
- [17] S. Wong and R. Bioletti, "Carbon dioxide separation technologies," Alberta: Carbon & Energy Management Alberta Research Council, 2002.
- [18] B. Mc Kee, "Solution for 21th century: zero emission technologies for fossil fuels," France: International Energy Agencies, 2002.
- [19] J. Zou and W. S. W. Ho, "CO₂-selective polymeric membranes containing amines in crosslinked poly(vinyl alcohol)," *J. Membr. Sci.*, pp. 310-321, 2006.
- [20] D.Q. Vu, W.J. Koros, and S. J. Miller, "Mixed matrix membranes using carbon molecular sieves: I. Preparation and experimental results," *J. Membr. Sci.*, vol. 211, p. 311, 2003.
- [21] A.F. Ismail, N. Ridzuan, and S. A. Rahman, "Latest development on the membrane formation for gas separation," *Songklanakarinn J. Sci. Technol.*, vol. 24(Suppl.), pp. 1025-1043, 2002.
- [22] D. Şen, "Effect of compatibilizers on the gas separation performance of polycarbonate membranes," in *The Department of Chemical Engineering*. vol. MSc.: The Middle East Technical University, 2003.
- [23] D. Shekhawat, D.R. Luebke, and H. W. Pennline, "A review of carbon dioxide selective membranes: a topical report," National Energy Technology Laboratory, United States Department of Energy, Pittsburgh 2003.
- [24] M. Mulder, *Basic principles of membrane technology*, 2nd ed. Dordrecht: Kluwer Academic, 1996.
- [25] S. Husain, "Mixed matrix dual layer hollow fiber membranes for natural gas separation," in *School of Chemical & Biomolecular Engineering*. vol. PhD: Georgia Institute of Technology, 2006.
- [26] L.M. Robeson, "Correlation of separation factor versus permeability for polymeric membranes," *J. Membr. Sci.*, vol. 62, p. 165, 1991.
- [27] T.-S. Chung, L.Y. Jiang, and S. K. Y. Li, "Mixed matrix membranes (MMMs) comprising organic polymers with dispersed inorganic fillers for gas separation," *Prog. Polym. Sci.*, vol. 32, p. 483, 2007.
- [28] C.M. Zimmerman, A. Singh, and W. J. Koros, "Tailoring mixed matrix composite membranes for gas separations," *J. Membr. Sci.*, vol. 137, p. 145, 1997.

- [29] A.F. Ismail and L. I. B. David, "A review on the latest development of carbon membranes for gas separation," *J. Membr. Sci.*, vol. 193, pp. 1-18, 2001.
- [30] D.Q. Vu, "Formation and characterization of asymmetric carbon molecular sieve and mixed matrix membranes for natural gas purification." vol. PhD: The University of Texas at Austin, 2001.
- [31] T.T. Moore, "Effect of materials, processing, and operating conditions on the morphology and gas transport properties of mixed matrix membranes, ." vol. PhD: The University of Texas at Austin, 2004.
- [32] M. Anson, J. Marchese, E. Garis, N. Ochoa, and C. Pagliero, "ABS copolymer-activated carbon mixed matrix membranes for CO₂/CH₄ separation, ," *J. Membr. Sci.*, vol. 243, p. 19, 2004.
- [33] S.P. Nunes, J. Schultz, and K. V. Peinemann, "Silicone membranes with silica nanoparticles," *J. Mater. Sci. Lett.*, vol. 15, pp. 1139-1141, 1996.
- [34] B.P. Singh, D. Singh, R.B. Mathur, and T. L. Dhami, "Influence of surface modified MWCNTs on the mechanical, electrical, and thermal properties of polyimide nanocomposites," *Nanoscale Res. Lett.*, vol. 3, pp. 444-453, 2008.
- [35] S. Kim, L. Chen, J.K. Johnson, and E. Marand, "Polysulfone functionalized carbon nanotube mixed matrix membranes for gas separation: Theory and experiment," *J. Membr. Sci.*, vol. 294, p. 147, 2007.
- [36] P. Pandey and R. S. Chauhan, "Membranes for gas separation," *Prog. Polym. Sci.*, vol. 26, pp. 853-893, 2001.
- [37] R.W. Baker, "Future directions of membrane gas separation technology," *Ind. Eng. Chem. Res.*, vol. 41, pp. 1393-1411, 2002.
- [38] J.-M. Duval, B. Folkers, M.H.V. Mulder, G. Desgrandchamps, and C. A. Smolders, "Adsorbent filled membranes for gas separation. Part 1. Improvement of the gas separation properties of polymeric membranes by incorporation of microporous adsorbents, ," *J. Membr. Sci.*, vol. 80, p. 189, 1993.
- [39] J.-M. Duval, A.J.B. Kemperman, B. Folkers, M.H.V. Mulder, G. Desgrandchamps, and C. A. Smolders, "Preparation of zeolite filled glassy polymer membranes," *J. Appl. Poly. Sci.*, vol. 54, pp. 409-418, 1994.
- [40] I.V.J. Vankelecom, E. Merckx, M. Luts, and J. B. Uytterhoeven, "Incorporation of zeolites in polyimide membranes," *J. Phys. Chem.*, vol. 99, p. 13187, 1995.
- [41] T.M. Gur, "Permselectivity of zeolite filled polysulfone gas separation membranes," *J. Membr. Sci.*, vol. 93, p. 283, 1994.

- [42] R. Mahajan, R. Burns, M. Schaeffer, and W. J. Koros, "Challenges in forming successful mixed matrix membranes with rigid polymeric materials," *J. Appl. Poly. Sci.*, vol. 86, pp. 881-890, 2002.
- [43] S.A. Stern, "Polymers for gas separations: the next decade," *J. Membr. Sci.*, vol. 94, pp. 1-65, 1994.
- [44] G.C. Kapantaidakis, S.P. Kaldis, X.S. Dabou, and G. P. Sakellaropoulos, "Gas permeation through PSF-PI miscible blend membranes," *J. Membr. Sci.*, vol. 110, pp. 239-247, 1996.
- [45] K. Sutherland, *Profile of the international membrane industry: market prospects to 2008*, 3rd ed. Oxford: Elsevier Advanced Technology, 2004.
- [46] K.M. Steel, "Carbon membranes for challenging gas separations," in *Chemical Engineering Department*. vol. PhD Austin: University of Texas at Austin, 2000.
- [47] D.R. Paul and D. R. Kemp, "The diffusion time lag in polymer membranes containing adsorptive fillers," *J. Polym. Sci. Polym. Phys.*, vol. 41, pp. 79-93, 1973.
- [48] M. Jia, K.V. Peinemann, and R.D. Behling, "Molecular sieving effect of the zeolite-filled silicone rubber membranes in gas permeation," *J. Membr. Sci.*, vol. 57, pp. 289-296, 1991.
- [49] S. Kulprathipanja, H. Estates, R.W. Neuzil, D. Grove, N.N. Li, and A. Heights, "Separation of fluids by means of mixed matrix membranes." vol. 4,740,219, U. S. Patent, Ed.: Allied-Signal Inc., 1988.
- [50] M.G. Sürer, N. Baç, and L. Yilmaz, "Gas permeation characteristic of polymer-zeolite mixed matrix membranes," *J. Membr. Sci.*, vol. 91, pp. 77-86, 1994.
- [51] R. Mahajan, C.M. Zimmerman, and W. J. Koros, "Fundamental and practical aspects of mixed matrix gas separation membranes," in *ACS Symposium Series No. 733*, B.D. Freeman and I. Pinnau, Eds. Washington DC: American Chemical Society, 1999, pp. 277-286.
- [52] I.F.J. Vankelecom, E. Scheppers, R. Heus, and J. B. Uytterhoeven, "Parameters influencing zeolite incorporation in PDMS membranes," *J. Phys. Chem.*, vol. 98, pp. 12390-12396, 1994.
- [53] M. Anson, J. Marchese, E. Garis, N. Ochoa, and C. Pagliero, "ABS copolymer-activated carbon mixed matrix membranes for CO₂/CH₄ separation," *J. Membr. Sci.*, vol. 243, pp. 19-28, 2004.
- [54] S. Kim, T.W. Pechar, and E. Marand, "Poly(imide siloxane) and carbon nanotube mixed matrix membranes for gas separation," *Desalination*, vol. 192, pp. 330-339, 2006.

- [55] I.F.J. Vankelecom, S. Van den Broeck, E. Merckx, H. Geerts, P. Grobet, and J. B. Utterhoeven, "Silylation to improve incorporation of zeolites in polyimide films," *J. Phys. Chem.*, vol. 100, pp. 3753-3758, 1996.
- [56] Y. Li, H.-M. Guan, T.-S. Chung, and S. Kulprathipanja, "Effect of novel silane modification of zeolite surface on polymer chain rigidification and partial pore blockage in polyethersulfone (PES)-zeolite A mixed matrix membranes," *J. Membr. Sci.*, vol. 275, p. 17, 2006.
- [57] S. Husain and W. J. Koros, "Mixed matrix hollow fiber membranes made with modified HSSZ-13 zeolite in polyetherimide polymer matrix for gas separation," *J. Membr. Sci.*, vol. 288, pp. 195-207, 2007.
- [58] H.H. Yong, H.C. Park, Y.S. Kanga, J.Won, and W. N. Kimb, "Zeolite-filled polyimide membrane containing 2,4,6-triaminopyrimidine," *J. Membr. Sci.*, vol. 188, pp. 151-163, 2001.
- [59] W.J. Koros, D.Q. Vu, R. Mahajan, and S. J. Miller, "Gas separation using mixed matrix membranes." vol. US 6,503,295 B1, U. S. Patent, Ed.: Chevron U.S.A. Inc., The University of Texas System, 2003.
- [60] W.A.W. Rafizah and A.F. Ismail, "Effect of carbon molecular sieve sizing with poly(vinyl pyrrolidone) K-15 on carbon molecular sieve-polysulfone mixed matrix membrane," *J. Membr. Sci.*, vol. 307, pp. 53-61, 2008.
- [61] R.C. Bansal and M. Goyal, *Activated carbon adsorption*. Boca Raton: Taylor & Francis Group, 2005.
- [62] C.C. Miller, "The Stokes-Einstein law for diffusion in solution," *Proceedings of Royal Society of London, Series A*, 1924.
- [63] W.W. Brandt, "Model calculation of the temperature dependence of small molecule diffusion in high polymers," *J. Phys. Chem.*, vol. 63, pp. 1080-1084, 1959.
- [64] A.T. DiBenedetto and D. R. Paul, "Molecular properties of amorphous high polymers. An interpretation of gaseous diffusion through polymers," *J. Polym. Sci. Part A*, vol. 1, pp. 3477-3487, 1964.
- [65] R.J. Pace and A. Dadyner, "Statistical mechanical model for diffusion of simple penetrants in polymers," *J. Polym. Sci. Polym. Phys. Ed.*, vol. 17, pp. 437-451, 1979.
- [66] W.J. Koros, A.H. Chan, and D.R. Paul, "Carbon dioxide sorption and transport in polycarbonate," *J. Polym. Sci. Part A-2 Polym Phys*, vol. 14, pp. 687-702, 1976.
- [67] J.H. Petropoulos, "Mechanisms and theories for sorption and diffusion of gasses in polymers," in *Polymeric gas separation membranes*, D.R. Paul and Y. P. Yampol'skii, Eds. Boca Raton: CRC Press, Inc., 1994, pp. 17-82.

- [68] M.R. Pixton and D. R. Paul, "Relationships between structure and transport properties for polymer with aromatic backbones," in *Polymeric gas separation membranes*, D.R. Paul and Y. P. Yampol'skii, Eds. Boca Raton: CRC Press, Inc., 1994, pp. 83-154.
- [69] J.M.D. Tascon, "Overview of carbon materials in relation to adsorption," in *Adsorption by carbons*, 1st ed, E.J. Bottani and J. M. D. Tascon, Eds. Amsterdam: Elsevier, 2008.
- [70] "UDEL Polysulfone," Solvay Membranes, 2010.
- [71] R.-C. Ruaan, T. Chang, and D.-M. Wang, "Selection criteria for solvent and coagulation medium in view of macrovoid formation in the wet phase inversion process," *J. Polym. Sci. B: Polym. Phys.*, vol. 37, pp. 1495-1502, 1999.
- [72] M.W. Marshall, S. Popa-Nita, and J. G. Shapter, "Measurement of functionalised carbon nanotube carboxylic acid groups using a simple chemical process," *Carbon*, vol. 44, pp. 1137-1141, 2006.
- [73] P. Vinke, M. Van Der Elik, M. Verbree, A.F. Voskamp, and H. V. Bekkum, "Modification of the surfaces of a gas-activated carbon and a chemically activated carbon with nitric acid, hypochlorite, and ammonia," *Carbon*, vol. 32, pp. 675-686, 1994.
- [74] H.P. Boehm, "Surface oxides on carbon and their analysis: a critical assessment," *Carbon*, vol. 40, pp. 145-149, 2002.
- [75] Z. Wu, C.U. Pittman Jr., and S. D. Gardner, "Nitric acid oxidation of carbon fibers and the effect of subsequent treatment in refluxing aqueous NaOH," *Carbon*, vol. 33, p. 597, 1995.
- [76] L.H. Sperling, *Introduction to physical polymer science*. New Jersey: John Wiley, 2006.
- [77] C. Torras, F. Ferrando, J. Paltakari, and R. Garcia-Valls, "Performance, morphology, and tensile characterization of activated carbon composite membranes for the synthesis of enzyme membrane reactors," *J. Membr. Sci.*, vol. 282, pp. 149-161, 2006.
- [78] D. Roylance, "Stress-strain curve," Cambridge: Department of Materials Science and Engineering Massachusetts Institute of Technology, 2001.
- [79] K.P. Menard, *Dynamic mechanical analysis: a practical introduction*, 2nd ed. Boca Raton: CRC Press, 2008.
- [80] J. Yang, J. Hu, C. Wang, Y. Qin, and Z. Guo, "Fabrication and characterization of soluble multi-walled carbon nanotubes reinforced P(MMA-co-EMA) composites," *Macromol. Mater. Eng.*, vol. 289, pp. 828-832, 2004.

- [81] R.M. Silverstein, F.X. Webster, and D.J. Kiemle, *Spectrometric identification of organic compounds*, 7th ed.: John Wiley & Sons, Inc., 2005.
- [82] P. Hacırlıoğlu, L. Toppare, and L. Yılmaz, "Effect of preparation parameters on the performance of dense homogeneous polycarbonate gas separation membranes," *J. Appl. Polym. Sci.*, vol. 90, pp. 776-785, 2003.
- [83] Y. Kishimoto and R. Ishii, "Differential scanning calorimetry of polysulfone at high pressures of CO₂ and N₂O," *Polymer Bulletin*, vol. 43, p. 255, 1999.
- [84] A. Alhamid, "Parametric analysis of CO₂ separation from natural gas," in *Chemical Engineering*. vol. MSc. Tronoh: Universiti Teknologi Petronas, 2006.
- [85] S. Matsumura, S. Sato, M. Yudasaka, A. Tomida, T. Tsuruo, S. Iijima, and K. Shiba, "Prevention of carbon nanohorn agglomeration using a conjugate composed of comb-shaped polyethylene glycol and a peptide aptamer.," *Mol. Pharm.*, vol. 6, pp. 441-447, 2009.
- [86] C. Pomchaitaward, I. Manas-Zloczower, and D. L. Feke, "Investigation of the dispersion of carbon black agglomerates of various sizes in simple-shear flows," *Che. Eng. Sci.*, vol. 58, pp. 1859-1865, 2002.
- [87] G. Tsagaropoulos and A. Eisenberg, "Dynamic mechanical study of the factors affecting the two glass transition behavior of filled polymers. Similarities and differences with random ionomers," *Macromolecules*, vol. 28, pp. 6067-6077, 1995.
- [88] J.-S. Kim, R.J. Jackman, and A. Eisenberg, "Filler and percolation behavior of ionic aggregates in styrene-sodium methacrylate ionomers," *Macromol.*, vol. 27, pp. 2789-2803, 1994.
- [89] B. Lauke, "On the effect of particle size on fracture toughness of polymer composites," *Compos. Sci. Technol.*, vol. 68, pp. 3365-3372, 2008.
- [90] P. Gou, H. Song, and X. Chen, "Interfacial properties and microstructures of multiwalled carbon nanotubes/epoxy composites," *Matter. Sci. Eng. A*, vol. 517, pp. 17-23, 2009.
- [91] M. Ito, T. Nakamura, and K. Tanaka, "Pulsed NMR study on the silica-filled rubber systems," *J. Appl. Polym. Sci.*, vol. 30, pp. 3493-3504, 1985.
- [92] P. Chingombe, B. Saha, and R. J. Wakeman, "Surface modification and characterisation of a coal-based activated carbon," *Carbon*, vol. 43, pp. 3132-3143, 2005.
- [93] A.I. Schepetkin, I.A. Khlebnikov, Y.S. Ah, B.S. Woo, C. Jeong, and N. O. Klubachuk, "Characterization and biological activities of humic substance from mumie," *J. Agric. Food. Chem.*, vol. 51, pp. 5245-5154, 2003.

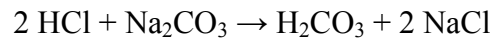
- [94] B. Cagnon, X. Py, A. Guillot, J.P. Joly, and R. Berjoan, "Pore structure modification of pitch-based activated carbon by NaOCl and air oxidation/pyrolysis cycles," *Microp. Mesop. Mater.*, vol. 80, 2005.
- [95] S. Biniak, G. Szymański, J. Siedlewski, and A. Świątkowski, "The characterization of activated carbons with oxygen and nitrogen surface groups," *Carbon*, vol. 35, pp. 1799-1810, 1997.
- [96] A. Marcías-García, M.A. Díaz-Díez, E.M. Cuerda-Correa, M. Olivares-Marín, and J. Gañan-Gómez, "Study of the pore size distribution and fractal dimension of HNO₃-treated activated carbons," *Appl. Surf. Sci.*, vol. 252, pp. 5972-5975, 2006.
- [97] P.A. Bazula, "Structure and pore structure modification of ordered mesoporous carbons via chemical oxidation approach," *Microp. Mesop. Mater.*, vol. 108, pp. 266-275, 2008.
- [98] W. Shen, Z. Li, and Y. Liu, "Surface chemical functional groups modification of porous carbon," *Recent Patents on Chemical Engineering*, vol. 1, pp. 27-40, 2008.
- [99] B.P. Grady, F. Pompeo, R.L. Shambaugh, and D. E. Resasco, "Nucleation of polypropylene crystallization by single-walled carbon nanotubes," *J. Phys. Chem. B*, vol. 106, p. 5852, 2002.
- [100] J. Yang, Y. Lin, J. Wang, M. Lai, J. Li, J. Liu, X. Tong, and H. Cheng, "Morphology, thermal stability, and dynamic mechanical properties of atactic polypropylene/carbon nanotube composites," *J. Appl. Polym. Sci.*, vol. 98, p. 1087, 2005.
- [101] Y.T. Sung, C.K. Kum, H.S. Lee, N.S. Byon, H.G. Yoon, and W. N. Kim, "Dynamic mechanical and morphological properties of polycarbonate/multi-walled carbon nanotube composites," *Polymer*, vol. 46, pp. 5656-5661, 2005.
- [102] T. Ramanathan, H. Liu, and L.C. Brinson, "Functionalized SWNT/polymer nanocomposites for dramatic property improvement," *J. Polym. Sci. B: Polym. Phys.*, vol. 43, p. 2269, 2005.
- [103] D.R. Paul and W. J. Koros, "Effect of partially immobilizing sorption on permeability and the diffusion time lag," *J. Polym. Sci.: Polym. Phys.*, vol. 14, pp. 675-685, 1975.
- [104] W.R. Vieth, M.A. Amini, A. Constantinides, and R. A. Ludolph, "Extension of the dual sorption theory and its relation to transport phenomena in biologically active membranes," *Ind. Eng. Chem., Fundam.*, vol. 16, 1977.
- [105] G.S. Huvard, V.T. Stannett, W.J. Koros, and H. B. Hopfenberg, "The pressure dependence of CO₂ sorption and permeation in poly(acrylonitrile)," *J. Membr. Sci.*, vol. 6, pp. 185-201, 1980.

PUBLICATION

1. International Conference on Chemical, Biological, and Environmental Engineering 2009 (Singapore, 9-11 October 2009)
“Development of Polysulfone-Carbon Molecular Sieves Mixed Matrix Membranes for CO₂ Removal from Natural Gas”
Amelia Suyono Wiryoatmojo, Hilmi Mukhtar, Zakaria Man
(Conference proceeding published by World Scientific World, indexed by Thomson ISI Proceeding, IACSIT Database, and Ei Compendex)
2. The 7th International Conference on Membrane Science and Technology (Malaysia, 12-15 May 2009)
“Effect of Annealing Treatment on Physical Properties of Polysulfone-Carbon Molecular Sieve Mixed Matrix Membranes”
Amelia Suyono Wiryoatmojo, Hilmi Mukhtar, Zakaria Man
(Conference proceeding published by Advanced Membrane Technology Research Centre of Universiti Teknologi Malaysia)
3. National Postgraduate Conference on Engineering, Science, and Technology (Malaysia, 31 March 2008)
“Development of Mixed Matrix Membrane Using Carbon Filter for CO₂ Removal from Natural Gas”
Amelia Suyono Wiryoatmojo, Hilmi Mukhtar, Zakaria Man
(Conference proceeding published by Universiti Teknologi Petronas)

APPENDIX A
ACIDIC CAPACITY OF CARBON MOLECULAR SIEVES

Acidic capacity of carbon molecular sieves were measured by its NaOH uptake capacity, which quantified by simple acid-base titration against HCl. Since hydrochloric acid (HCl) is not a primary standard, before it used as titrant in the acid-base titration, it should be standardized first. Primary standard which used in this study is 0.05 M of sodium carbonate (Na₂CO₃). The reaction between HCl and Na₂CO₃ shown below:

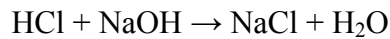


5.4 ml of HCl were needed to neutralized 25 ml of Na₂CO₃, therefore the concentration of HCl (C_{HCl}) could be calculated as:

$$C_{\text{HCl}} = \frac{2 \times C_{\text{Na}_2\text{CO}_3} \times V_{\text{Na}_2\text{CO}_3}}{V_{\text{HCl}}}$$

$$C_{\text{HCl}} = \frac{2 \times 0.05 \text{ M} \times 25 \text{ ml}}{5.4 \text{ ml}} = 0.463 \text{ M}$$

The known HCl concentration was then used to neutralize NaOH, with reaction as follow:



The concentration of NaOH (C_{NaOH}) could be calculated by using:

$$C_{\text{NaOH}} = \frac{C_{\text{HCl}_3} \times V_{\text{HCl}}}{V_{\text{NaOH}}}$$

The concentration of NaOH control solution is:

$$C_{\text{NaOH}} = \frac{0.463 \text{ M} \times 26 \text{ ml}}{20 \text{ ml}} = 0.602 \text{ M}$$

The number of mole of NaOH in the blank solution is:

$$n_{\text{NaOH}} = \frac{C_{\text{NaOH}}}{V_{\text{NaOH}}} = \frac{0.602 \text{ M}}{20 \text{ ml}} = 30.1 \mu\text{mol}$$

1 gram of the un-oxidized and nitric acid-oxidized CMS powder were then soaked in 50 ml of NaOH solution and shaken for 72 hours. 20 ml aliquots of the filtered solutions were titrated by the standardized HCl solution. Data series from the titration is given in Table A.1.

Table A.1: Acid-base titration data of oxidized-carbon molecular sieves.

CMS	Run no.	V _{HCl} (ml)	C _{NaOH} (M)	Average C _{NaOH} (M)	n _{NaOH} (μmol)	Average n _{NaOH} (μmol)
Un-oxidized	1	26.0	0.602	0.596	30.10	29.81
	2	25.5	0.590		29.52	
2M HNO ₃	1	25.5	0.590	0.590	29.52	29.52
	2	25.5	0.590		29.52	
5M HNO ₃	1	25.0	0.579	0.579	28.94	28.94
	2	25.0	0.579		28.94	
8M HNO ₃	1	23.0	0.535	0.535	26.62	26.62
	2	23.0	0.535		26.62	
11M HNO ₃	1	22.5	0.521	0.521	26.04	26.04
	2	22.5	0.521		26.04	

The acidic capacity of CMS calculated from the difference between the number of moles of NaOH in the blank solution and in the sample. It is assumed that the difference is equal to the number of moles of NaOH neutralized by the acidic functional group on the surface of 1 gram of CMS powder.

$$\text{Total Acidic Capacity} = \frac{n_{\text{control}} - n_{\text{sample}}}{W_{\text{sample}}}$$

Therefore the Total Acidic Capacity (TAC) for all samples could be calculated by the above equation. TAC for all samples are tabulated in Table A.2.

Table A.2: Total acidic capacity of oxidized-carbon molecular sieves.

CMS	Run no.	TAC ($\mu\text{mol/g}$)	Average TAC ($\mu\text{mol/g}$)
Un-oxidized	1	0.0050	0.294
	2	0.5838	
2M HNO ₃	1	0.5838	0.584
	2	0.5838	
5M HNO ₃	1	1.1625	1.163
	2	1.1625	
8M HNO ₃	1	3.4775	3.478
	2	3.4775	
11M HNO ₃	1	4.0563	4.056
	2	4.0563	

APPENDIX B
PERMEABILITY OF MEMBRANE CALCULATION

Permeability of a membrane was measured by considering the volumetric flow rate of certain gas through the membrane. Gas permeation measurement was performed using gas membrane permeation unit. Pure CO₂ and CH₄ were employed as tests gases. Membrane was cut into a circular with effective area 14.53 cm² and mounted into the module. Before measurement, the system was vacuumed to remove any gases or vapours sorbed into the membrane. Experiments were carried out in 25°C, with pressure at the upstream side vary from 2-10 barg, and done until steady state condition accomplished.

As example, in 25°C and feed pressure 2 bar, a 106.43 μm of polysulfone (PSU) membrane was able to permeate a 0.07 cm³ CO₂ gas in 600 seconds with permeate in atmospheric pressure. The permeability of CO₂ gas can be determined as follows:

CO₂ volumetric flow rate, Q , was calculated as follows:

$$Q_i = \frac{\Delta V_i}{\Delta t_i}$$

$$Q_{CO_2} = \frac{0.07 \text{ cm}^3}{600 \text{ s}}$$

$$= 1.167 \times 10^{-4} \text{ cm}^3 / \text{s}$$

The volumetric flow rate was then corrected to standard pressure and temperature condition (1 atm, 0°C), Q_{STP} , as follows:

$$Q_{STP_i} = Q_i \times \frac{T_{STP}}{T_i}$$

$$= 1.167 \times 10^{-4} \text{ cm}^3 / \text{s} \times \frac{273K}{298K}$$

$$= 1.069 \times 10^{-4} \text{ cm}^3 (STP) / \text{s}$$

CO₂ flux is expressed as the volumetric flow rate of CO₂ gas per unit membrane area, calculated as follows:

$$J_i = \frac{Q_{STP}}{A}$$

$$J_{CO_2} = \frac{1.069 \times 10^{-4} \text{ cm}^3 (\text{STP}) s^{-1}}{14.53 \text{ cm}^2}$$

$$= 7.356 \times 10^{-6} \text{ cm}^3 (\text{STP}) / \text{cm}^2 s$$

CO₂ permeability is a pressure- and thickness-normalized flux of the gas through the membrane and defined by:

$$P_i = \frac{J_i \ell}{\Delta p_i}$$

Since, $p_{CO_2, feed} = 2 \text{ bar} = 150.0128 \text{ cmHg} + 76.0002 \text{ cmHg} = 226.013 \text{ cmHg}$; and

$$p_{CO_2, permeate} = 1 \text{ atm} = 76.0002 \text{ cmHg}$$

$$P_{CO_2} = \frac{(7.356 \times 10^{-6} \text{ cm}^3 (\text{STP}) / \text{cm}^2 s) \times (106 \times 10^{-4} \text{ cm})}{(226.013 - 76.0002) \text{ cmHg}}$$

$$= 5.22 \times 10^{-10} \text{ cm}^3 (\text{STP}) \text{ cm} / \text{cm}^2 s \text{ cmHg}$$

Permeability is often expressed in customary unit of Barrer, which
 $1 \text{ Barrer} = 1 \times 10^{-10} \text{ cm}^3 (\text{STP}) \text{ cm} / \text{cm}^2 s \text{ cmHg}$

Therefore, $P_{CO_2} = 5.22 \text{ Barrer}$

By using similar step permeability of CH₄ gas can be calculated. For the same experiment condition, permeability of CH₄ was obtained 1.49 Barrer. Therefore, the ideal selectivity (α) of CO₂/CH₄ can be determined by taking the ratio of permeability of one penetrant over another, as follows:

$$\alpha_{CO_2/CH_4} = \frac{P_{CO_2}}{P_{CH_4}}$$

$$= \frac{5.22 \text{ Barrer}}{1.49 \text{ Barrer}}$$

$$= 3.50$$

From permeation that has been done the result can be seen in following Tables.

Table B.1: Gas permeation results of polysulfone membranes.

Membrane	Run no.	P (bar)	tCO ₂ (s)	tCH ₄ (s)	VCO ₂ (cm ³)	VCH ₄ (cm ³)	PCO ₂ (Barrer)	PCH ₄ (Barrer)	α_{CO_2/CH_4}
M1	1	2	600	1200	0.070	0.040	5.22	1.49	3.50
	2		600	1200	0.068	0.038	5.07	1.42	3.58
	Average		600	1200	0.069	0.039	5.14	1.45	3.54
	SD		0	0	0.001	0.001	0.11	0.05	0.06
M2	1	2	600	1200	0.068	0.042	5.07	1.57	3.24
	2		600	1200	0.062	0.040	4.62	1.49	3.10
	Average		600	1200	0.065	0.041	4.85	1.53	3.17
	SD		0	0	0.004	0.001	0.32	0.05	0.10
M1	1	4	600	6000	0.118	0.180	4.40	0.67	6.63
	2		600	6000	0.124	0.184	4.62	0.69	6.74
	Average		600	6000	0.121	0.182	4.51	0.68	6.68
	SD		0	0	0.004	0.003	0.16	0.01	0.08
M2	1	4	600	6000	0.122	0.190	4.55	0.71	6.49
	2		600	6000	0.130	0.180	4.85	0.67	7.22
	Average		600	6000	0.126	0.185	4.70	0.69	6.86
	SD		0	0	0.006	0.007	0.21	0.03	0.52
M1	1	6	600	3000	0.172	0.084	4.27	0.42	10.24
	2		600	3000	0.174	0.090	4.32	0.45	9.67
	Average		600	3000	0.173	0.087	4.30	0.43	9.95
	SD		0	0	0.001	0.004	0.04	0.02	0.40
M2	1	6	600	3000	0.170	0.082	4.23	0.41	10.37
	2		600	3000	0.168	0.080	4.18	0.40	10.24
	Average		600	3000	0.169	0.081	4.20	0.40	10.30
	SD		0	0	0.001	0.001	0.04	0.01	0.09
M1	1	8	600	3000	0.208	0.070	3.88	0.26	14.86
	2		600	3000	0.220	0.070	4.10	0.26	16.18
	Average		600	3000	0.214	0.070	3.99	0.26	15.52
	SD		0	0	0.008	0.000	0.16	0.00	0.93
M2	1	8	600	3000	0.210	0.072	3.91	0.27	14.58
	2		600	3000	0.220	0.080	4.10	0.30	14.10
	Average		600	3000	0.215	0.076	4.01	0.28	14.34
	SD		0	0	0.007	0.006	0.13	0.02	0.34
M1	1	10	600	3600	0.256	0.050	3.82	0.12	32.00
	2		600	3600	0.260	0.052	3.88	0.13	27.86
	Average		600	3600	0.258	0.051	3.85	0.13	29.93
	SD		0	0	0.003	0.001	0.04	0.00	2.93
M2	1	10	600	3600	0.260	0.050	3.88	0.12	31.20
	2		600	3600	0.270	0.056	4.03	0.14	28.93
	Average		600	3600	0.265	0.053	3.95	0.13	30.06
	SD		0	0	0.007	0.004	0.11	0.01	1.61

Table B.2: Gas permeation results of mixed matrix membranes contain 10 wt.% CMS.

Membrane	Run no.	P (bar)	tCO ₂ (s)	tCH ₄ (s)	VCO ₂ (cm ³)	VCH ₄ (cm ³)	PCO ₂ (Barrer)	PCH ₄ (Barrer)	α_{CO_2/CH_4}
M1	1	2	300	2400	0.036	0.054	5.37	1.01	5.33
	2		300	2400	0.032	0.054	4.77	1.01	4.74
	Average		300	2400	0.034	0.054	5.07	1.01	5.04
	SD		0	0	0.003	0.000	0.42	0.00	0.42
M2	1	2	300	2400	0.032	0.052	4.77	0.97	4.92
	2		300	2400	0.036	0.052	5.37	0.97	5.54
	Average		300	2400	0.034	0.052	5.07	0.97	5.23
	SD		0	0	0.003	0.000	0.42	0.00	0.44
M1	1	4	300	2400	0.070	0.058	5.22	0.54	9.66
	2		300	2400	0.060	0.058	4.47	0.54	8.28
	Average		300	2400	0.065	0.058	4.85	0.54	8.97
	SD		0	0	0.007	0.000	0.53	0.00	0.98
M2	1	4	300	2400	0.062	0.050	4.62	0.47	9.92
	2		300	2400	0.068	0.050	5.07	0.47	10.88
	Average		300	2400	0.065	0.050	4.85	0.47	10.40
	SD		0	0	0.004	0.000	0.32	0.00	0.68
M1	1	6	300	2400	0.094	0.060	4.67	0.37	12.53
	2		300	2400	0.088	0.044	4.37	0.27	16.00
	Average		300	2400	0.091	0.052	4.52	0.32	14.27
	SD		0	0	0.004	0.011	0.21	0.07	2.45
M2	1	6	300	2400	0.082	0.052	4.08	0.32	12.62
	2		300	2400	0.090	0.052	4.47	0.32	13.85
	Average		300	2400	0.086	0.052	4.27	0.32	13.23
	SD		0	0	0.006	0.000	0.28	0.00	0.87
M1	1	8	300	2400	0.110	0.040	4.10	0.19	22.00
	2		300	2400	0.108	0.042	4.03	0.20	20.57
	Average		300	2400	0.109	0.041	4.06	0.19	21.29
	SD		0	0	0.001	0.001	0.05	0.01	1.01
M2	1	8	300	2400	0.100	0.046	3.73	0.21	17.39
	2		300	2400	0.120	0.044	4.47	0.21	21.82
	Average		300	2400	0.110	0.045	4.10	0.21	19.60
	SD		0	0	0.014	0.001	0.53	0.01	3.13
M1	1	10	300	3600	0.130	0.044	3.88	0.11	35.45
	2		300	3600	0.140	0.044	4.18	0.11	38.18
	Average		300	3600	0.135	0.044	4.03	0.11	36.82
	SD		0	0	0.007	0.000	0.21	0.00	1.93
M2	1	10	300	3600	0.130	0.046	3.88	0.11	33.91
	2		300	3600	0.138	0.044	4.12	0.11	37.64
	Average		300	3600	0.134	0.045	4.00	0.11	35.77
	SD		0	0	0.006	0.001	0.17	0.00	2.63

Table B.3: Gas permeation results of mixed matrix membranes contain 20 wt.% CMS.

Membrane	Run no.	P (bar)	tCO ₂ (s)	tCH ₄ (s)	VCO ₂ (cm ³)	VCH ₄ (cm ³)	PCO ₂ (Barrer)	PCH ₄ (Barrer)	α_{CO_2/CH_4}
M1	1	2	300	2400	0.039	0.038	5.82	0.71	8.21
	2		300	2400	0.041	0.037	6.11	0.69	8.86
	Average		300	2400	0.040	0.038	5.96	0.70	8.54
	SD		0	0	0.001	0.001	0.21	0.01	0.46
M2	1	2	300	2400	0.041	0.038	6.11	0.71	8.63
	2		300	2400	0.040	0.037	5.96	0.70	8.56
	Average		300	2400	0.041	0.038	6.04	0.70	8.59
	SD		0	0	0.001	0.000	0.11	0.01	0.05
M1	1	4	300	2400	0.070	0.041	5.22	0.39	13.53
	2		300	2400	0.068	0.042	5.07	0.39	12.95
	Average		300	2400	0.069	0.042	5.14	0.39	13.24
	SD		0	0	0.001	0.000	0.11	0.00	0.41
M2	1	4	300	2400	0.071	0.042	5.29	0.39	13.52
	2		300	2400	0.070	0.042	5.22	0.39	13.33
	Average		300	2400	0.071	0.042	5.26	0.39	13.43
	SD		0	0	0.001	0.000	0.05	0.00	0.13
M1	1	6	300	2400	0.091	0.040	4.52	0.25	18.20
	2		300	2400	0.092	0.040	4.57	0.25	18.40
	Average		300	2400	0.092	0.040	4.55	0.25	18.30
	SD		0	0	0.001	0.000	0.04	0.00	0.14
M2	1	6	300	2400	0.094	0.040	4.67	0.25	18.99
	2		300	2400	0.092	0.041	4.57	0.25	17.95
	Average		300	2400	0.093	0.040	4.62	0.25	18.47
	SD		0	0	0.001	0.001	0.07	0.01	0.73
M1	1	8	300	2400	0.110	0.031	4.10	0.15	28.03
	2		300	2400	0.112	0.032	4.18	0.15	28.00
	Average		300	2400	0.111	0.032	4.14	0.15	28.01
	SD		0	0	0.001	0.000	0.05	0.00	0.02
M2	1	8	300	2400	0.112	0.033	4.18	0.15	27.15
	2		300	2400	0.116	0.032	4.32	0.15	28.82
	Average		300	2400	0.114	0.033	4.25	0.15	27.99
	SD		0	0	0.003	0.001	0.11	0.00	1.18
M1	1	10	300	3900	0.138	0.039	4.12	0.09	45.77
	2		300	3900	0.134	0.039	4.00	0.09	44.44
	Average		300	3900	0.136	0.039	4.06	0.09	45.10
	SD		0	0	0.003	0.000	0.08	0.00	0.94
M2	1	10	300	3900	0.136	0.039	4.06	0.09	45.33
	2		300	3900	0.140	0.039	4.18	0.09	46.67
	Average		300	3900	0.138	0.039	4.12	0.09	46.00
	SD		0	0	0.003	0.000	0.08	0.00	0.94

Table B.4: Gas permeation results of mixed matrix membranes contain 30 wt.% CMS.

Membrane	Run no.	P (bar)	tCO ₂ (s)	tCH ₄ (s)	VCO ₂ (cm ³)	VCH ₄ (cm ³)	PCO ₂ (Barrer)	PCH ₄ (Barrer)	α_{CO_2/CH_4}
M1	1	2	300	2400	0.046	0.024	6.56	0.43	15.33
	2		300	2400	0.048	0.027	6.84	0.49	14.01
	Average		300	2400	0.047	0.026	6.70	0.46	14.67
	SD		0	0	0.001	0.002	0.20	0.04	0.93
M2	1	2	300	2400	0.050	0.026	7.13	0.46	15.38
	2		300	2400	0.048	0.026	6.84	0.46	14.77
	Average		300	2400	0.049	0.026	6.98	0.46	15.08
	SD		0	0	0.001	0.000	0.20	0.00	0.44
M1	1	4	300	2400	0.080	0.036	5.70	0.32	17.78
	2		300	2400	0.076	0.040	5.42	0.36	15.20
	Average		300	2400	0.078	0.038	5.56	0.34	16.49
	SD		0	0	0.003	0.003	0.20	0.03	1.82
M2	1	4	300	2400	0.076	0.034	5.42	0.31	17.67
	2		300	2400	0.076	0.030	5.42	0.27	20.27
	Average		300	2400	0.076	0.032	5.42	0.29	18.97
	SD		0	0	0.000	0.003	0.00	0.03	1.83
M1	1	6	300	2400	0.100	0.034	4.75	0.20	23.67
	2		300	2400	0.098	0.027	4.66	0.16	28.61
	Average		300	2400	0.099	0.031	4.70	0.18	26.14
	SD		0	0	0.001	0.005	0.07	0.03	3.50
M2	1	6	300	2400	0.096	0.036	4.56	0.21	21.33
	2		300	2400	0.102	0.040	4.85	0.24	20.40
	Average		300	2400	0.099	0.038	4.70	0.23	20.87
	SD		0	0	0.004	0.003	0.20	0.02	0.66
M1	1	8	300	2400	0.122	0.026	4.35	0.11	37.83
	2		300	2400	0.114	0.025	4.06	0.11	35.91
	Average		300	2400	0.118	0.026	4.20	0.11	36.87
	SD		0	0	0.006	0.000	0.20	0.00	1.36
M2	1	8	300	2400	0.128	0.024	4.55	0.11	42.53
	2		300	2400	0.120	0.024	4.28	0.11	40.00
	Average		300	2400	0.124	0.024	4.41	0.11	41.27
	SD		0	0	0.005	0.000	0.19	0.00	1.79
M1	1	10	300	3600	0.144	0.024	4.11	0.06	71.40
	2		300	3600	0.154	0.026	4.39	0.06	71.63
	Average		300	3600	0.149	0.025	4.25	0.06	71.52
	SD		0	0	0.007	0.001	0.20	0.00	0.16
M2	1	10	300	3600	0.140	0.026	3.99	0.06	64.62
	2		300	3600	0.150	0.025	4.28	0.06	72.58
	Average		300	3600	0.145	0.025	4.13	0.06	68.60
	SD		0	0	0.007	0.001	0.20	0.00	5.63

Table B.5: Gas permeation results of mixed matrix membranes contain 10 wt.% CMS with annealing treatment.

Membrane	Run no.	P (bar)	tCO ₂ (s)	tCH ₄ (s)	VCO ₂ (cm ³)	VCH ₄ (cm ³)	PCO ₂ (Barrer)	PCH ₄ (Barrer)	α CO ₂ /CH ₄
M1	1	2	1200	3600	0.109	0.040	3.88	0.48	8.16
	2		1200	3600	0.109	0.038	3.88	0.45	8.59
	Average		1200	3600	0.109	0.039	3.88	0.46	8.37
	SD		0	0	0.000	0.001	0.00	0.02	0.30
M2	1	2	1200	3600	0.110	0.041	3.91	0.49	8.02
	2		1200	3600	0.110	0.040	3.91	0.48	8.14
	Average		1200	3600	0.110	0.041	3.91	0.48	8.08
	SD		0	0	0.000	0.000	0.00	0.01	0.08
M1	1	4	1200	3600	0.160	0.056	2.85	0.33	8.54
	2		1200	3600	0.168	0.054	2.99	0.32	9.37
	Average		1200	3600	0.164	0.055	2.92	0.33	8.95
	SD		0	0	0.006	0.002	0.10	0.01	0.58
M2	1	4	1200	3600	0.163	0.053	2.91	0.31	9.27
	2		1200	3600	0.160	0.053	2.85	0.31	9.09
	Average		1200	3600	0.162	0.053	2.88	0.31	9.18
	SD		0	0	0.002	0.000	0.04	0.00	0.13
M1	1	6	1200	3600	0.229	0.046	2.72	0.18	14.79
	2		1200	3600	0.228	0.040	2.71	0.16	17.10
	Average		1200	3600	0.228	0.043	2.71	0.17	15.95
	SD		0	0	0.001	0.005	0.01	0.02	1.63
M2	1	6	1200	3600	0.221	0.049	2.63	0.19	13.54
	2		1200	3600	0.232	0.048	2.76	0.19	14.53
	Average		1200	3600	0.227	0.049	2.69	0.19	14.03
	SD		0	0	0.008	0.001	0.09	0.00	0.69
M1	1	8	1200	3600	0.300	0.032	2.67	0.10	27.78
	2		1200	3600	0.278	0.032	2.48	0.09	26.23
	Average		1200	3600	0.289	0.032	2.57	0.10	27.00
	SD		0	0	0.016	0.000	0.14	0.00	1.10
M2	1	8	1200	3600	0.300	0.030	2.67	0.09	30.41
	2		1200	3600	0.300	0.033	2.67	0.10	26.95
	Average		1200	3600	0.300	0.032	2.67	0.09	28.68
	SD		0	0	0.000	0.003	0.00	0.01	2.45
M1	1	10	1200	3600	0.346	0.019	2.47	0.05	54.63
	2		1200	3600	0.380	0.021	2.71	0.05	54.31
	Average		1200	3600	0.363	0.020	2.59	0.05	54.47
	SD		0	0	0.024	0.001	0.17	0.00	0.22
M2	1	10	1200	3600	0.330	0.023	2.35	0.05	43.81
	2		1200	3600	0.376	0.022	2.68	0.05	51.27
	Average		1200	3600	0.353	0.022	2.52	0.05	47.54
	SD		0	0	0.033	0.000	0.23	0.00	5.28

Table B.6: Gas permeation results of mixed matrix membranes contain 20 wt.% CMS with annealing treatment.

Membrane	Run no.	P (bar)	tCO ₂ (s)	tCH ₄ (s)	VCO ₂ (cm ³)	VCH ₄ (cm ³)	PCO ₂ (Barrer)	PCH ₄ (Barrer)	α_{CO_2/CH_4}
M1	1	2	1200	3600	0.118	0.031	4.20	0.37	11.27
	2		1200	3600	0.113	0.030	4.02	0.35	11.36
	Average		1200	3600	0.115	0.031	4.11	0.36	11.31
	SD		0	0	0.004	0.001	0.13	0.01	0.06
M2	1	2	1200	3600	0.116	0.028	4.13	0.34	12.25
	2		1200	3600	0.112	0.028	3.99	0.33	11.91
	Average		1200	3600	0.114	0.028	4.06	0.34	12.08
	SD		0	0	0.003	0.000	0.10	0.00	0.24
M1	1	4	1200	3600	0.178	0.041	3.17	0.24	12.96
	2		1200	3600	0.162	0.041	2.89	0.24	11.91
	Average		1200	3600	0.170	0.041	3.03	0.24	12.44
	SD		0	0	0.011	0.000	0.20	0.00	0.74
M2	1	4	1200	3600	0.174	0.040	3.10	0.24	13.12
	2		1200	3600	0.182	0.040	3.24	0.24	13.65
	Average		1200	3600	0.178	0.040	3.17	0.24	13.38
	SD		0	0	0.006	0.000	0.10	0.00	0.38
M1	1	6	1200	3600	0.246	0.034	2.93	0.13	21.87
	2		1200	3600	0.250	0.041	2.97	0.16	18.29
	Average		1200	3600	0.248	0.037	2.95	0.15	20.08
	SD		0	0	0.003	0.005	0.03	0.02	2.53
M2	1	6	1200	3600	0.235	0.034	2.79	0.13	20.74
	2		1200	3600	0.228	0.033	2.71	0.13	20.48
	Average		1200	3600	0.232	0.034	2.75	0.13	20.61
	SD		0	0	0.005	0.000	0.06	0.00	0.18
M1	1	8	1200	3600	0.312	0.026	2.78	0.08	35.95
	2		1200	3600	0.290	0.024	2.58	0.07	36.55
	Average		1200	3600	0.301	0.025	2.68	0.07	36.25
	SD		0	0	0.015	0.002	0.14	0.00	0.42
M2	1	8	1200	3600	0.328	0.022	2.92	0.07	44.73
	2		1200	3600	0.306	0.023	2.73	0.07	39.91
	Average		1200	3600	0.317	0.023	2.82	0.07	42.32
	SD		0	0	0.016	0.001	0.14	0.00	3.40
M1	1	10	1200	5400	0.386	0.018	2.75	0.03	96.50
	2		1200	5400	0.408	0.021	2.91	0.03	87.43
	Average		1200	5400	0.397	0.020	2.83	0.03	91.96
	SD		0	0	0.016	0.002	0.11	0.00	6.41
M2	1	10	1200	5400	0.350	0.019	2.49	0.03	83.78
	2		1200	5400	0.338	0.018	2.41	0.03	84.50
	Average		1200	5400	0.344	0.018	2.45	0.03	84.14
	SD		0	0	0.008	0.001	0.06	0.00	0.51

Table B.7: Gas permeation results of mixed matrix membranes contain 30 wt.% CMS with annealing treatment.

Membrane	Run no.	P (bar)	tCO ₂ (s)	tCH ₄ (s)	VCO ₂ (cm ³)	VCH ₄ (cm ³)	PCO ₂ (Barrer)	PCH ₄ (Barrer)	α CO ₂ /CH ₄
M1	1	2	1200	3600	0.124	0.023	4.42	0.28	16.03
	2		1200	3600	0.124	0.023	4.40	0.27	16.12
	Average		1200	3600	0.124	0.023	4.41	0.27	16.08
	SD		0	0	0.000	0.000	0.01	0.00	0.06
M2	1	2	1200	3600	0.120	0.023	4.28	0.27	15.79
	2		1200	3600	0.126	0.022	4.49	0.26	17.34
	Average		1200	3600	0.123	0.022	4.38	0.26	16.56
	SD		0	0	0.004	0.001	0.15	0.01	1.10
M1	1	4	1200	3600	0.196	0.031	3.49	0.18	19.09
	2		1200	3600	0.191	0.032	3.41	0.19	18.04
	Average		1200	3600	0.194	0.031	3.45	0.19	18.56
	SD		0	0	0.003	0.001	0.06	0.00	0.74
M2	1	4	1200	3600	0.185	0.032	3.29	0.19	17.11
	2		1200	3600	0.193	0.033	3.44	0.20	17.56
	Average		1200	3600	0.189	0.033	3.37	0.19	17.34
	SD		0	0	0.006	0.000	0.11	0.00	0.32
M1	1	6	1200	3600	0.260	0.025	3.09	0.10	31.45
	2		1200	3600	0.256	0.025	3.04	0.10	30.24
	Average		1200	3600	0.258	0.025	3.06	0.10	30.84
	SD		0	0	0.003	0.000	0.03	0.00	0.86
M2	1	6	1200	3600	0.260	0.026	3.09	0.10	30.23
	2		1200	3600	0.260	0.025	3.09	0.10	31.71
	Average		1200	3600	0.260	0.025	3.09	0.10	30.97
	SD		0	0	0.000	0.001	0.00	0.00	1.04
M1	1	8	1200	7200	0.328	0.020	2.92	0.03	97.31
	2		1200	7200	0.329	0.021	2.93	0.03	94.06
	Average		1200	7200	0.328	0.021	2.93	0.03	95.68
	SD		0	0	0.001	0.001	0.01	0.00	2.30
M2	1	8	1200	7200	0.329	0.019	2.93	0.03	103.96
	2		1200	7200	0.318	0.021	2.83	0.03	91.73
	Average		1200	7200	0.324	0.020	2.88	0.03	97.84
	SD		0	0	0.008	0.001	0.07	0.00	8.65
M1	1	10	1200	9000	0.384	0.010	2.74	0.01	282.35
	2		1200	9000	0.394	0.014	2.81	0.01	211.07
	Average		1200	9000	0.389	0.012	2.77	0.01	246.71
	SD		0	0	0.007	0.003	0.05	0.00	50.40
M2	1	10	1200	9000	0.388	0.009	2.77	0.01	323.33
	2		1200	9000	0.389	0.010	2.77	0.01	291.90
	Average		1200	9000	0.389	0.010	2.77	0.01	307.62
	SD		0	0	0.001	0.001	0.01	0.00	22.23

Table B.8: Gas permeation results of mixed matrix membranes contain 10 wt.% oxidized-CMS.

Membrane	Run no.	P (bar)	tCO ₂ (s)	tCH ₄ (s)	VCO ₂ (cm ³)	VCH ₄ (cm ³)	PCO ₂ (Barrer)	PCH ₄ (Barrer)	α CO ₂ /CH ₄
M1	1	2	1200	3600	0.138	0.057	4.92	0.68	7.24
	2		1200	3600	0.142	0.063	5.06	0.75	6.74
	Average		1200	3600	0.140	0.060	4.99	0.72	6.99
	SD		0	0	0.003	0.004	0.10	0.05	0.35
M2	1	2	1200	3600	0.139	0.057	4.97	0.68	7.31
	2		1200	3600	0.138	0.067	4.91	0.79	6.19
	Average		1200	3600	0.139	0.062	4.94	0.74	6.75
	SD		0	0	0.001	0.007	0.04	0.08	0.79
M1	1	4	1200	3600	0.211	0.062	3.76	0.37	10.15
	2		1200	3600	0.234	0.064	4.16	0.38	11.02
	Average		1200	3600	0.222	0.063	3.96	0.37	10.59
	SD		0	0	0.016	0.001	0.28	0.01	0.61
M2	1	4	1200	3600	0.218	0.067	3.88	0.40	9.79
	2		1200	3600	0.214	0.066	3.81	0.39	9.79
	Average		1200	3600	0.216	0.066	3.85	0.39	9.79
	SD		0	0	0.003	0.001	0.05	0.01	0.00
M1	1	6	1200	3600	0.315	0.062	3.74	0.25	15.25
	2		1200	3600	0.316	0.051	3.75	0.20	18.44
	Average		1200	3600	0.316	0.057	3.75	0.22	16.85
	SD		0	0	0.001	0.007	0.01	0.03	2.26
M2	1	6	1200	3600	0.305	0.052	3.62	0.21	17.58
	2		1200	3600	0.309	0.058	3.67	0.23	15.97
	Average		1200	3600	0.307	0.055	3.64	0.22	16.78
	SD		0	0	0.003	0.004	0.03	0.02	1.14
M1	1	8	1200	3600	0.351	0.040	3.13	0.12	26.47
	2		1200	3600	0.372	0.046	3.31	0.14	24.37
	Average		1200	3600	0.362	0.043	3.22	0.13	25.42
	SD		0	0	0.015	0.004	0.13	0.01	1.49
M2	1	8	1200	3600	0.484	0.046	4.31	0.14	31.84
	2		1200	3600	0.410	0.044	3.65	0.13	28.08
	Average		1200	3600	0.447	0.045	3.98	0.13	29.96
	SD		0	0	0.052	0.001	0.47	0.00	2.66
M1	1	10	1200	3600	0.480	0.039	3.42	0.09	37.11
	2		1200	3600	0.488	0.037	3.48	0.09	39.80
	Average		1200	3600	0.484	0.038	3.45	0.09	38.46
	SD		0	0	0.006	0.001	0.04	0.00	1.90
M2	1	10	1200	3600	0.492	0.037	3.51	0.09	40.11
	2		1200	3600	0.500	0.037	3.56	0.09	40.32
	Average		1200	3600	0.496	0.037	3.53	0.09	40.22
	SD		0	0	0.006	0.000	0.04	0.00	0.15

Table B.9: Gas permeation results of mixed matrix membranes contain 20 wt.% oxidized-CMS.

Membrane	Run no.	P (bar)	tCO ₂ (s)	tCH ₄ (s)	VCO ₂ (cm ³)	VCH ₄ (cm ³)	PCO ₂ (Barrer)	PCH ₄ (Barrer)	$\alpha_{\text{CO}_2/\text{CH}_4}$
M1	1	2	1200	3600	0.140	0.049	5.00	0.58	11.27
	2		1200	3600	0.168	0.047	5.99	0.56	11.36
	Average		1200	3600	0.154	0.048	5.49	0.57	11.31
	SD		0	0	0.020	0.001	0.70	0.02	0.06
M2	1	2	1200	3600	0.145	0.044	5.15	0.53	12.25
	2		1200	3600	0.153	0.044	5.44	0.52	11.91
	Average		1200	3600	0.149	0.044	5.30	0.52	12.08
	SD		0	0	0.006	0.000	0.21	0.00	0.24
M1	1	4	1200	3600	0.225	0.054	4.01	0.32	12.96
	2		1200	3600	0.238	0.052	4.24	0.31	11.91
	Average		1200	3600	0.231	0.053	4.12	0.32	12.44
	SD		0	0	0.009	0.001	0.17	0.01	0.74
M2	1	4	1200	3600	0.232	0.052	4.13	0.31	13.12
	2		1200	3600	0.246	0.054	4.38	0.32	13.65
	Average		1200	3600	0.239	0.053	4.26	0.31	13.38
	SD		0	0	0.010	0.001	0.18	0.01	0.38
M1	1	6	1200	3600	0.320	0.048	3.81	0.19	21.87
	2		1200	3600	0.328	0.046	3.90	0.18	18.29
	Average		1200	3600	0.324	0.047	3.85	0.19	20.08
	SD		0	0	0.005	0.001	0.06	0.01	2.53
M2	1	6	1200	3600	0.342	0.045	4.07	0.18	20.74
	2		1200	3600	0.332	0.045	3.94	0.18	20.48
	Average		1200	3600	0.337	0.045	4.01	0.18	20.61
	SD		0	0	0.007	0.000	0.09	0.00	0.18
M1	1	8	1200	3600	0.424	0.035	3.78	0.10	35.95
	2		1200	3600	0.429	0.035	3.82	0.10	36.55
	Average		1200	3600	0.426	0.035	3.80	0.10	36.25
	SD		0	0	0.003	0.000	0.03	0.00	0.42
M2	1	8	1200	3600	0.410	0.032	3.65	0.10	44.73
	2		1200	3600	0.414	0.033	3.69	0.10	39.91
	Average		1200	3600	0.412	0.033	3.67	0.10	42.32
	SD		0	0	0.003	0.001	0.03	0.00	3.40
M1	1	10	1200	3600	0.498	0.021	3.55	0.05	96.50
	2		1200	3600	0.520	0.018	3.71	0.04	87.43
	Average		1200	3600	0.509	0.020	3.63	0.05	91.96
	SD		0	0	0.016	0.002	0.11	0.01	6.41
M2	1	10	1200	3600	0.486	0.022	3.47	0.05	83.78
	2		1200	3600	0.516	0.022	3.68	0.05	84.50
	Average		1200	3600	0.501	0.022	3.57	0.05	84.14
	SD		0	0	0.021	0.000	0.15	0.00	0.51

Table B.10: Gas permeation results of mixed matrix membranes contain 30 wt.% oxidized-CMS.

Membrane	Run no.	P (bar)	tCO ₂ (s)	tCH ₄ (s)	VCO ₂ (cm ³)	VCH ₄ (cm ³)	PCO ₂ (Barrer)	PCH ₄ (Barrer)	$\alpha_{\text{CO}_2/\text{CH}_4}$
M1	1	2	1200	3600	0.170	0.034	6.06	0.40	15.00
	2		1200	3600	0.165	0.031	5.88	0.37	16.07
	Average		1200	3600	0.168	0.032	5.97	0.38	15.54
	SD		0	0	0.004	0.002	0.13	0.03	0.76
M2	1	2	1200	3600	0.16	0.03	5.6944	0.35635	15.98
	2		1200	3600	0.176	0.034	6.2717	0.40148	15.62
	Average		1200	3600	0.168	0.032	5.98	0.38	15.80
	SD		0	0	0.011	0.003	0.41	0.03	0.25
M1	1	4	1200	3600	0.268	0.041	4.78	0.24	19.53
	2		1200	3600	0.252	0.043	4.49	0.25	17.66
	Average		1200	3600	0.260	0.042	4.63	0.25	18.60
	SD		0	0	0.011	0.001	0.20	0.01	1.32
M2	1	4	1200	3600	0.264	0.038	4.7038	0.2245	20.95
	2		1200	3600	0.248	0.04	4.4187	0.23875	18.51
	Average		1200	3600	0.256	0.039	4.56	0.23	19.73
	SD		0	0	0.011	0.002	0.20	0.01	1.73
M1	1	6	1200	3600	0.348	0.034	4.13	0.13	30.71
	2		1200	3600	0.348	0.039	4.14	0.15	27.06
	Average		1200	3600	0.348	0.036	4.13	0.14	28.88
	SD		0	0	0.000	0.003	0.00	0.01	2.58
M2	1	6	1200	3600	0.352	0.033	4.1811	0.13066	32
	2		1200	3600	0.344	0.036	4.0908	0.14333	28.54
	Average		1200	3600	0.348	0.035	4.14	0.14	30.27
	SD		0	0	0.005	0.002	0.06	0.01	2.45
M1	1	8	1200	3600	0.439	0.019	3.91	0.06	69.28
	2		1200	3600	0.426	0.018	3.80	0.05	70.22
	Average		1200	3600	0.432	0.019	3.85	0.06	69.75
	SD		0	0	0.009	0.001	0.08	0.00	0.66
M2	1	8	1200	3600	0.44	0.023	3.9198	0.06949	56.41
	2		1200	3600	0.448	0.021	3.9911	0.06236	64
	Average		1200	3600	0.444	0.022	3.96	0.07	60.21
	SD		0	0	0.006	0.002	0.05	0.01	5.37
M1	1	10	1200	7200	0.526	0.016	3.75	0.02	192.44
	2		1200	7200	0.508	0.017	3.62	0.02	179.29
	Average		1200	7200	0.517	0.017	3.68	0.02	185.87
	SD		0	0	0.013	0.000	0.09	0.00	9.29
M2	1	10	1200	7200	0.538	0.017	3.8357	0.02043	187.74
	2		1200	7200	0.506	0.017	3.6062	0.01996	180.71
	Average		1200	7200	0.522	0.017	3.72	0.02	184.23
	SD		0	0	0.023	0.000	0.16	0.00	4.97